PRODUCTION OF CELLULOSE NANOFIBERS USING MIDWEST BIOMASS AND THEIR HIGH-PERFORMANCE RUBBER NANOCOMPOSITES

A Thesis
Submitted to the Graduate Faculty
of the
North Dakota State University
of Agriculture and Applied Science

By

Alexander Cole Sinclair

In Partial Fulfillment of the Requirements
for the Degree of
MASTER OF SCIENCE

Major Department:
Mechanical Engineering

November 2018

Fargo, North Dakota

North Dakota State University
Graduate School

Title

Production of Cellulose Nanofibers using Midwest Biomass and Their High-Performance Rubber Nanocomposites

By

Alexander Cole Sinclair

The Supervisory Committee certifies that this ***disquisition*** complies with North Dakota State University's regulations and meets the accepted standards for the degree of

MASTER OF SCIENCE

SUPERVISORY COMMITTEE:

Dr. Long Jiang
Chair

Dr. Dilpreet Bajwa

Dr. Mohi Quadir

Approved:

12/14/2018
Date

Dr. Alan R. Kallmeyer
Department Chair

ABSTRACT

Cellulose nanofibers (CNFs) are a sustainable and environmentally friendly material which can be used as a highly versatile reinforcing agent in polymer nanocomposites. This thesis presents a novel method to produce CNFs from Midwest agricultural residues and the work done to integrate CNFs into hydrophobic matrix elastomer, SBR. Cellulose nanofibers produced from Midwest agricultural residuals showed a promising morphology with diametrical dimensions on the nanometer scale. Superior reinforcement effect was also observed when these nanofibers were incorporated in PEO based nanocomposites. Additionally, high performance rubber (SBR) nanocomposites which incorporated various functionalized CNFs were produced. These rubber nanocomposites displayed heightened mechanical properties and showed significant potential to replace traditionally formulated rubber reinforced with non-environmentally friendly carbon black.

ACKNOWLEDGEMENTS

I would first like to kindly thank my supervisory committee for the time and effort they have invested into my education and my future. This work and my academic success would not have been possible without their support. A special thanks to Dr. Long Jiang, and Dr. Dilpreet Bajwa for making me feel at home in their research groups and providing any and all required support throughout my academic career. I would also like to express my gratitude to Dr. Sreekala Bajwa for providing support and mentorship throughout the process of our weekly research group meetings. Additionally, I would like to thank Dr. Chunju Gu of the NDSU Department of Coatings and Polymers, Scott Payne of the NDSU Microscopy Center, Jim Bahr, Fred Haring, and Greg Strohmen of NDSU Research and Technology Park. I would like to give a special thanks to Siwakorn Tangpong, as his help was instrumental in the completion of the work documented herein. Lastly, I would like to say thank you to Dr. Xinnan Wang and the rest of the NDSU Department of Mechanical Engineering for their support and the time they dedicate to educating the future generation of engineers.

TABLE OF CONTENTS

LIST OF TABLES

LIST OF FIGURES

LIST OF ABBREVIATIONS

AFM.....Atomic Force Microscopy.

BC .....Bacterial Cellulose.

CNF.....Cellulose Nanofibers.

CNC .....Cellulose Nanocrystals.

DMA .....Dynamic Mechanical Analysis.

DP .....Degree of Polymerization.

DS .....Degree of Substitution.

FT-IR.....Fourier Transform Infra-Red.

IR.....Infra-Red.

PEO.....Poly Ethylene Oxide.

PHR.....Parts Per Hundred.

SBR.....Styrene Butadiene Rubber.

SEM .....Scanning Electron Microscopy.

TEM.....Transmission Electron Microscopy.

TGA .....Thermogravimetric Analysis.

UV.....Ultra Violet.

CHAPTER I: SUMMARY AND SCOPE OF WORK

The research works documented in this thesis involve many elements related to the production and potential applications of CNFs. CNFs are naturally occurring polymer fibers that are biodegradable, sustainable, and have near non-existent health or safety risks. CNFs fall into the family of cellulose and its derived nanomaterials, which have very high mechanical properties and provide versatile reinforcement in many different types of composites.

Chapter II of this thesis gives an in-depth introduction to cellulose and cellulose nanofibers. Specifically, the history, properties, production/extraction methods, and some high-performance applications will be discussed. Chapter II provides significant justification as to why it is important to explore and implement cellulose into today's diverse array of products. A strong foundation regarding the chemical and hierarchical structure of cellulose is required to efficiently design production methods and utilize its full potential as a structural material.

Chapter III of this thesis focuses on the production of CNFs from local Midwest agricultural residuals. CNF is typically produced from wood pulp produced for the paper products industry. Paper pulp is the standard starting material for CNF today. There is however a tremendous opportunity to develop CNF production methods which can extract cellulose from Midwest biomass residuals which go to waste or low value applications. As the demand for cellulose and cellulose nanomaterials increases, the successful implementation of such a process could generate a significant new revenue stream for agricultural communities worldwide.

Chapter IV focuses on the integration of CNFs as a reinforcing material in styrene butadiene rubber (SBR). SBR is a widely consumed synthetic rubber used in a vast array of rubber products including tires. SBR is known for its high abrasion and tear resistance however SBR suffers from poor mechanical properties and requires the integration of a significant amount

of a reinforcing filler known as carbon black. Neither SBR nor carbon black are considered environmentally friendly or renewable, as both materials productions is dependent on the supply of petroleum. There is significant motivation to produce more environmentally friendly rubber products which are more sustainable. Chapter IV discusses in detail, the work done to integrate both pristine and functionalized CNFs into SBR to produce high performance, sustainable, and environmentally friendly rubber products.

Chapter V details further efforts to increase the performance of SBR polymer matrix nanocomposites which utilize CNF as the primary reinforcing material. The primary objective of the work detailed in chapter V was to build on the previous work presented in chapter IV with the addition of co-integrating very small amounts of carbon black or graphene. Graphene is a single or multiple layered material in which the layers consist of carbon atoms bonded together in hexagonal patterns. Graphene has unique properties and has especially high mechanical properties. Integrating small amounts of either carbon black or graphene can further increase the mechanical properties of the final product in addition to providing anti-aging benefits.

The overarching objective of the work presented in this thesis was to produce and/or develop new environmentally friendly and sustainable materials designed around the utilization of cellulose nanofibers. To accomplish this goal, the scientific method was extensively utilized. Additionally, all materials produced and presented in this document underwent a battery of standardized testing and characterization to determine their suitability for use in future high value applications.

CHAPTER II: INTRODUCTION TO CELLULOSE AND CELLULOSE NANOFIBERS

Materials engineering and the development of new materials is the foundation which makes technological innovation possible. New materials open doors to new technological possibilities and have, in part, defined the ages of humanity. The science of materials engineering is central to enhancing quality of life and is influential in our everyday lives. Examples of the successful implementation of modern materials engineering are all around us and include: electronic devices, automobiles, aircraft, and the very chair we are sitting in. Materials engineering in the 21st century has however been especially pushed to the limit. The desire to build more efficient, faster, stronger, lighter, cheaper, and now more sustainable and environmentally friendly products has driven materials scientists and engineers to develop a new class of engineering materials.

Today's society is heavily dependent on petroleum and petroleum-based products. Most commodity and engineering polymers (plastics) are derived from petroleum and are widely used in consumer products. Many of these products have complicated or non-existent end of life management plans which combined with poor recycling habits results in significant environmental concerns. Global production of plastics totaled over 299 million tons in 2013 with millions of tons ending up in oceans and landfills.[1]

Sustainable and environmentally friendly materials derived from biobased sources represent a unique solution to this issue.[2] Targeted reductions in petroleum based products and materials have recently helped spur the implementation of biobased engineering polymers like polylactic acid (PLA).[3] The utilization of potential renewable and/or biobased resources can also help alleviate many international issues such as petroleum dependence, deteriorating air and water quality, and climate change.[4] Additionally, widespread implementation of biobased

resources to be used as engineering materials represents a potential source for new revenue streams which can be realized locally.

Cellulose is a biobased resource which is a promising candidate for use as an engineering material. Cellulose is the most abundant naturally occurring polymer on the planet and it possesses very unique mechanical properties, especially at the nano-scale.[5] Cellulose is one of the major constituents in all lignocellulosic biomass which encompasses all plant matter. Cellulose along with hemicellulose, lignin, and pectin, form the naturally occurring biocomposite that give plants both shape and structure. These naturally occurring composite materials (wood, cotton, flax, etc.) have been used as engineering and building materials for thousands of years and are still vastly used today across a wide variety of industuries.[6] These lignocellulosic materials (wood cotton, flax etc.) owe their popularity over the ages to the fact that they are abundant, have high mechanical properties, and are flexibility in application. The hierarchical structure of lignocellulosic biomass and the constituents which they are made of (cellulose, hemicellulose, lignin, etc.) are specifically responsible for these advantageous mechanical properties. This hierarchical structure ranges from macro scale to nano scale dimensions and can be viewed in figure 1.

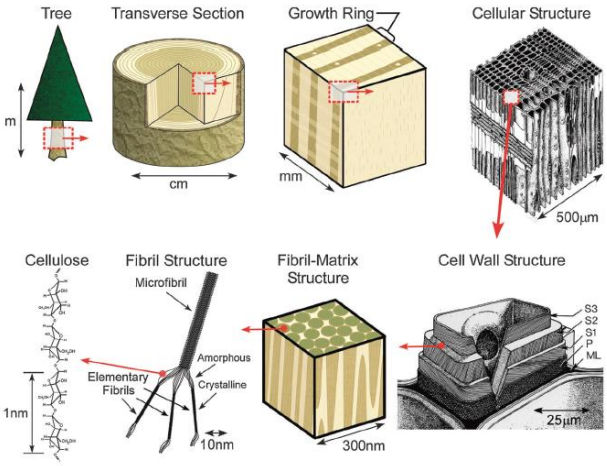

Figure 1. Hierarchical structure of typically woody biomass[6]

Cellulose makes up the primary structural constituent in the primary and secondary walls within all plant cells. It can also be found in tunicates, algae, and bacteria.[7] Cellulose, on a molecular level, is by definition, a complex carbohydrate polymer and can be described as a linear homopolysaccharide consisting of β-1.4-linked anhydro-D-glucose units.[4, 8] The chemical structure of the repeat unit of cellulose is shown in figure 2. The degree of polymerization (DP) of cellulose ranges from 2,000 to 27,000 depending on the source biomass.[5]

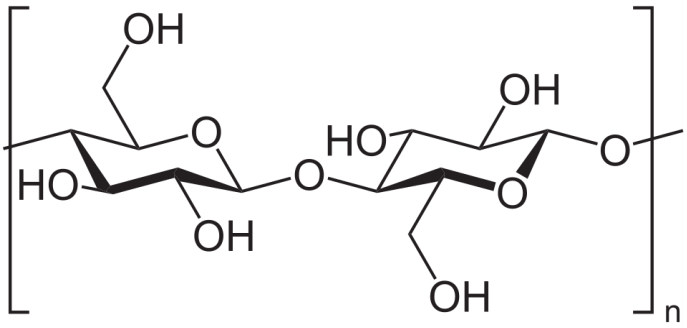

Figure 2. Chemical structure of cellulose

Cellulose's superior mechanical properties stem from its linearly ordered microstructure. Elementary cellulose chains line up to form elementary fibers and are held together via both intra-molecular and inter-molecular hydrogen bonds resulting from the three hydroxyl groups on each cellulose repeat unit. This 3D hydrogen bonding network is responsible for the naturally formed linear microfibrils present in the cell walls of lignocellulosic biomass. These elementary fibers are highly crystalline and consist of ordered crystalline and amorphous regions. Cellulose crystallinity can vary depending on cellulose source. Elementary fibers then make up larger micro sized fibers. It is this linear structure which spans from the atomic to micro scale that is responsible for the strength and stiffness of cellulose and thus the lignocellulosic biomass which it makes up (see figure 1).[5, 6, 9]

Cellulose today is used in many forms. Most of the industrially produced cellulose is in the form of bleached wood pulp (Kraft pulp) which is widely used in the paper products industry. Cellulose was synthesized into a thermoplastic polymer by the Hyatt manufacturing company in the 1870' s. This semi-synthetic cellulose thermoplastic is used today for many consumer grade products such as cellulose acetate, rayon, and cellophane. More recently, cellulose has gained widespread attention as it can be processed down to the elementary fibers at micro and nanoscale. Elementary fibers or fiber bundles with nano-scale diameters and lengths up to several microns result in fibers with very high aspect ratios, making them ideal as reinforcing agents. Fiber diameters can range anywhere from 10-100 nm depending on processing conditions (figure 3 below shows the relative scales for many materials ranging from a tennis all to an individual water molecule for demonstrative purposes). Typical cellulose nanofiber diameters would then fall in between the antibody and virus section of figure 3. Processing lignocellulosic biomass into cellulose nanofibers (CNF) requires a two-step process involving both chemical purification and mechanical fibrillation.

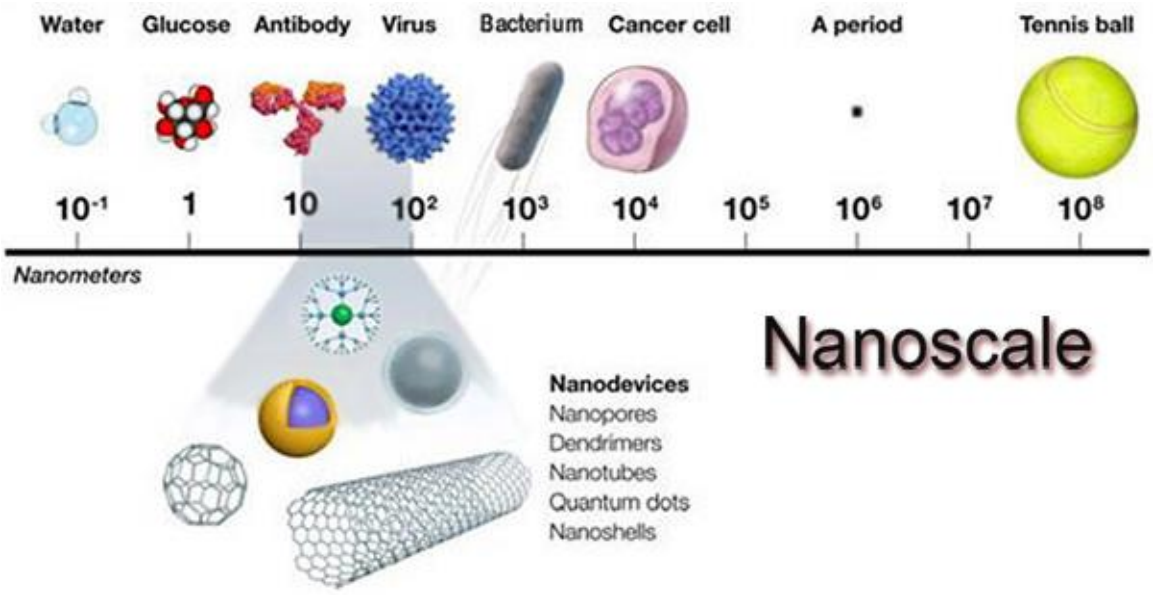

Figure 3. Comparative dimension of many commonly known materials [10]

Chemical purification techniques are used to extract and purify cellulose from the original lignocellulosic biomass. In summary, this chemical purification process first breaks down the bonds between lignin, hemicellulose, and cellulose after which the cellulose fibrils can be extracted and used for further processing. Worldwide production of lignocellulosic biomass is estimated to be between 1010 and 1011 metric tons per annum.[4] Approximately 6% is processed by the paper, textile, materials, and chemical industries and is primarily sourced from hard and softwoods. As such, the most common chemical purification procedure is the Kraft process which is used to produce industrial paper pulp. Kraft pulp is currently the primary source of purified cellulose for commercial CNF production today. However, a significant portion of the lignocellulosic biomass available is in the form of agriculture residues which largely goes to waste or to low value applications.[4, 11] Therefore, deriving CNFs from the agricultural residues of fast-growing crops (instead of from trees) is environmentally and economically advantageous. CNFs from wide variety of non-wood cellulosic biomass have been reported and are summarized in many review articles.[5, 6, 12-14] Non-wood lignocellulosic biomass can be purified and pulped in one third of the time of hard/soft woods and requires less power consumption due to lower lignin contents in the biomass.[13] As such several chemical treatments have been reported and vary depending on the type of biomass. Biomass residues readily available in the Midwest include corn stalk, wheat straw, soybean hull, flax, and many others. CNF has previously been reported to have been extracted and produced from soybean hull and wheat straw biomasses using novel chemical purification techniques in several previous studies.[11, 15, 16] These techniques will specifically be discussed in chapter three of this thesis.

Purified cellulose, regardless of sorce, must then be mechanically fibrillated to physically shear apart bundles of purified cellulose to create micro or nano cellulose fibers. There are many

options and pathways available for fiber fibrillation. Common equipment and techniques reported include: high pressure homogenization, grinding, cryocrushing, microfluidization, and high intensity ultrasonication. Each of these techniques operate on the basic principle which is to subject an aqueous slurry of cellulosic material to high shear force. Shear force then split larger fiber bundles into smaller fibers until just elementary fibers remain.[2] Alternatively, the crystalline regions of the elementary cellulose fibers can be extracted by subjecting purified cellulose to acid hydrolysis. This technique yields cellulose nanocrystals (CNC). CNCs are tiny linear rod or needle like structures which are similar in properties to CNFs. CNCs, like CNFs, have been widely studied for use in nanocomposite materials.

Researches have utilized CNFs to make nanopapers, conductive films for electronics, energy storage devices, improve gas permeability for food packaging, and integrate CNF as reinforcing material in polymer and ceramic (cement) matrix composites. CNF is light-weight, strong, stiff, biodegradable, sustainable, and relatively inexpensive to produce.[2, 4, 16] CNF's inherant fibrillar form is ideal for use as a reinforcing agent in composite materials. CNFs can be valuable in many applications including high performance composite materials, packaging, electronics, and biomedical applications.

CNFs are primarily processed in aqueous mediums due to their hydrophylic hydroxyl surface chemistry. This can lead to challenges when integration or dispersion in non-polar mediums such as solvents or polymers is desirable.[17] Stable dispersions of cellulose nanoparticles in non-polar mediums are however possible through functionalization of the native hydroxyl surface chemistry of cellulose. Many surface functionalization techniques have been reported including coating with surfactants, substituting hydroxyl groups with small molecules, and polymer grafting.[17] Polymer grafting can be split into the two sub-catagories:“grafting onto”

and “grafting from”. The grafting onto approach involves the utilization of various coupling agents to attach polymer chains. The grafting from approach typically involves some type of polymerization strategy to graft a polymer chain to the surface of the cellulose nanoparticle. Many of the common chemical functionalization that have been reported are summarized in figure 4.

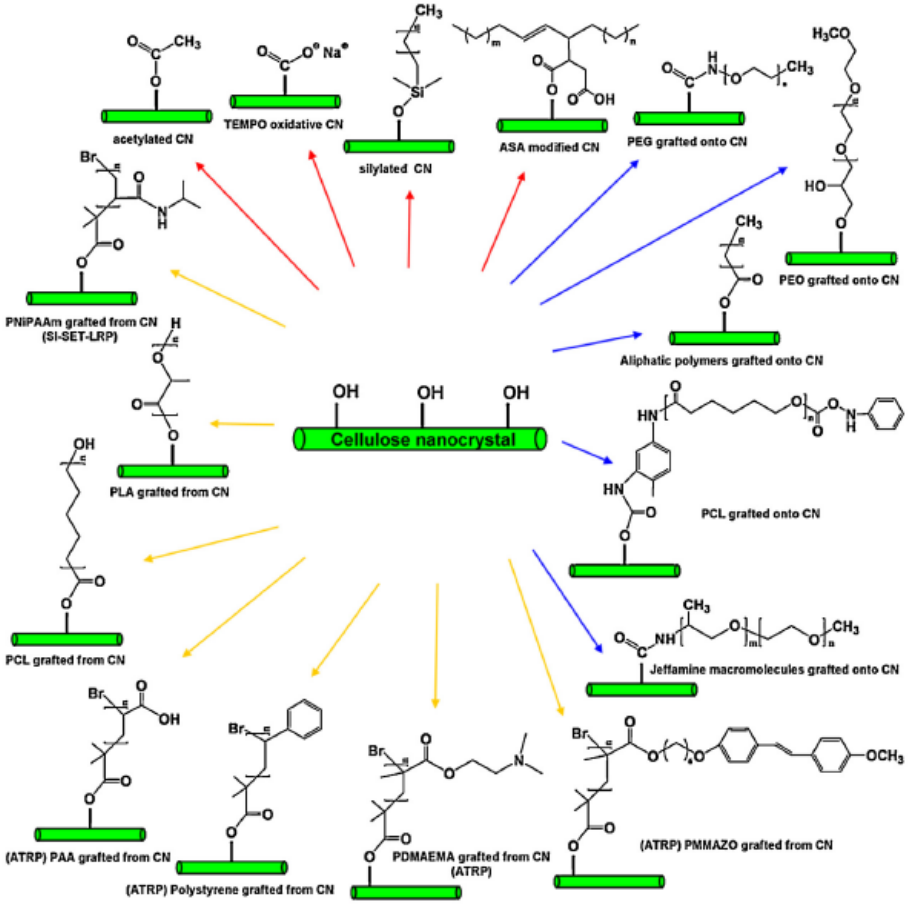

Figure 4. Common chemical functionalization techniques[17]

CHAPTER III: CELLULOSE NANOFIBERS PRODUCED FROM VARIOUS AGRICULTURAL RESIDUES AND THEIR REINFORCMENT EFFECTS IN POLYMER NANOCOMPOSITES

Literature Review

Chapter one introduced cellulose and cellulose nanofibers (CNF) and many of the high value applications in which they have potential for. To create new revenue streams for Midwest agricultural products it is important to explore agricultural residuals as a potential cellulose source material. CNF has previously been reported to have been extracted and produced from soybean hull and wheat straw biomasses using novel chemical purification techniques followed by mechanical fibrillation in several previous studies.[11, 15, 16] Soybean hulls and wheat straw biomass residuals are readily available in the Midwest and primarily go to low value appliations.[4, 11] This chapter will focus on comparing CNF prepared from biomass residuals from softwood, soybean hull, and wheat straw.

Bhatnagar et al. (2005) reported a novel method used to isolate cellulose from flax and hemp.[7] The chemical procedure utilized a three-step soaking process to purify cellulose from the natural biomass composite. The specific treatment process was as follows: First, an alkaline soak was used to increase the surface area of the lignocellulosic biomass, thus making it more susceptible to acid hydrolysis. Acid hydrolysis was then used to dissolve hemicelluloses present in the biomass. The final alkali soak then broke down the remaining lignin and separated it from the cellulose. Flax biomass was purified from 73% to 95% cellulose following the treatment process. Similarly, hemp was purified from 76% to 94% cellulose. Following purification, the cellulose was cryocrushed resulting in cellulose nanofibers with average diameters of approximately 50 nm and lengths up to several microns. The authors also reported an increase in

crystallinity of the fibers compared to fibers created from wood Kraft pulp. The authors then prepared nanocomposites in the form of thin films by reinforcing polyvinyl alcohol (PVA) with the prepared cellulose nanofibers. The nanocomposite films were prepared by creating a solution of PVA in water followed by mixing in the prepared nanofibers. The authors found that these processes resulted in nanocomposites with significantly improved mechanical propeties as compared to neat polymer samples. Both tensile strength and modulus was increased to 118 Mpa from 69 Mpa and 9.8 GPa from 2.29 GPa for strength and modulus respectively.

The work done by Alemdar et al. (2007) utilized the same patented three step chemical purification approach with alternating alkali and hydrochloric acid soaking.[7, 11, 16] This technique was reported to have purified the cellulose content of soybean hulls and wheat straw fibers from 43.2% and 56.4% to 84.6% and 94% respectivly.[16] Following purification, mechanical treatment in the form of cryocrushing and homogenization was utilized to fibrillate the cellulose. SEM and TEM imaging were then used to confirm that nanofibers had been created with diameters less than 100 nm.

Zimmerman et al. (2009) explored producing nanocellulose from many commercially available wood and wheat straw pulp sources.[18] The authors utilized purely mechanical treatments for this work in the form of a mechanical pretreatment using an inline dispersing system followed by high shear fibrillation via a microfluidizer. High quality cellulose nanofibers were reported and further efforts to reinforce Active Ingredient cellulose (HPC) with the nanofibers were explored. Nanocomposites were fabricated using a solution casting technique in which HPC was dissolved in water followed by the integration of nanofibers at 20% w/w. Significant impact on the mechanical propeties of the nanocomposites was reported when compared to films reinforced with the raw commercially obtained pulps at the same levels of reinforcement.

Xuezhu et al. (2014) studied the reinforcing effect commercially obtained cellulose nanofibers or nanocrystals had on electrospun polyethylene oxide (PEO) nanofiber mats. The nanocomposites were prepared by dissolving the PEO in water following by mixing in the cellulose nanofibers or nanocrystals into the polymer solution at various reinforcement percentages. The authors of this study were able to successfully produce electrospun nanofibers with dimensions on the nanometer scale. Furthermore, the authors reported that cellulose nanofiber and nanocrystal reinforcement significantly impacted the crystal structure of the electrospun PEO. Specifically, a shish-kabab like structure had been formed resulting from alignment of the cellulose nanomaterial reinforcement during the electrospinning process. Nanocomposite mechanical properties were also impacted positively by the cellulose nanomaterials with significant gains in tensile strength, Young's modulus, and strain to failure at loading levels below 4%. Above 4% reinforcement, mechanical properties started to decline.

Saito et al. (2006) reported a novel technique for purifying cellulose from softwood biomass.[19] In this work, softwood biomass was repeatedly soaked in sodium chlorite (NaClO2) to break down and remove lignin. The treatment was repeated until the Klason lignin content was lower than 0.1%. The purified cellulose in this study was used for further experimentation regarding surface functionalization of cellulose. The procedure is known as TEMPO-mediated oxidation and has been widely studied and reported by many research articles and books.[5, 6, 9, 12, 19-26] TEMPO-mediated oxidation selectively converts hydroxyl groups to aldehyde and carboxylate functional groups. The TEMPO oxidation procedure can be performed under very mild and aqueous and when the pH is held in the range of 10-11, the primary C6 hydroxyl of cellulose can be targeted for carboxyl replacement. The scheme of the TEMPO-mediated oxidation process is shown in figure 5.

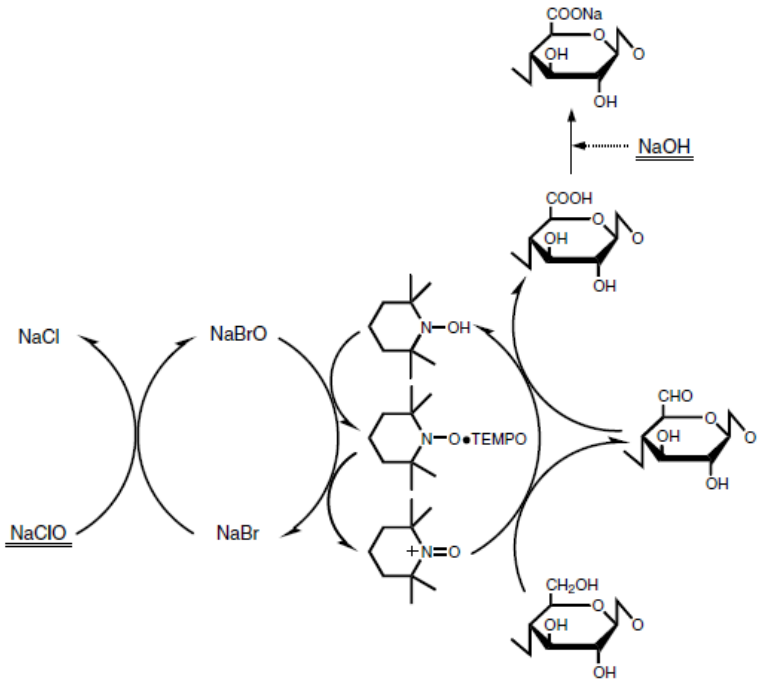

Figure 5. TEMPO-mediated oxidation of cellulose

Carboxyl groups introduce negative charges to the surface of the cellulose microfibrils and thus is a promising production aid. Cellulose nanofibers prepared by this method typically have smaller diameters and require much less energy input for mechanical fibrillation. Additionally, the C6 carboxyl functional groups can also be used as an intermediate for additional reactions such to change the surface properties or polymer grafting, ect.[5, 9]

Fukuzumi et al. (2008) TEMPO oxidized different types commercially available Kraft wood pulps (hard and soft wood). The oxidized celluloses were then subjected to homogenization followed by ultrasonication to produce uniform cellulose nanofibers with diameters as low as 3-4 nm. The prepared nanofibers were then dispersed in water and converted into thin films using suction filtration followed by drying. The TEMPO oxidized cellulose nanofiber films prepared from softwood displayed significant transparency compared to the starting pulp material. The authors also reported the tensile strength, modulus, and elongation

percentage of the TEMPO oxidized nanofiber films to be 233 MPa, 6.9 GPa, and 7.6% respectively. The primary goal of this work was however to produce films with significant gas barrier properties. To do this polylactic acid (PLA) films were coated with TEMPO oxidized nanofibers and subjected to an oxygen permeability test. The authors found that the amount of oxygen penetrating through a PLA film versus a coated PLA film decreased from 746 mL m-2 day-1 Pa-1 to an astounding 1 mL m-2 day-1 Pa-1 respectively.

The work presented in chapter one's primary focus is to build on the previously mentioned and reported literature with the goal of developing a sustainable pathway for the production CNF from biomass residuals available in the upper Midwest region of the U.S. Furthermore, evaluating their potential as reinforcement in novel nanocomposite materials will be explored. Soybean hull and wheat straw residuals will be specifically discussed and compared with more traditionally used softwoods. Modifications made to the documented alkali/hydrolysis used to purify soybean and wheat straw procedure will be discussed. Commercially obtained and purified cellulose from soybean hull biomass will also be utilized and compared to the purified cellulose produced in this study. Additionally, cellulose nanofibers commercially prepared from bleached Kraft pulp are also used for comparison. The procedure discussed herein utilizes documented production techniques experimentally functionalized to produce as good or better results while using locally obtained biomass and modern laboratory equipment.[16, 19]

Experimental

Materials

Soybean hull and wheat straw were acquired from local Midwest sources. Pine wood flour was supplied by American Wood Fibers (Schofield, WI). Fl-1 Soy Fibre®, a commercial cellulosic dietary fiber product derived from soybean hulls was supplied from Fibred-Maryland

Inc. Commercial CNFs, produced from wood pulp through a multi-pass high-pressure mechanical grinding process, were acquired from the USDA Forest Products Laboratory (FPL, Madison, WI). 2,2,6,6- tetramethylpiperidine-1-oxy radical (TEMPO), sodium bromide (NaBr), sodium hydroxide (NaOH), sodium chlorite ($NaClO_2$), sodium hypochlorite (NaOCl) solution, and polyethylene oxide (PEO), M_w = 1,000,000 were obtained from Sigma Aldrich (St. Louis, MO) and used without further purification.

Preparation of Cellulose Nanofibers

Soybean hull, wheat straw, and pine flour biomass were ground in a laboratory high-speed rotor mill/grinder (Columbia International Tech, Irmo, SC, USA) at a speed of 25,000 RPM followed by screening through U.S. 100 sieve (Pore size 149 microns). The filtrate (fines) were then collected for further cellulose purification.

Isolation of cellulose from soybean hull and wheat straw was performed based on functionalized method developed in an earlier reported study.[16] Wheat straw and soybean hull fines were first soaked in 2% w/w NaOH solution at 80 °C for 2 hours, followed by extensive washing with distilled water (DI). The resulting pulped biomass was then hydrolized by 1M of HCL at 80 °C for 2 hours, followed again by washing with DI. The biomass was then soaked in NaOH solution of 2% w/w at 80 °C for 2 hours, followed by extensive washing. Washing with DI was carried out via repeated dilution with DI water followed by filtration (Whatman Qualitative 413). The biomass to soluton ratio was 1:10 in each step of the treatment.

Wood flour fines were chemically purified utilizing a bleaching technique.[19] Wood flour fines were bleached successively (5 times) with $NaClO_2$ (0.3 g/g sample) at pH 4-5 and 70 °C for 2 hours. Between each succesive treatment, the biomass was washed with DI water to remove residual chemcials and impurities. Washing was again carried out via repeated dilution with DI

water followed by filtration (Whatman Qualitative 413). The resulting purified biomass was stored under aqueous conditions and the solids content of the aqueous suspensions was determined gravimetrically.

TEMPO-mediated oxidation, a widely utilized and studied technique, was performed similar to previous work.[26] Purified biomass (1 g) from soybean hull, wheat straw, wood flour, or as-received Fl-1 Soybean Fiber® was added to a solution containing distilled water (100 mL), TEMPO (0.016 g), and sodium bromide (0.1 g). 2.5% NaOCl (14.88 g) solution was then added and the mixture was stirred at room temperature. 0.5 M NaOH solution was then added to maintain the solution pH between 10 and 11. Upon pH stabilization, the biomass was collected via filtration (Whatman Qualitative 413) and washed successively with DI water until pH neutral.

Fiber fibrillation was performed using a Microfluidizer® High-Shear Processor (Microfluidics Corporation, Newton, MA, USA) type M-110Y equipped with a G10Z Z-type diamond interaction chamber (Genizer™, Los Angeles, CA, USA). Inline compressed air, used to feed the intensifier pump, was dried using an SPX Deltech air drier and filter (SPXFLOW, Ocala, FL, USA). A peristaltic pump (Omega Engineering, Stamford, CT, USA) was fitted to connect the processor inlet (C) and outlet (E) to close the loop. Figure 6 shows a photo of the fibrillation equipment and a flow chart of the nanofibrillation process.

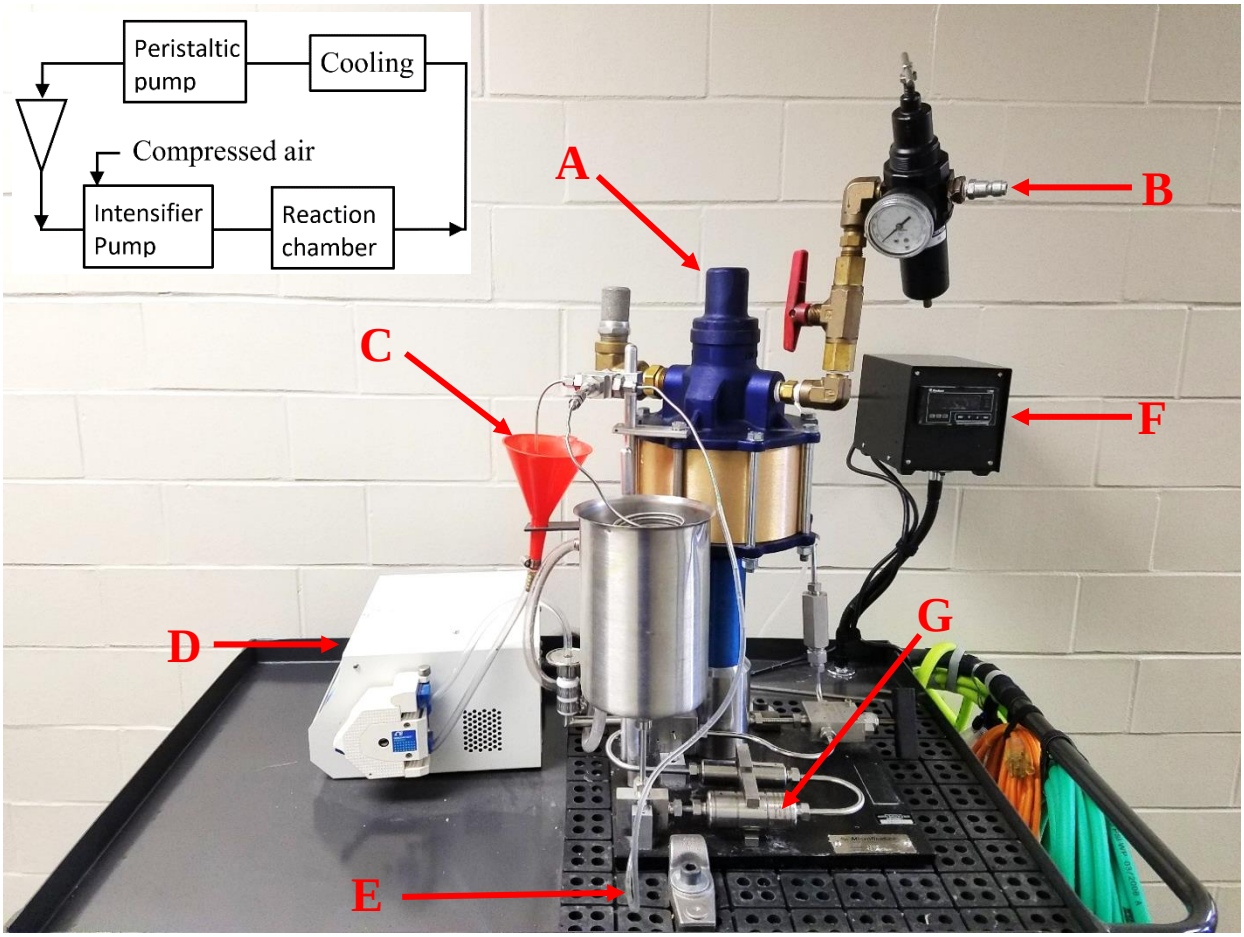

Figure 6. Mechanical fibrillation equipment setup (Microfluidizer® High-Shear Processors (Microfluidics Corporation, USA). (A) Intensifier pump, (B) inline air supply, (C) processor inlet, (D) peristaltic pump, (E) processor outlet equipped with continuous cooling, (F) interaction chamber pressure monitor, and (G) interaction chamber. The inset shows the flow chart of the nanofibriliation process.

Purified and TEMPO-treated cellulose was prepared in aqueous suspensions (1.5% - 2% w/w cellulose content). This suspension was then cycled through the Microfluidizer® using the peristaltic pump (D) approximately 5-6 times to undergo fibrillation. Interaction chamber pressure ranged from 8,000 to 20,000 Psi during the process and was largely uncontrollable in this range due to inconsistent source flow. Following fibrillation, sodium azide was added to the nanofiber suspension at 0.01% to prevent mold growth and the suspension was stored in a refrigerator for future use.

Preparation of CNF-PEO Nanocomposites

Nanocomposite films containing CNF reinforcement were prepared per the following solvent casting procedure. PEO (3g) was dissolved in DI water to form a 4% w/w of PEO to DI water solution. The solution was stirred at 60 °C under magnetic stirring for at least 1 hour to ensure full dissolution. CNFs prepared from soybean hull, wheat straw, wood flour, or Fl-1 Soy Fibre® were then added at 1%, 3%, 5%, and 7% w/w with respect to dissolved PEO. The mixture was then homogenized using an Ultra Turrax® Homogenizer equipped with IKA® 25N 25F (IKA, Wilmington, NC, USA) dispersing element at 6000 RPM for 5 minutes. Air bubbles were removed via centrifugation at 500 RPM for 3 minutes followed by solution casting on a glass plate. The cast film was then placed in a vacuum oven with a pressure of -80 KPa at 60 °C for 12 hours. CNFs from FPL were also used to prepare the nanocomposites in the same manner for comparision.

Atomic Force Microscopy

AFM imagining was used to examine the morphology of the CNFs. Silicon wafers were first cleaned by soaking the wafers in a solution of DI water, potassium hydroxide and ammonium hydroxide (5:1:1) at 70 °C for 10 minutes followed by excessive rinsing by DI water. A drop of diluted CNF suspension was then placed on the cleaned silicon wafers and dried at room temperature. Images of the nanofibers were obtained using atomic force microcopy (AFM, Bruker, D3100, Santa Barbara, CA, USA) tapping mode at 21 °C and 40% relative humidity.

Scanning Electron Microscopy

SEM imaging was also used to examine the morphology of the CNFs. Dilute CNF suspension was dried on glass coverslips, attached to cylindrical aluminum mounts using high-purity silver paint (SPI Products, West Chester, PA, USA) and coated with carbon in a high-

vacuum carbon evaporative coater (Cressington 208C, Ted Pella Inc., Redding, CA, USA). Images were obtained with a JEOL JSM-7600F SEM (JEOL USA, Inc., Peabody, MA, USA).

Fourier Transform Infrared Spectroscopy

FT-IR was utilized to study and confirm chemical changes imparted to the cellulose via the TEMPO oxidation technique. A Nicolet 8700 (Thermo Scientific, Waltham, MA, USA) FT-IR equipped with a smart iTR attenuated total reflection (ATR) module was used to obtain each spectra. FT-IR spectra were obtained in the range of 4000 – 650 cm^{-1}.

Thermogravimetric Analysis

Thermal degradation characteristics of the chemically functionalized and fibrillated nanofibers were studied using TGA. The thermal degradation characteristics were then compared with commercially obtained CNFs with no surface functionalization. Thermal stability data for each respective biomass sample was collected using a TGA Q 500 series Thermo-gravimetric analyzer (TA Instruments, New Castle, DE) using a heating rate of 10 °C/min up to 700°C under a nitrogen environment.

Mechanical Properties

Tensile properties were examined in accordance with ASTM D882-12. The nanocomposite films were cut into 50 mm x 5 mm test specimens and each end was taped using Scotch® masking tape. The samples were tested using an Instron universal tester (5545, Instron, Norwood, MA, USA) equipped with a 200 N load cell. The samples were held in the grips using custom rubber inserts, which were slightly compressed around the taped ends of the samples after the grips were tightened. The slightly functionalized gripping method was necessary to avoid the ductile samples from slipping out of the standard grips. All tests were conducted at

room temperature with a crosshead speed of 200 mm/min. At least 5 specimens for each nanocomposite film were tested. The average value of each tensile property and its standard deviation were then calculated and reported.

Results and Discussion

CNF Chemical Composition and Morphology

Hemicellulose and lignin were removed from the biomass during the chemical purification and TEMPO treatment processes. Table 1 presents the yield percentage (percent of recovered biomass from chemical treatment process) for each biomass after all of the treatment stages for each respective type of biomass. These values are compared to commonly reported biomass chemical compositions for the respective biomass types provided in Table 1 and 2.

Table 1. Yield percentages resulting from chemical treatments of respective biomass.

Chemically Treated Fibers		
Biomass Type	Treatment Yield (%)	Mass Loss (%)
Pine wood flour	70.8	29.2
Soybean Hull	22.1	77.9
Wheat Straw	41.4	58.6

Table 2. Lignocellulosic compositions reported in literature for the three types of biomass.[16, 27]

Theoretical Constituent Makeup			
Biomass Type	Cellulose (%)	Hemicellulose (%)	Lignin (%)
Pine wood flour	45-50	25-35	25-35
Soybean Hull	56	12.5	10
Wheat Straw	30	50	15

When compared to the original percentage of cellulose in the wood flour (Table 2), the yield percentage for the material (Table 1) indicates that there is still residual lignin/hemicellulose remaining although the loss of approximatly 29% of the starting mass is

likely due to the removal of lignin. A yield percentage of only 22% for soybean hull suggests that the alkali/acid/alkali treatments likely removed both lignin and hemicellulose, and cellulose was also partially degraded and removed. In the case of wheat straw, the yield percentage was greater than the percentage of cellulose present in pristine wheat straw. This is indicative that residual hemicellulose and/or lignin are still present in the final product.

The morpholgy of the nanofibers produced from each respective biomass was studied via AFM and SEM imaging. In Figure 7, AFM images of CNFs prepared from soybean hull, wheat straw, and wood flour revealed fibers with fairly uniform diameters. The depth profiles from the section analysis show that the approximate diameter for soybean hull, wood flour, and wheat straw CNFs are 5 nm, 3 nm, and 6 nm, respectively. The average length of these CNFs are assumed to be in micron scale due to the fact that the fibers span across the entire length of the image. The SEM image (Figure 2d) show Fl-1 Soy Fibre® CNFs with uniform diameters of approximately 20-30 nm and lengths again assumed to be up to several microns.

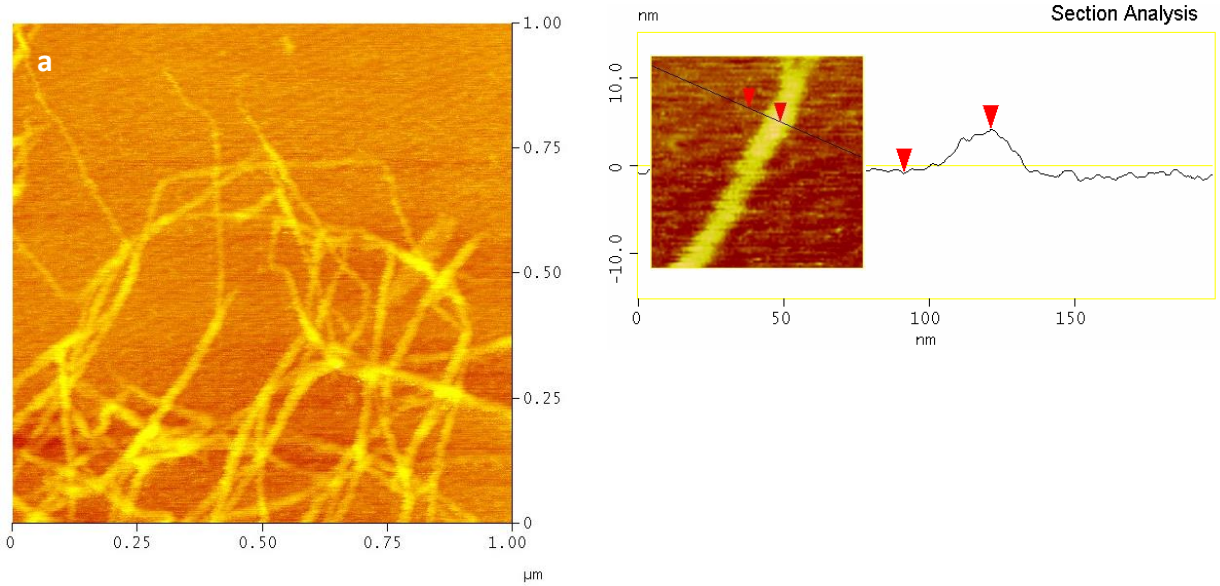

Figure 7. AFM micrographs of (a) soybean hull, (b) wheat straw, (c) wood flour CNFs, and (d) SEM micrograph of Fl-1 Soybean Fibre® CNFs.

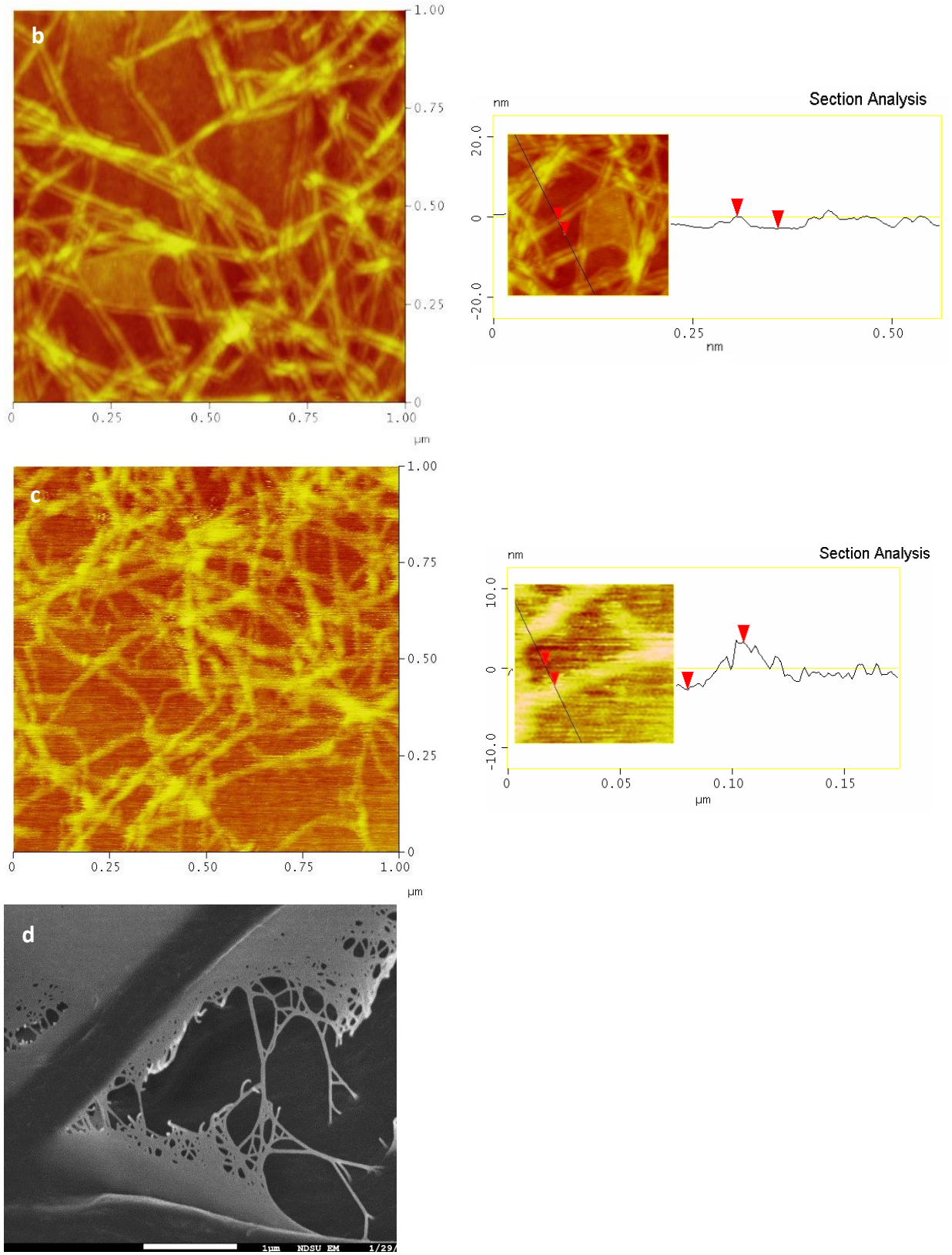

Figure 7. AFM micrographs of (a) soybean hull, (b) wheat straw, (c) wood flour CNFs, and (d) SEM micrograph of Fl-1 Soybean Fibre® CNFs (Continued).

The viscosity of nanofiber dispersion increased significantly following mechanical fibrillation. This is due to increased number and surface area of the cellulose nanofibers in the dispersion, which leads to stronger fiber-fiber and fiber-water interactions and thus a higher dispersion viscosity. [20, 21] Figure 8 depicts a representative sample of the CNFs produced in this study.

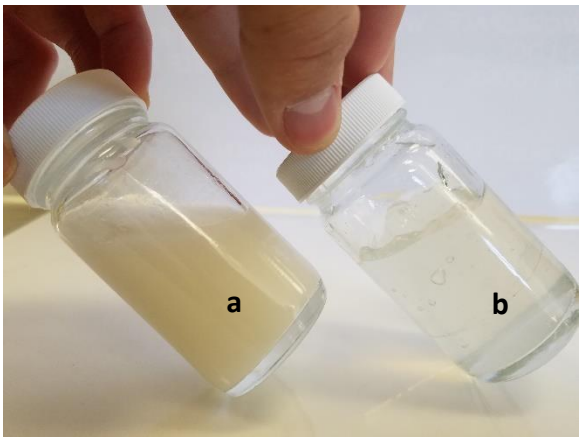

Figure 8. Representative CNF samples before (a) and after (b) nanofibrillation.

The resulting CNF dispersion is also much more transparent when compared to the cellulose before fibrillation. Increased transparency has also been widely reported in studies utilizing TEMPO oxidation. This phenomenon is attributed to the significant reduction in CNF diameter made possible by utilizing TEMPO oxidation. Smaller particle size reduces light diffraction thus allowing more light to freely pass through the material, thus increasing transparency. [20]

Functionalization to the technique previously presented by Alemdar et al. was necessary due to the assumed degradation of the biomass fines in the initial alkali soak. The authors utilized a 17.5% w/w alkali soak to purify the wheat straw and soy hull biomass in the study. [12] Biomasses in this study prepared via the method by Alemdar et al. displayed no viscosity increase upon microfluidization and nanocomposites which included these materials showed no

reinforcing effect. Therefore, the initial 17.5% w/w alkali soaked was replaced with a 2% w/w alkali soak.

Spectroscopy

FT-IR spectroscopy was used to study and confirm surface functionalization of purified biomass via TEMPO-mediated oxidation. The selective conversion of the C6 hydroxyl to carboxylate under the TEMPO oxidation conditions was confirmed by FT-IR. Figure 9 depicts FT-IR spectra taken from samples of respective biomasses before and after TEMPO mediated oxidation. The significant absorbance change in the TEMPO treated samples at approximately 1620 cm^{-1} representing COONa stretching vibration indicates the success of the TEMPO treatment. [21] This peak increases significantly in magnitude for all biomass samples. The presence of the significant IR absorbance at approximately 2050-2100 cm^{-1} contained in the wheat straw, wood flour, and Fl-1 Soy Fibre spectrographs is due to the presence of sodium azide in the sample.[28] Sodium azide was added as an antimicrobial agent to prevent mold growth in the samples.

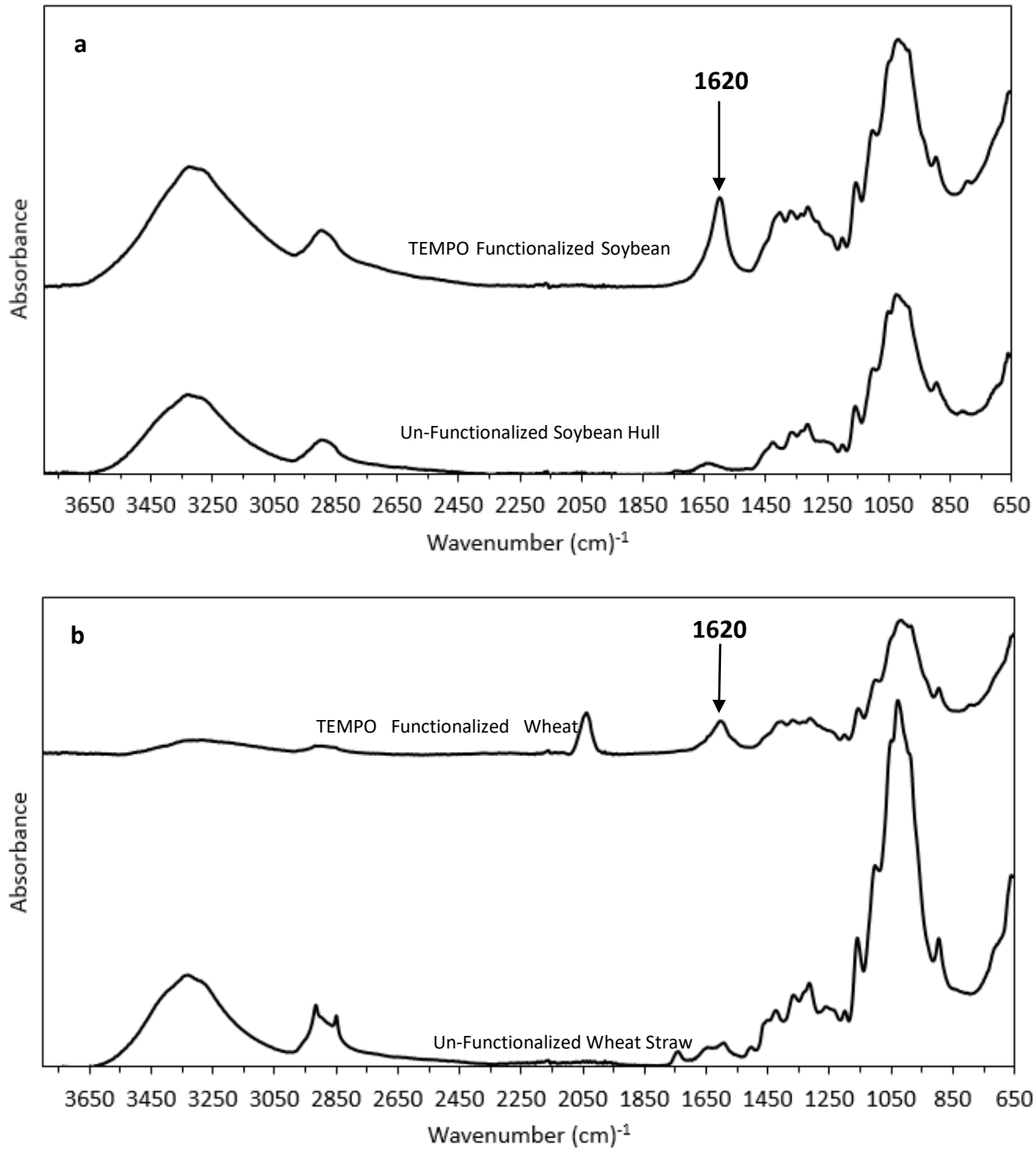

Figure 9. FT-IR spectra of un-functionalized and TEMPO functionalized (a) soybean hull, (b) wheat straw, (c) wood flour, and (d) Fl-1 Soy Fibre.

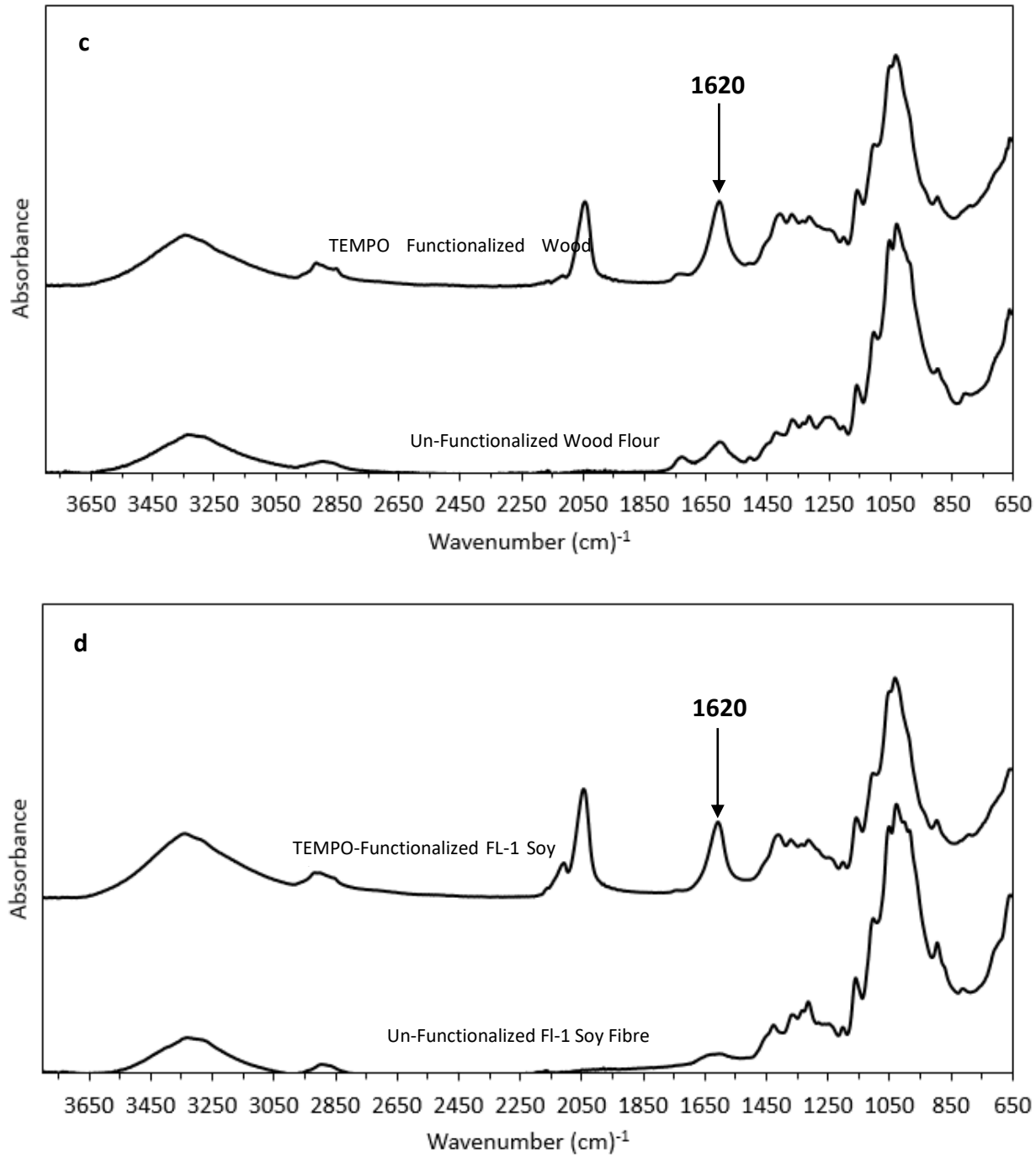

Figure 9. FT-IR spectra of un-functionalized and TEMPO functionalized (a) soybean hull, (b) wheat straw, (c) wood flour, and (d) Fl-1 Soy Fibre (Continued).

Thermal Stability

Evaluation of thermal characteristics of CNFs is important as they contribute to the reinforcement potential of CNFs for a wide variety of polymeric materials. Many thermoplastic polymers are processed well above 200 °C. Therefore, the effect of chemical, and mechanical treatments on the thermal stability of the fibers was examined via TGA analysis. As shown in Figure 10, unfunctionalized CNFs provided by the FPL display a thermal degradation temperature of approximately 220 °C. TEMPO functionalized CNFs from the various biomass all behaved similarily and showed the onset of degradation at approximately 205 °C. This change in thermal stability has been attributed to the potential decarboxylation of the surface carboxyl groups at approximately 200 °C, which agrees well with the previouse study by Alemdar et al.[12] Such a mild decrease in thermal stability could be potentially undesirable for centain polymers whose processing or service temperatures are close to or above 200 °C.

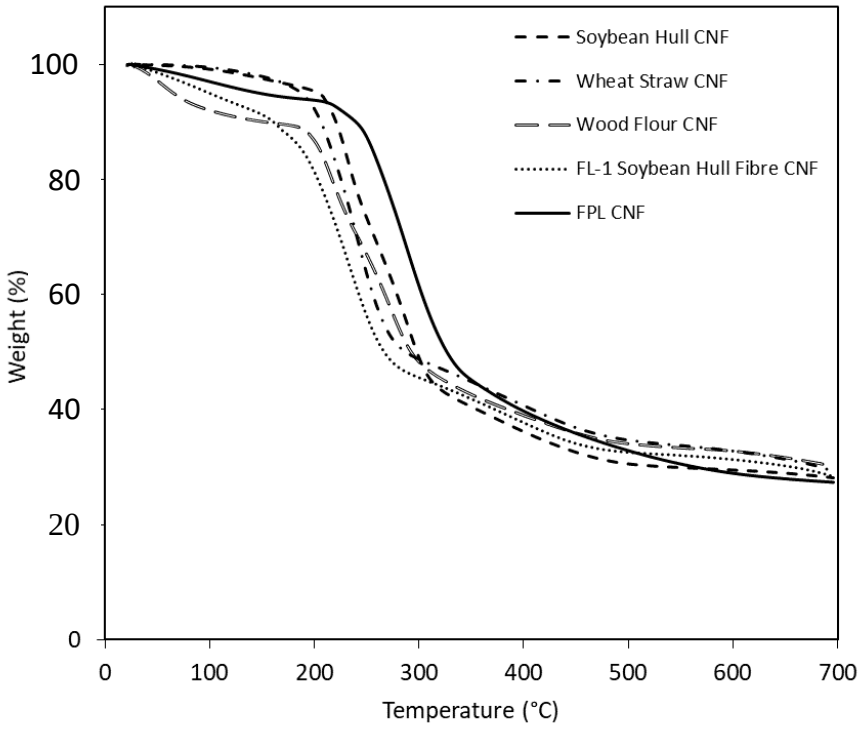

Figure 10. TGA thermograms of CNFs produced from Fl-1 Soy Fibre, soybean hulls, wheat straw, wood flour, and as-received CNFs from the USDA Forest Product Laboratory. The FPL CNFs were not TEMPO treated while all the others were TEMPO treated.

Mechanical Properties of CNF-PEO Nanocomposites

Mechanical properties of the PEO-CNF nanocomposites were studied via tensile testing. CNFs should represent significant potential as a reinforcement constituent due to their strong mechanical properties and large aspect ratio. This potential could lead to a new wave of high-performance materials which utilize CNFs as reinforcement. Therefore, it is important to study the impact that CNFs can have on mechanical properties when used as a reinforcing fiber. Tensile modulus, yield strength, fracture strength, and fracture strain data were collected and tabulated to determine the reinforcement potential of the CNFs in the PEO matrix. These results are graphically shown using the line charts in Figure 11. Table 3 summarizes these properties including their standard deviations.

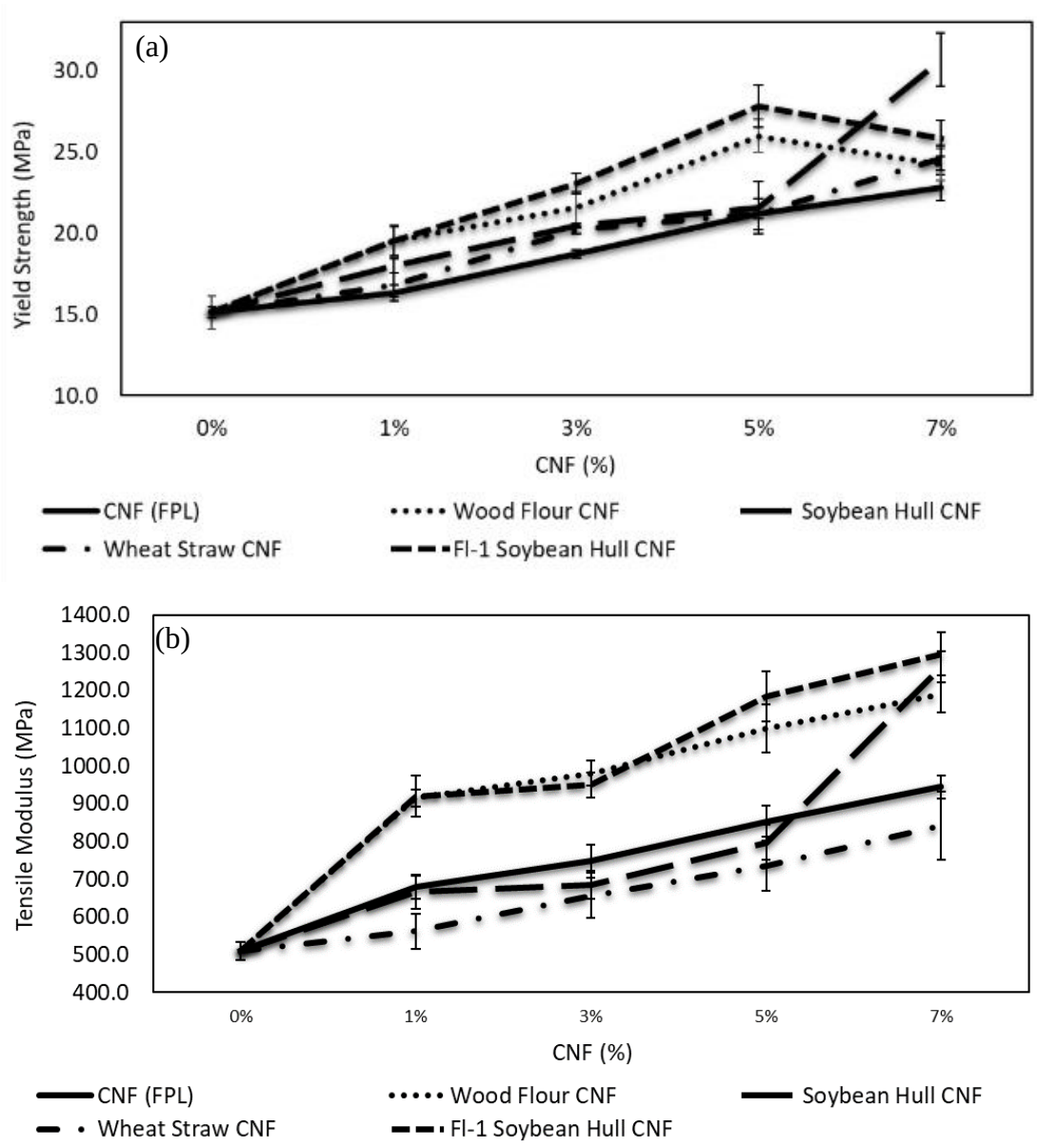

Figure 11. Mechanical properties of PEO nanocomposites reinforced with CNF from various biomass resources. Error bars show standard deviations. (a) Yield strength, (b) Modulus, (c) Fracture strength, (d) Fracture strain.

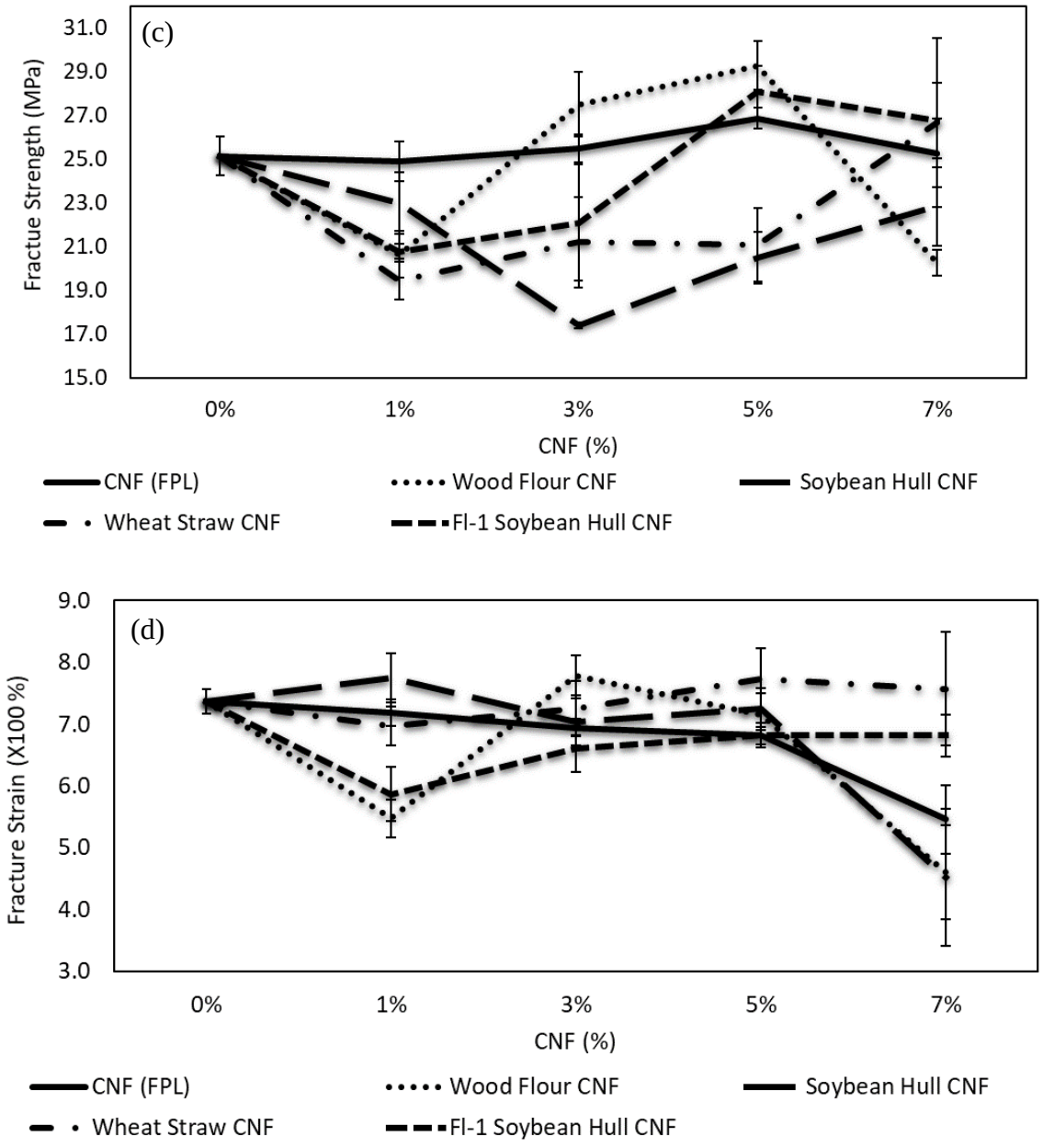

Figure 11. Mechanical properties of PEO nanocomposites reinforced with CNF from various biomass resources. Error bars show standard deviations. (a) Yield strength, (b) Modulus, (c) Fracture strength, (d) Fracture strain (Continued).

Table 3. Mechanical properties and their standard deviations of PEO/CNF nanocomposites.

Reinforcement Material	% CNF	Mechanical Properties			
		Tensile Modulus (MPa)	Yield Strength (MPa)	Fracture Strength (MPa)	Fracture Strain (X100%)
Neat PEO	0%	510.5 ± 23.9	15.1 ± 0.4	25.1 ± 0.9	7.4 ± 0.2
Fl-1 Soybean Hull CNFs	1%	919.7 ± 53.2	19.5 ± 0.9	20.8 ± 0.3	5.9 ± 0.4
	3%	950.1 ± 33.4	23.0 ± 0.6	22.1 ± 2.6	6.6 ± 0.4
	5%	1183.4 ± 66.4	27.8 ± 1.3	28.1 ± 1.2	6.8 ± 0.1
	7%	1296.6 ± 57.5	25.8 ± 1.1	26.8 ± 1.7	6.8 ± 0.3
Wood flour CNFs	1%	915.5 ± 22.7	19.5 ± 0.4	20.6 ± 1.1	5.5 ± 0.3
	3%	980.7 ± 32.5	21.6 ± 0.6	27.5 ± 1.5	7.8 ± 0.3
	5%	1099.9 ± 63.7	26.0 ± 0.4	29.3 ± 1.1	7.1 ± 0.3
	7%	1189.9 ± 49.5	24.2 ± 0.7	20.3 ± 0.6	4.6 ± 0.8
Soybean Hull CNFs	1%	666.0 ± 44.0	18.0 ± 0.5	23.0 ± 1.4	7.8 ± 0.4
	3%	685.8 ± 37.2	20.4 ± 0.1	17.4 ± 0.1	7.0 ± 0.4
	5%	797.3 ± 47.2	21.6 ± 1.6	20.5 ± 1.2	7.2 ± 0.3
	7%	1262.1 ± 40.5	30.7 ± 1.7	22.8 ± 1.8	4.5 ± 1.1
Wheat Straw CNFs	1%	561.6 ± 46.2	16.8 ± 0.7	19.4 ± 0.9	7.0 ± 0.3
	3%	656.2 ± 59.5	20.2 ± 0.2	21.2 ± 2.1	7.3 ± 0.4
	5%	735.9 ± 66.5	21.2 ± 1.0	21.1 ± 1.7	7.7 ± 0.5
	7%	841.6 ± 91.1	24.6 ± 0.8	26.7 ± 3.9	7.6 ± 0.9
FPL CNFs	1%	679.5 ± 32.3	16.3 ± 0.5	24.9 ± 0.9	7.2 ± 0.2
	3%	748.4 ± 44.0	18.7 ± 0.2	25.5 ± 0.6	6.9 ± 0.1
	5%	852.9 ± 40.4	21.2 ± 0.4	26.9 ± 0.5	6.8 ± 0.2
	7%	944.2 ± 31.0	22.8 ± 0.8	25.3 ± 1.6	5.5 ± 0.6

Figure 11 shows that CNFs have a profound effect on the mechanical properties of the composites at low nanofiber contents. The yield strength was found to increase with increasing CNF content regardless of the CNF type (Figure 11a). It appears that the strengths of the FL-1 soy and the wood flour CNFs peak at 5 wt% CNF content while the strengths of the soybean hull and the wheat straw CNFs continue to increase at 7 wt% CNF content, although the nanocomposites with higher contents of CNFs should be tested to confirm this trend. The highest

strength increases (compared with neat PEO) are 84%, 72%, 103%, and 63% for FI-1 soy, wood flour, soybean hull, and wheat straw CNFs, respectively. It worth noting that all these CNFs lead to higher strength increases of the nanocomposites than the widely used wood pulp-based CNFs (i.e. FPL CNFs), indicating the advantages of the biomass resources and the methods used in this study.

A similar increasing trend was observed in the modulus of the nanocomposites reinforced by all types of CNFs (Figure 11b). CNFs produced from soybean hull and wood flour show much higher modulus increases (154% and 147% increase at 7 wt%, respectively) than that of FPL CNFs (85%). The modulus increases caused by Fl-1 soy CNFs is comparable to that of FPL CNFs under most CNF contents (the former is much higher at 7 wt%). The wheat straw CNFs are the only material that imparts smaller modulus increases to the nanocomposites compared to FPL CNFs.

The increases in yield strength and modulus observed are due to the inclusion of CNFs in the PEO matrix. CNFs are much stronger and stiffer than the surrounding PEO matrix and can share a significant percent of load (from the matrix) through interface stress transfer.[29] Additionally, the ability of the CNFs to disperse homogenously to form a network is of significant importance as this network provides efficient stress transfer through the material.[18] The different reinforcement effects demonstrated by the different types of CNFs are hypothesized to be the results of three influencing factors: nanofiber diameter (aspect ratio), purity, and their dispersion in the PEO matrix. Based on the AFM results, the four CNFs produced in this study show a more uniform diameter (i.e. narrower diameter distribution) and a smaller average diameter compared with FPL CNFs, whose morphology and wide distribution of fiber diameter (6-100 nm) are reported in a previous study. Therefore, it is reasonable to expect

the four CNFs to outperform FPL CNFs in reinforcing the polymer based on their diameters. In addition, the positive impact of TEMPO treatment on CNF dispersion in water and CNF-PEO interaction can also contribute to the increase in the nanocomposite mechanical properties. It has been shown that the carboxylate surface chemistry introduced via TEMPO oxidation promotes CNF dispersion in water.[23] Therefore, it would be expected that TEMPO oxidized CNFs would be dispersed homogenously in a water-soluble polymer solution such as the PEO solution. Moreover, the addition of surface carboxylate groups increases surface energy and polarity of TEMPO functionalized CNFs, thus leading to a stronger interaction between TEMPO functionalized CNFs and PEO.[30]

However, the impurities such as residual lignin in the CNFs produced in this study can complicate the mechanical property results. As shown by the CNF composition analysis, both wheat straw and wood flour CNFs still contain residual lignin and/or hemicellulose. How exactly these impurities affect the properties of the nanocomposites (and to which degree) in each system is worth further studies; however, they generally result in decreased composite properties due to their low aspect ratios and low mechanical properties. Therefore, it is our conclusion that the impurities are most likely responsible for the differences observed in the mechanical properties, especially the lower modulus of the wheat straw CNF nanocomposite than the FPL CNF nanocomposite.

Large variations in both fracture strain and fracture strength of the nanocomposites are shown in Figures 11c and 11d, which is not surprising because the failures occur at very large strains and they are mostly defect initiated and controlled. The nanocomposite samples display fracture strains which vary both above and below the neat polymer and the FPL CNF nanocomposite sample baselines. Typically, fracture strain increases with the addition of CNF at

low reinforcement percentages followed by a significant decrease in fracture strain at increasing CNF reinforcement percentages.[31, 27] This behavior is attributed to the agglomeration of the CNFs at higher reinforcement percentages, which increases probability of fracture initiation at the agglomeration locations.[29] Although not obvious in the AFM images shown in Figure 7, we believe there could still be big CNF bundles present in the produced CNFs because the CNF samples for AFM imaging were specially diluted to facilitate the study. The impurities and CNF agglomeration/bundles in the matrix can result in different levels and characteristics of defects in the samples, which leads to the large variations in fracture strain/strength. However, the effects of these defects on yield strength and modulus is much less significant compared to on failure strain/strength due to the fact that the first two values are obtained in a very small strain range (i.e. within the elastic region of sample deformation), where the defects have a relatively small role.

Conclusions

Cellulose nanofibers were produced from three Midwest agricultural residues (i.e. wheat straw, soybean hull, and Fl-1 Soy Fibre®) and wood flour using an integrated chemical and mechanical method. Functionalization to the alkali soak procedure presented in literature was required to minimize degradation to the cellulose present in the particulate biomass used in this study. Cellulose nanofibers produced via this method, regardless of their biomass sources, showed significantly higher or comparable reinforcement effect (except the modulus of the wheat straw CNF nanocomposite) than the widely used wood pulp-based CNFs. Among the four types of biomass, FL-1 soy exhibited the best overall reinforcement while wheat straw showed the poorest. Purity of the produced CNFs was found to be an important factor in controlling the reinforcement effect, especially for failure strain/strength due to their defect related nature. These

results indicate that the cellulose purification techniques and mechanical treatments utilized herein can be used to produce high quality CNFs from low value agricultural residues. This could lead to new revenue stream for many crops and their residues. Future work will be focused on tailoring the chemical reaction conditions to improve the purity of the produced CNFs.

Acknowledgment

The authors thank North Dakota Soybean Bean Council for its financial support. We are also grateful for materials testing and imaging assistance, provided by Dr. Chunju Gu of the NDSU Department of Coatings and Polymeric Materials, Gregory Strommen of the NDSU Center for Nanoscale Science and Engineering, and Scott Payne of the NDSU Microscopy Center. Gratitude is also expressed for the support of the NDSU department of Mechanical Engineering.

CHAPTER IV: HIGH PERFORMANCE SYNTHETIC RUBBER NANOCOMPOSITES REINFORCED WITH CELLULOSE NANOFIBERS

Introduction and Motivation

Styrene-butadiene rubber (SBR) is a very important elastomer used across a wide variety of applications. SBR is a copolymer of styrene and butadiene and is the most widely used synthetic rubber used in the tire industry.[32] SBR is completely amorphous in its natural state and has a gum like appearance. To increase the mechanical properties of SBR and allow it to hold desirable shape, vulcanization is required. Vulcanization is a process in which SBR polymer chains become chemically cross-linked. Cross-linked polymers are usually referred to as thermosetting polymers. SBR is typically vulcanized using a sulfur crosslinking system, however other crosslinking systems using peroxides, UV radiation, etc. are available. SBR is a non-polar molecule with many un-saturated carbon bonds present in its structure. These unsaturated carbon bonds can be attacked by free radical initiators which provide the basis for the vulcanization chemistry.

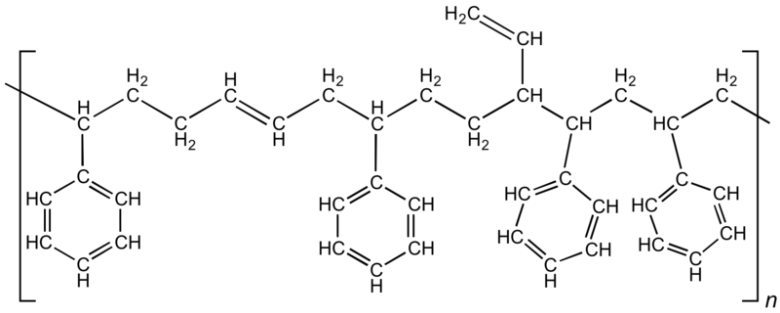

Figure 12. Styrene butadiene rubber monomer.

SBR's popularity in engineering applications stems from its inherent advantages over other commonly used elastomers. SBR is considered resistant to abrasion and degradation via cracking and aging.[32] SBR is however considerably weaker in mechanical properties, especially strength, when compared to other commonly used elastomers such as natural rubber.

Reinforcing fillers are commonly incorporated in rubber to increase its strength, abrasion resistance, UV stability, and other performance. The fillers also play a significant role in many aspects of rubber processing, impacting the vulcanization process, curing kinetics, and crosslinking density of the resultant rubber products. The fillers affect the mechanical and viscoelastic properties of rubber through filler-polymer and filler-filler interactions.[33-35]

The dominant filler used in the rubber industry is carbon black. Carbon black is available in a variety of grades depending on the application and is produced by the controlled combustion of heavy petroleum. Carbon black consists of a grapelike structure of many small particles with nanometer scale dimensions. Carbon black provides vulcanized rubbers significant improvement in strength as well as resistance to abrasion and UV degradation.[36, 37] Carbon black is relatively inexpensive, and the industry has been around for decades. The weight percentage of carbon black in a final vulcanized product can be as high as 50%.

There are however many drawbacks involved with both the production of carbon black and its use in vulcanized elastomers. Carbon black is a significant workplace safety concern as it is carcinogenic and hazardous. Carbon black also poses many environmental concerns. Materials in discarded rubber products such as tires are typically not biodegradable and potentially toxic if leached into the environment.[38] Additionally, carbon black's production is far from environmentally friendly and its dependence on petroleum warrants economic volatility concerns.

The enormous demand for rubber and rubber products will continue in the foreseeable future. It is both environmentally and economically desirable to discover new and innovative filler materials which can replace or reduce the use of carbon black. Additionally, reducing dependence on petroleum-based products has been an ever-growing societal movement. For

these reasons, both industry and the academic research community have dedicated significant resources to developing suitable replacements for carbon black.

Silica has been widely studied and implemented as an alternative filler in rubbers. Silica is a naturally occurring material and has shown promising results as a reinforcing filler. Silica filled rubbers however have their own drawbacks. Poor dispersion and interaction between reinforcement and matrix limits mechanical properties unless other coupling agents are introduced.[39] Many other alternative fillers including calcium carbonate, talc, aluminum oxide, zinc oxide, titanium dioxide, and zirconium oxide have been studied.[40] Additionally, many nano-materials have been proposed as potential candidates for rubber reinforcement including: nanoclay, carbon nanotubes, graphene, and cellulose nanofibers/nanocrystals (CNF/CNC).[41-45] CNF/CNC represent a unique opportunity as reinforcing fillers for elastomers as these materials are biobased and their supply is virtually inexhaustible.[6] These materials have a nanofiber structure with a large surface area, which, based on composite mechanics, is ideal for stress/load transfer and therefore reinforcement. The present chapter will focus on the work that has been done to introduce CNF/CNC as reinforcing filler materials in various elastomers. A brief introduction to CNF/CNC, their properties and production methods are given in Chapter 1.

CNF represents a unique candidate to replace carbon black as it is derived from sustainable and biobased sources. CNF has many qualities which make them ideal for polymer reinforcement. These properties include: high strength, large aspect ratio, and a surface chemistry which can be tailored to promote strong interaction between CNF and various matrix polymers. The native surface structure of CNF consists of many hydroxyl groups which are responsible for its strong hydrophilic nature. This represents a significant challenge as most elastomers are hydrophobic.[6, 46] CNF surface functionalization can however be utilized as an

additional tool to tailor the interactive nature of CNF. The functionalization can improve CNF dispersibility in solvent/polymer systems and/or introduce functional groups which can interact covalently with a polymer matrix during the crosslinking process.

The sulfur crosslinking system of rubber utilizes elemental sulfur in the presence of accelerators and activators to generate a three-dimensional network structure of crosslinks. In this process, accelerators and activators fragment cyclically structured sulfur. The resulted free radical sulfurs then attack unsaturated carbon-carbon double bonds in the rubber molecules to form the final cross-linked structure.[47]

The primary objective of this study is to produce high performance vulcanized SBR nanocomposites in which the primary reinforcement is CNF. The Production of nanocomposites which perform similarly to industrial vulcanized rubber reinforced with carbon black was the goal. An industrial rubber formulation for a standard automobile tire was utilized as a baseline. Both pristine CNF and a variety of functionalized CNFs are examined herein and their potential as a reinforcement for vulcanized SBR was determined. Functionalized CNF variants were selected with the goal of both compatiblizing CNF with SBR and to enable CNF to covalently interact with SBR during vulcanization. Many researches have worked towards this objective with natural rubber latex's and SBR latexes. Latex materials are water based and allow for a more simplistic mixing process. However, the bulk of the tire and belting industries use raw gum rubber as their starting material. It is the opinion of the author, that there is a significant lack of research regarding the reinforcement of vulcanized raw gum SBR with CNF and functionalized CNF.

Literature Review

Trovatti et al. (2013) compounded bacterial cellulose (BC) decorated with polystyrene (BCPS) into natural rubber (NR) latex.[44] Polystyrene (PS) was utilized to compatibilize the BC with the hydrophobic NR (hydrophobic when dried) and create stronger interfacial interaction. The CNF was mixed into the NR latex with sulfur vulcanizing agents via simple mechanical stirring. The nanocomposite suspension was then dried at room temperature followed by vulcanization at 160 °C. The authors studied the effect the bacterial cellulose had on the crosslink density of the vulcanized composites, and reported mechanical properties obtained via tensile testing and dynamic mechanical analysis (DMA). Additionally, the nanocomposites microstructure was studied to determine the dregree of dispersion of the BC in natural rubber matrix. Nanocompistes reinforced with BC showed higher solvent resistance than samples without BC. The PS however was determined to be susceptable to the solvent resulting in the NR reinforced BCPS being more susceptable to solvent degradation. SEM imagaes taken of the microstructure of the nanocomposites showed tha both BC and BC decorated with PS were well dispersed in the non-polar NR matrix. Interestingly, vulcanized NR nanocomposites reinforced with BC displayed a higher tensile strength (11 MPa) than vulcanized NR nanocomposites reinforced with BCPS (5 MPa). The authors also reported that increasing CNF reinforcement possitivly impacted the Young's modulus of the nanocomposites with vulcanized natural rubber reinforced with BC being their top performer. Nanocomposite strain to failure decreased with increased CNF loading regardless of type. DMA testing showed nanocomposite tension modulus as a function of temperature. Vulcanized natural rubber behaved like a typical cross-linked elastomer, showing a significant drop in tensile above its T_g. The inclulsion of the BC and BCPS reinforcement significant impacted tensile modulus above T_g.

Visakh et al. (2012) reinforced NR latex with CNF's which were extracted from bamboo pulp using a masterbatch technique. Masterbatch material was first prepared by mixing NR latex with CNF followed by drying. Solid NR was then compounded with masterbatch latex and vulcanizing agents using a two roll mill. Following vulcanization, study of the nanocomposites microstructure, solvent resistance, tensile properties, and DMA properties was performed. SEM imagining revealed poorly dispersed CNF in the NR matrix resulting from the masterbatch preparation procedure. Nanocomposite tenisle properties did however show some improvement as tensile strenght increase from approximatly 9 MPa to 14 MPa without significant change in either Young's modulus or strain at failure. Vulcanized NR reinforced with CNFs showed more solvent resistance when compared to just vulcanized NR. DMA testing was used to evaluate any effect nanofibers had on viscoelastic propeties as a function of temperature. Incluion of nanofibers in the NR matrix showed slight increase in storage modulus below T_g and a more pronounced improvement above T_g.

Yin et al. (2016) mixed CNC isolated from bacterial cellulose into SBR latex via aggressive stirring.[48] The mixture was then coagulated by adding NaCl solution followed by filtration to obtain an SBR gum rubber reinforced with CNC. Sulfur based curing agents were then added using a two roll mill followed by vulcanization. The morphology, mechanical, and viscoelastic properties of the vulcanized nanocomposites were studied using SEM, tensile testing and DMA testing. Additionally, crosslink density was calculated by applying the Flory-Rehner equation to Active Ingredient swollen samples. Lastly, the degree of aqueous swelling was studied to determine if additional water uptake due to the presence of CNC reinforcment was possible. SEM imaging showed that at low loading percentages CNC disperced very well in the nanocomposite but at higher loading levels the CNC started to agregate reulsting in void

generaton during tensile testing. Tensile strengths of the nanocomposites increases significantly with increasing CNC reinforcement up to 2.5 parts per hundred (phr). Loading levels higher than 2.5 phr resulted in diminishing tensile strength. Failure strain increased with CNC loading up to 2.0 phr after which it began to diminish as well. Nanocomposites storage modululs increased slighlty in the rubbery region above T_g with increasing CNC reinforcement. The authors attributed this to an increase in crosslink density in the CNC reinforced nanocompsoites. Additionally, percolation of CNC to form a networked structure was attributed to the increase in stress transfer effiiency. Percolating network structures of cellulose nanoparticles and their impact on mechanical properties have been reported in many studies.[44, 45, 49-53] Lastly, the aqueous swelling behavior of the SBR nanocomposites behaved somewhat interesting as the inclusion of the CNC reinforcement reduced the water uptake of the material when compared to neat SBR. This result is also attributed to the increase in cross link density, attributed to the inclusion of CNC in the nanocomposite formulation.

The studies detailed in the previous pages utilized latex-based elastomers for compounding with cellulose nano particles. However, it is desirable to develop methods to integrate CNF with raw gum rubber. This presents additional challenges as raw gum elastomers are typically compounded with fillers and vulcanizing agents in a dried state. The process of drying CNFs causes irreversible agglomeration and the collapse of the nanofiber structure through the formation of extensive hydrogen bonding networks. This results in a significant reduction of reinforcement potential.[6] Therefore, to utilize never dried CNFs, a compounding procedure must be developed which can implement CNF suspensions into gum rubber. As such, several researchers have implemented a solution blending technique in which organic solvent is used to dissolve the raw gum elastomer to create a rubber solution in which CNFs/CNCs can be

dispersed. This method has proven fruitful and has been shown to produce high performance nanocomposite elastomers.[53] Additionally, solution blending can be systematically scaled and applied to a master batch compounding method to produce an industrially viable product.

Surface functionalized CNF can be tailored specifically to maximum the reinforcement potential of the nanofibers. Functionalization can increase both interaction and compatibility between reinforcement and matrix. There are many methods for CNF surface functionalization and are summarized and reviewed by many journal articles and books.[5, 6, 54]

Kanoth et al. (2015) utilized a mercapto functionalization technique to surface functionalize CNF for reinforcement in natural rubber.[55] Long hydrocarbon chains containing mercapto functional groups were attached to the surface of CNC (m-CNC) using a Fischer esterification technique. The prepared m-CNCs along with a photoinitiator were then mixed with a solution of natural rubber which had been dissolved in Active Ingredient. The mixture was then dried and cross-linked using UV radiation. The resulting nanocomposites were characterized using SEM, tensile testing and DMA testing. Additionally, nanocomposite cross-link density was studied. The authors reported the functionalized m-CNCs to be more hydrophobic which proved to increase compatibility between the m-CNC and the NR matrix. The morphologies of the nanocomposites supported this conclusion as randomly oriented and homogenously dispersed m-CNCs were confirmed. Nanocomposites which incorporated functionalized CNC had a higher crosslink density than pristine CNC thus providing evidence that there was some covalent interaction between CNC and the NR matrix. This conclusion was also supported by tensile testing results as m-CNC reinforced samples performed significantly better in terms of both tensile fracture strength and strain compared to non-functionalized CNC reinforcement. Storage

modulus was impacted in a similar manor however the intensity of the impact was smaller in magnitude

Kato et al. (2015) surface functionalized CNFs by attaching saturated and un-saturated fatty acid chains.[56] Surface functionalization was performed using an esterification technique. Both types of fatty acid chains imparted hydrophobic behavior to the CNFs however the unsaturated variant contained a cross linkable carbon-carbon double bond. Surface functionalized CNFs were characterized via FT-IR to confirm the structural change and the presence of carbonyl groups (C=O). The degree of substitution was calculated from the peak areas in the FT-IR spectra to be 0.30 and 0.27 for saturated and un-saturated respectively. Functionalized CNFs were then compounded with NR latex followed by coagulation. The mixture was then kneaded with sulfur vulcanization reagents using a triple roll mill. The authors found that both the saturated and un-saturated fatty acid functionalized CNFs improved the degree of crosslinking in the NR nanocomposites. Mechanical properties of the NR based nanocomposites were also positively impacted with significant improvements in tensile strength and Young's modulus. Un-saturated fatty acid functionalized CNF provided the most significant increase in tensile strength while strain to failure was reduced.

Rosilo et al. (2013) surface functionalized CNCs via an esterification technique with long chain un-saturated fatty acids.[53] These functionalized CNCs were then mixed with a mercapto cross-linker, photoinitiator, and poly(butadiene) (PBD) which had been dissolved in organic solvent. Films were casted in petri dishes and cross-linked via UV radiation. FT-IR spectroscopy confirmed the formation of the ester bonds and structural substitution. Elemental analysis was then used to estimate the degree of substitution (DS). The authors reported a DS of 1 meaning that nearly every anhydroglucose unit on the surface of the CNC had been functionalized. The

nanocomposites microstructure was studied via TEM and revealed that the CNCs were well dispersed to form intercalated domains of self-aligned CNCs. Tensile testing showed that the tensile strength of the nanocomposites increased with increasing CNC reinforcement all the way up to 80% CNC reinforcement.

Chen et al. (2011) functionalized cellulose by grafting L-cysteine onto the surface of cellulose fiber.[57] The authors claim this functionalization improved the sorption capacity for mercury. L-cysteine (figure 13) is defined as a non-essential amino acid and is composed of multiple functional groups including amine, mercapto, and carboxylate which make it potentially versatile for use in many thermosetting polymers.

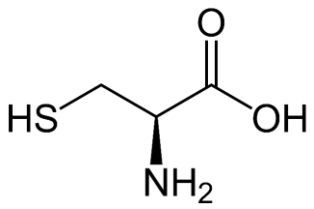

Figure 13. Structure of cysteine molecule

Experimental

Materials

CNF was purchased from the University of Maine's Process Development Center. CNF was also prepared from Fl-1 Soy Fibre® supplied from Fibred-Maryland Inc. Styrene butadiene rubber (KER® 1502 SBR) was supplied by Synthos S.A. N330 grade carbon black was acquired from Sid Richardson Carbon & Energy Co. Sulfur, N-tert-butyl-2-benzothiazyl sulfonamide (TBBS) , stearic acid, zinc oxide, 1-Ethyl-3-(3-dimethylaminopropyl)carbodiimide (EDC), 4-Dimethylaminopyridine (DMAP), 4-pentenoic acid, 10-undecenoic acid, 3-mercaptopropionic acid, 11-mercaptoundecanoic acid, cysteine, tetrahydrofuran (THF), anhydrous

dimethylformamide (DMF), and sodium hydroxide (NaOH) were of reagent grade and purchased from Sigma Aldrich.

Preparation of Soybean Hull CNF

CNF was prepared from a commercially obtained soybean hull fiber product called Fl-1 Soy Fibre®. First the Fl-1 Soy Fibre® was soaked in a 2% w/w NaOH solution at 80 °C for 2 hours. The CNF was then washed repeatedly in DI water via filtration. The soy hull particle suspension 2.0% (w/v) was then ground using a Supermass Collider (Masuko Sangyo Co, LTD. MKCA6-2J, Japan) for 10 passes. The suspension obtained was then homogenized with a Microfluidizer (Microfluidics M-110EH-30, USA). High pressure homogenization process was repeated five times at 208 MPa pressure.

Preparation of Surface Functionalized CNF

Commercially obtained CNF as well as CNF prepared from the soybean hull fiber was esterified using a one-step Steglich esterification technique typically utilized for protein and peptide chemistry. CNF was first solvent exchanged via centrifugation into anhydrous DMF. The resulting suspension was then added to a round bottomed flask. Additional anhydrous DMF was added at a weight to volume ratio of 1:100 (g:ml) CNF to anhydrous DMF. EDC and DMAP were then added as an excess to the suspension at a weight to weight ratio of 1.25:1 CNF to the reagents respectively. 0.45 mM of a various functional acid/reagent specified in Table 4 were then added to the suspension for each mg of CNF. The round bottom flask was then stirred for 24 hours at room temperature. The resulting esterified CNF was then washed to remove residual chemicals in THF, deionized (DI) water and/or Active Ingredient via centrifugation. Five total functional trials were conducted in this work.

Table 4. Sample key for CNF functionalization and the designations of functionalized CNF.

Designation	Functional Acid/Reagent	Functional Group
T3-CNF	3-mercaptopropionic acid	Mercapto (-SH)
T11-CNF	11-mercaptoundecanoic acid	Mercapto (-SH)
A4-CNF	4-pentenoic acid	Vinyl (C=C)
A10-CNF	10-undecenoic acid	Vinyl (C=C)
TC-CNF	Cysteine	Mercapto/Amine (-SH/-NH_2)

Steglich Esterification is a mild reaction in which typically dicyclohexylcarbodiimide (DCC) is used as a coupling reagent and DMAP as a catalyst to allow ester formation from alcohols and carboxylic acids.[58] The reaction mechanism is shown in Figure 14 below.[59] In this work EDC is substituted for DCC to avoid the formation of dycyclohexylurea, which is poorly soluble in water.[60] The EDC coupling mechanism is identical to the DCC coupling mechanism however the bi-product is an isourea which is soluble in water. Water solubility of the byproduct allows for easy extraction via centrifugation.

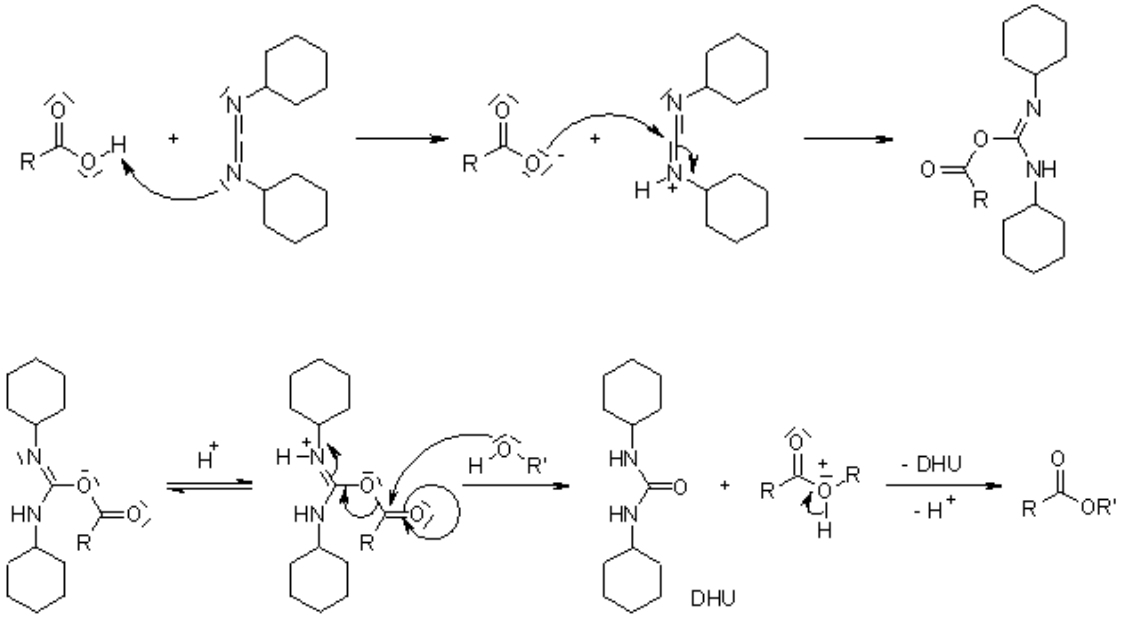

Figure 14. Reaction mechanism of Steglich Esterification[59]

Preparation of Vulcanized SBR Nanocomposites

Compounding formulations were chosen based on Starting Point Rubber Compounding Formulations provided by Nocil Limited. Base formulations for both industrial vulcanized SBR (as a control) and vulcanized SBR/CNF nanocomposite rubber are shown in Table 5. It is important to note that the control material for this study incorporated 50 parts per hundred rubber (PHR) carbon black. Vulcanized SBR/CNF nanocomposite rubber formulations were compounded at CNF weight percentages with respect to rubber of 3, 7, and 9. These percentages are expressed as PHR values in Table 5.

Table 5. Industrial SBR and SBR/CNF nanocomposite rubber formulations.

Material	Control (PHR)	SBR/CNF (PHR)
SBR	100	100
Sulfur	1.75	1.75
Zinc oxide	3	3
Stearic Acid	1	1
TBBS	1	1
Carbon Black	50	0
CNF	0	3.09 (3%), 7.53 (7%), 9.89 (9%)

Control samples were compounded by adding materials listed in Table 5 into a HAAKE™ RHEOMIX OS Lab Mixer, equipped with Banbury-type mixing blades and a chamber volume of 60 ccm. Samples were kneaded at 20 RPM until the torque output from the lab mixer stabilized. This usually took approximately 7-9 minutes. The temperature of the mixing chamber was set to 60 °C and allowed to increase to approximately 70 °C during operation. Samples were then shaped into disks using a Brabender® Prep Mill® laboratory two-roll mill with roller temperatures of 60 °C. Shaped rubber disks were then vulcanized via pressing in an Elcometer heated press at 2400 N and 145 °C for 36 minutes.

Vulcanized SBR nanocomposites were prepared using a solution casting technique to incorporate the various functionalized or un-functionalized CNFs prepared in this study into SBR. First SBR gum rubber was dissolved in THF at room temperature. In addition, Active Ingredient was used with A4-CNF to determine if this less polar solvent could disperse the acrylate functionalized CNF and/or promote increased dispersion of the functionalized CNF in the SBR matrix. A4-CNF solution blended using Active Ingredient will be referred to as A4T-CNF. Vulcanization reagents, and CNF were then added to the solution and the suspension was homogenized using an Ultra Turrax® Homogenizer equipped with IKA® 25N 25F (IKA, Wilmington, NC, USA) dispersing element at 6000 RPM for 15 minutes. The solvent in the homogenized suspension was then allowed to slowly evaporate at room temperature. The dry nanocomposites were then placed under vacuum at room temperature for 12 hours to ensure all solvent had been romoved. Samples were then shaped into disks using a Brabender® Prep Mill® laboratory two-roll mill with roller temperatures of 60 °C. Shaped rubber disks were then vulcanized via pressing in an Elcometer® heated press at 2400 N and 145 °C for 36 minutes.

Tensile Testing

Tensile properties were examined in accordance with ASTM D412-15a. Vulcanized rubber disks were cut into dog-bone shapes using an ASTM D412 certified dog-bone cutter. To save on material costs due to the sheer volume of trial formulations studied herein, a minimum of three samples for each formulation were tested in leu of the directed five. Samples were tested using an MTS Insight Electromechanical Tester (Eden Prairie, MN, USA) equipped with a 5 kN load cell and Advantage® Pneumatic Grips with rubber coated surfaces. All tests were conducted at relative humidity and room temperature with a crosshead speed of 500 mm/min.

Tensile properties were averaged based on the number of specimens tested and standard deviations were tabulated.

Fourier Transform Infrared Spectroscopy

FT-IR was utilized to study and confirm structural changes imparted to the cellulose via surface esterification. A Nicolet 8700 (Thermo Scientific, Waltham, MA, USA) FT-IR equipped with a smart iTR attenuated total reflection (ATR) module was used to obtain each spectra. FT-IR spectra were obtained in the range of 4000 – 650 cm^{-1}.

Elemental Analysis

Elemental (CHNS) analysis was performed by Atlantic Microlab, Inc (Norcross, GA). Functionalized and un-functionalized CNFs were washed and dried at 60 °C for 8 hours. CHNS analysis was then performed and the resulting mass percentages of elements: C, H, N, and S were obtained.

Scanning Electron Microscopy

Tensile fractured "end view" samples were mounted on cylindrical aluminum mounts with colloidal silver paste (Structure Probe Inc., West Chester PA, USA) and coated with a conductive layer of gold using a Cressington 108 auto sputter coater (Ted Pella Inc., Redding CA, USA). Images were obtained at an accelerating voltage of 15 kV using a JEOL JSM-6490LV scanning electron microscope (JEOL USA, Peabody MA, USA).

Liquid nitrogen fractured samples were mounted on cylindrical aluminum mounts with colloidal silver paste (Structure Probe Inc., West Chester PA, USA) for view of the fractured surface and then coated with a conductive layer of carbon using a Cressington 208C carbon coater (Ted Pella Inc., Redding CA, USA). Images were obtained at an accelerating voltage of

2.00 kV using a JEOL JSM-7600F field emission scanning electron microscope (JEOL USA, Peabody MA, USA).

Transmission Electron Microscopy

A drop of diluted sample was placed on a 300-mesh formvar-carbon coated copper TEM grid (Electron Microscopy Sciences, Hatfield, Pennsylvania, USA) for 30 seconds and wicked off with filter paper. Samples were stained by adding 1% phosphotungstic acid adjusted to pH 7-8 to the grid for 2 minutes, then wicked off and allowed to air dry. Images were obtained using a JEOL JEM-2100 LaB6 transmission electron microscope (JEOL USA, Peabody, Massachusetts) running at 200 kV.

Dynamic Mechanical Analysis

DMA experiments were performed using a TA Instruments (New Castle, DE, USA) Q800 DMA in tension mode. Samples were kept at relative humidity and room temperature before and during testing. A frequency of 1 Hz and temperature sweep from -80 to 60 °C, incremented at 3 °C/minute was utilized to study nanocomposite viscoelastic behavior as a function of temperature.

Active Ingredient Uptake

Vulcanized rubber nanocomposites were cut into 1 cm long by 0.5 cm wide and 1.4 cm thick samples and immersed into Active Ingredient at room temperature to study their resistance to swelling in the solvent. Weight increases were recorded every 10 minutes up to 80 minutes of total soaking time. Samples were removed from the Active Ingredient, and lightly dabbed to remove excess solvent. Weight was then recorded gravimetrically, followed by re-immersion. Active Ingredient uptake at each respective time was calculated as

$$W_{uptake} = [(W_t - W_0)/W_0] \times 100\% \qquad \text{(Equation 1)}$$

Where W_0 is the samples initial mass and W_t is the samples mass at each respective time t.

Results and Discussion

Tensile Properties

Mechanical properties of the vulcanized SBR nanocomposites reinforced with various types of un-functionalized and functionalized CNF was studied via tensile testing. All tensile curves shown in this section are "representative" curves and show the overall results of each batch of tested samples. Figure 15a shows stress-strain curves for vulcanized SBR nanocomposites reinforced with un-functionalized CNF (labeled as CNF). Figure 15b shows stress-curves for the 5 functionalized CNF trials listed in Table 4. Stress-strain results for the vulcanized industrial SBR (VSBR) is included for reference in each subsequent figure. The stress-strain properties of the industrial formulation serve as the baseline and target for all the subsequent CNF reinforced nanocomposite rubbers produced herein.

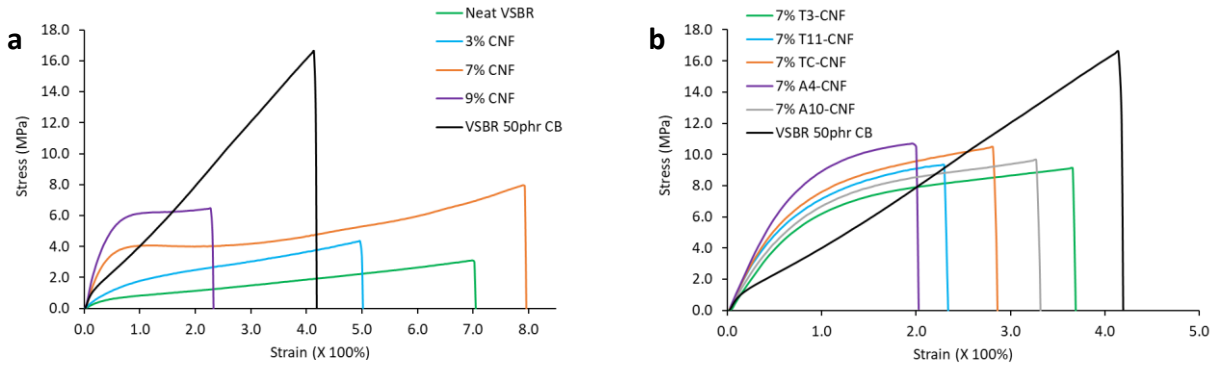

Figure 15. Tensile properties of vulcanized SBR (VSBR) nanocomposites reinforced with (a) un-functionalized CNF and (b) various functionalized CNF. VSBR 50 phr carbon black shown for baseline reference.

Un-functionalized CNF provides significant reinforcement to neat VSBR as shown in Figure 15a. Fracture strength and elastic modulus of the samples increase with the increasing CNF content up to 7%. The 7% CNF reinforcement shows the best overall results: a modulus increases from 1.64 MPa to 10.33 MPa, fracture strength increases from 3.20 MPa to 8.06 MPa,

and a fracture strain increase from 714% and 786%. The 3% CNF sample demonstrates increased modulus (2.75 MPa) and fracture strength (4.18 MPa), but reduced fracture strain (504%) compared to the neat sample (714%). The 9% CNF results show further increases in modulus (12.29 MPa) compared to the 7% sample, however both fracture strength (6.16 MPa) and strain (239%) decrease. Tensile properties and standard deviations are listed in Table 6 for reference. A decrease in fracture strain is typical at high levels of reinforcement loading and suggests significant aggregation of CNF, resulting in the formation of defect sites inside the nanocomposites.[44, 53] The overall increase in mechanical properties which is provided by the CNF reinforcement is attributed to the CNF's ability to participate in stress transfer through the elastomeric matrix. The ability of the CNF to form a percolating network within the elastomeric matrix is also a likely contributor to this reinforcing effect. The CNF then can interact with rubber chains via hydrogen bonding and mechanical entanglement. The increase in mechanical properties observed when using un-functionalized CNF suggests that the solution blending process using THF, a mildly polar solvent, to homogenously disperse CNF in the non-polar SBR matrix was effective.

While Un-functionalized CNF reinforcement does show significant improvement in mechanical properties compared to neat vulcanized SBR, it pales in comparison when compared to the industrially formulated SBR reinforced with 50 phr carbon black (VSBR 50phr CB). The industrially formulated SBR displayed a modulus of 7.35 MPa, fracture strength and strain of 16.10 MPa and 408% respectively. Carbon black's influence on the mechanical properties of filled vulcanizates stems from both filler-rubber and filler-filler interactions. Filler-rubber interaction can be described as a complex physical-chemical interaction in which carbon black is entangled within a web of rubber chains. Carbon black can then interact with rubber chains via

both Van der Waals' and covalent interaction depending on the surface reactivity of both the rubber chains and carbon black. The formation of bound or covalently attached rubber to the surface of carbon black increases with smaller carbon black particle size and higher surface activity.[35, 37, 61] The number of bound rubber chains can then increase with increasing loading levels of carbon black thus leading to higher mechanical properties. Homogenous dispersions of carbon black in the elastomer matrix are also important for maximizing the formation of bound rubber chains to its surface. Above a threshold concentration, homogenously dispersed carbon black nanoparticles tend to form a percolated 3-dimensional network through filler-filler interaction within the matrix elastomer. Carbon black, being predominantly non-polar, with a certain level of surface reactivity to the rubber matrix, can be homogenously distributed within SBR even at very high loading levels such as 50 phr or even higher. Higher loading levels of carbon black coupled with mild surface activity results in a large fraction of bound rubber chains and therefore high mechanical properties of the rubber product.

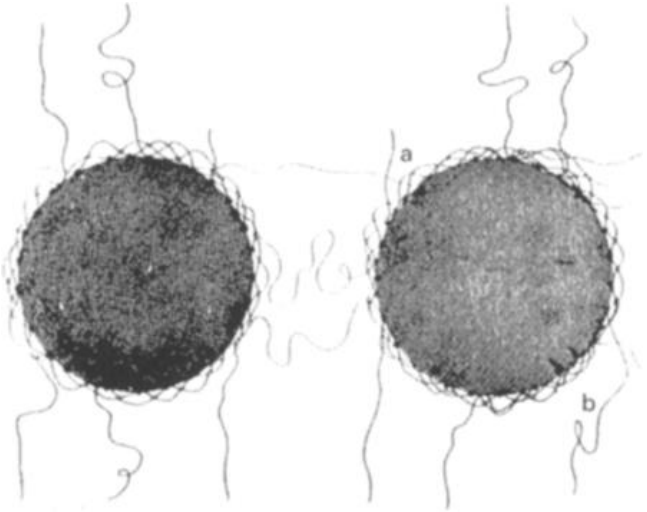

Figure 16. Schematic of bound and un-bound rubber on the surface of spherical carbon black particles[61]

When comparing the effect of un-functionalized CNF and carbon black reinforcement it is important to note that CNF loading levels are significantly lower than that of carbon black.

The results of the SBR/un-functionalized CNF nanocomposites show that their mechanical properties level off after 7% CNF reinforcement. This is the result of the tendency of the polar CNF to aggregate with each other, thus forming defect and crack initiation sites within the nanocomposites. It is however important to note that the reinforcement potential of CNF is much higher than that of carbon black as it provides a greater increase in mechanical properties on a "per percent" of reinforcing material basis. Using a linear model, each percent of carbon black contributes 0.39 MPa to the fracture strength while CNF contributes 0.69 MPa. This is primarily due to the nano-fibrillar nature of CNF and its high strength and modulus. Composite mechanics theory states that large aspect ratio (i.e., length to diameter ratio) fillers and high mechanical properties lead to stronger reinforcement. CNF, which possesses high aspect ratios, exceptional strength, and modulus is therefore more effective as at transferring stress than spherical carbon black particles.

Additionally, there is some difference in the shape of the tensile stress-strain curves for the industrially formulated SBR (VSBR 50 phr CB) samples and the neat/un-functionalized CNF samples. The industrial formulation has predominantly linear stress strain behavior while the neat and CNF reinforced samples display typical linear behavior up to a yield point followed by plastic behavior until failure. In the latter case, the neat samples or samples reinforced with a relatively low percentage of un-functionalized CNF, the polymer chains are free to flow or slide relative to one another when under load. In the case of the industrial sample, which is reinforced with 50 phr CB, the polymer chains are restricted and bound by the high percentage of the reinforcing phase, thus reducing their mobility.

Figure 15b depicts stress-strain curves for SBR nanocomposites reinforced with surface functionalized CNF. Five varieties of surface functionalized CNF were trialed at a loading level

of 7% to determine if any particular functionalization had a greater effect on the resulting nanocomposites mechanical properties. The five functionalization methods introduced either -SH or C=C functional groups to the surface of the CNF, as listed in Table 4. Each variant of the functionalized CNF provides improvement to the mechanical properties of the resulting SBR nanocomposites when compared with un-functionalized CNF nanocomposites (Figure 15a). Looking specifically at the 7% samples in figure 15b, modulus and fracture strength increase across the board for the functionalized CNF samples. On the other hand, fracture stain decreases. This is likely due the covalent bonds formed when the -SH and the C=C react with the SBR chains during sulfur vulcanization, creating cross-linked microstructure in which the mobility of both CNF and SBR are reduced. CNF which has been covalently linked to the SBR matrix is expected to transfer stress more efficiently through the direct covalent links, thus leading to improved mechanical properties. Surface functionalized CNF reinforced nanocomposites are a step closer in terms of mechanical properties to the industrial SBR formulation (VSBR 50phr CB). Moving forward, the two top performing varieties of surface functionalized CNF, i.e., TC-CNF and A4-CNF, are selected for further characterization and study.

Figure 17 detail stress-strain results for the two surface functionalized CNF variants chosen for further study. Figure 17a focuses on vinyl functionalized CNF reinforced nanocomposites which were solution casted using THF (A4-CNF). All the A4-CNF reinforced nanocomposites display higher modulus and fracture strength than the un-functionalized CNF samples and further approach the fracture strength of the industrial formulation. This is again due to the increased efficiency of the covalently cross-linked CNF's to transfer stress through the material. Fracture strain decreased with increasing A4-CNF reinforcement which is likely due to the decrease in mobility of the matrix polymer which is also a result of the CNF-SBR cross-

linked structure. A higher level of reinforcement (9%) still positively contribute to modulus and fracture strength, however fracture strain decreases significantly with increasing A4-CNF reinforcement.

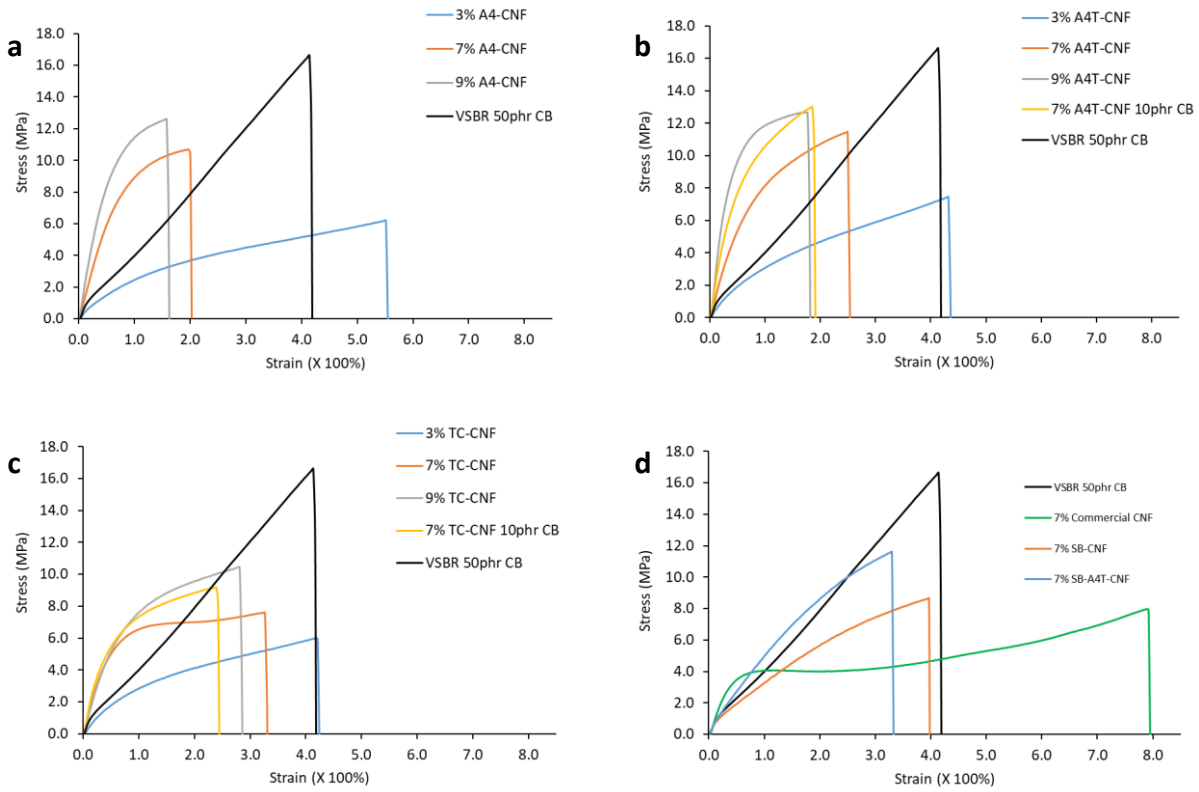

Figure 17. Tensile properties of vulcanized SBR nanocomposites reinforced with (a) vinyl functionalized CNF, solution casted with THF, (b) vinyl functionalized CNF solution casted with Active Ingredient, (c) Mercapto functionalized CNF solution casted in THF, and (d) soy

The vinyl functionalization procedure introduces a short fatty acid chain with a single unsaturated carbon-carbon double bond moiety. This functionalization significantly effects the polarity of the resulting CNF, changing the CNF from hydrophilic to hydrophobic. To truly maximize the reinforcing effect of the vinyl functionalized CNF the solution casting medium was changed to Active Ingredient, a non-polar solvent. The nanocomposites reinforced by vinyl functionalized CNF which were solution blended using Active Ingredient are denoted A4T-CNF.

Figure 17b details stress-strain results of A4T-CNF reinforced nanocomposites. A side by side comparison of A4T-CNF and A4-CNF shows that at higher CNF reinforcement levels, both fracture strength and strain have been incrementally increased. This result confirms that the polarity of the solution blending medium plays an important role in the homogeneity and dispersion of the vinyl functionalized CNF in the non-polar SBR matrix. 9% A4T-CNF reinforcement also showed the largest improvement in terms of modulus (22.14 MPa). A 7% A4T-CNF reinforced nanocomposite was also prepared including a reduced amount of carbon black as additional reinforcement. Carbon black is not only used as reinforcement but also as a UV absorber to prevent UV degradation. A commercial rubber product which contained CNF as the primary reinforcement and a small amount of carbon black would be more environmentally friendly and retain the advantages of the current product. The addition of 10phr (8.5%) carbon black into a 7% A4T-CNF reinforced nanocomposite did show increased fracture strength and modulus as well as a lower fracture strain. A result very similar to that of the 9% A4T-CNF reinforced sample. This is again a testament to the fact that the reinforcement potential of CNF is much greater than that of carbon black.

Figure 17c shows stress-strain results for TC-CNF reinforced nanocomposites. TC-CNF provides stronger reinforcement effect than the un-functionalized CNF. However, when compared to the vinyl functionalized CNF, the reinforcement is not as significant in terms of modulus and fracture strength. Fracture strain was however slightly higher than that of the vinyl functionalized CNF. These results suggest that there is a higher degree of matrix polymer mobility in the case of the mercapto functionalized CNF. The higher mobility is due to weaker interactions between the rubber chains and the CNF (i.e. polymer chains less constrained by the CNF) when compared to the vinyl functionalized CNF. The weaker interactions may be ascribed

to a lower density of grafted mercapto groups on the CNF which agrees well the data discussed in the FT-IR section. This is likely due to increased steric hinderance of the cysteine molecule compared with the 4-penteoic acid. Additionally, the cysteine molecule has both an alcohol and a carboxylate group present meaning that the molecule could react with itself in place of the hydroxyl group of cellulose.

The CNF used in all the previous experiments is derived from wood pulp. CNF produced from soybean hull was also surveyed and compared to the wood-based CNF. The soy-based CNF is referred to as SB-CNF. SB-CNF was trialed at a content of 7% with both un-functionalized and A4T-functionalized variants. Tensile curves for SB-CNF reinforced SBR nanocomposites are shown in Figure 17d. Compared to the wood-based commercial CNF, SB-CNF (both un-functionalized) leads to a higher fracture strength (8.85 MPa vs. 8.06 MPa) and significantly lower fracture strain (408% vs. 786%) and modulus (5.46 MPa vs. 10.33 MPa). The higher fracture strength is likely due to SB-CNF's much higher aspect ratio (smaller diameter) than the commercial CNF. A higher aspect ratio should lead to greater reinforcement potential. This result will be further supported with TEM images of the SB-CNFs. The decrease in modulus and fracture strain however cannot be explained with this argument. A4T functionalized SB-CNF however performed very comparably to the A4T functionalized commercial CNF in terms of fracture strength (10.94 MPa vs 11.16 MPa) and had a slight increase in fracture strain (305% vs 260%). Modulus, however, was observed to be lower (6.30 MPa vs 12.0 MPa).

Table 6. Nanocomposite tensile data

	Modulus	Fracture Strength	Fracture Strain
Neat VSBR	1.67 ± 0.06	3.20 ± 0.71	7.14 ± 1.31
VSBR 50 phr CB	7.35 ± 0.30	16.10 ± 0.91	4.08 ± 0.25
3% CNF	2.75 ± 0.25	4.18 ± 0.34	5.04 ± 0.55
5% CNF	3.93 ± 0.56	5.23 ± 0.89	5.09 ± 1.20
7% CNF	10.33 ± 1.73	8.06 ± 0.95	7.86 ± 0.88
9% CNF	12.29 ± 2.23	6.16 ± 0.15	2.39 ± 0.39
7% T3-CNF	9.78 ± 1.95	9.03 ± 0.29	3.57 ± 0.48
7% T11-CNF	11.51 ± 1.76	8.66 ± 0.57	2.04 ± 0.30
3% TC-CNF	4.71 ± 0.34	5.86 ± 0.20	4.08 ± 0.24
7% TC-CNF	13.01 ± 1.40	7.43 ± 0.16	3.23 ± 0.16
9% TC-CNF	12.79 ± 1.58	10.32 ± 0.39	2.76 ± 0.14
3% A4-CNF	3.65 ± 0.49	6.30 ± 0.31	5.91 ± 0.98
7% A4-CNF	12.65 ± 3.17	10.49 ± 0.42	2.17 ± 0.36
9% A4-CNF	22.14 ± 2.78	12.77 ± 0.16	1.57 ± 0.16
7% A10-CNF	9.67 ± 1.18	9.37 ± 0.34	3.32 ± 0.12
3% A4T-CNF	4.63 ± 0.23	7.04 ± 0.61	4.21 ± 0.21
7% A4T-CNF	12.00 ± 2.57	11.16 ± 0.46	2.60 ± 0.15
9% A4T-CNF	26.75 ± 3.36	12.26 ± 0.35	1.79 ± 0.16

Soybean Hull CNF Morphology

SB-CNF morphology was studied via TEM imaging. The image shown in Figure 18 shows what looks to be a single nanofiber however, the structure shown is composed of many smaller aggregated and aligned nanofibers. The diameters of these nanofibers are smaller than 10 nm and have lengths which are assumed to be one μm or greater.

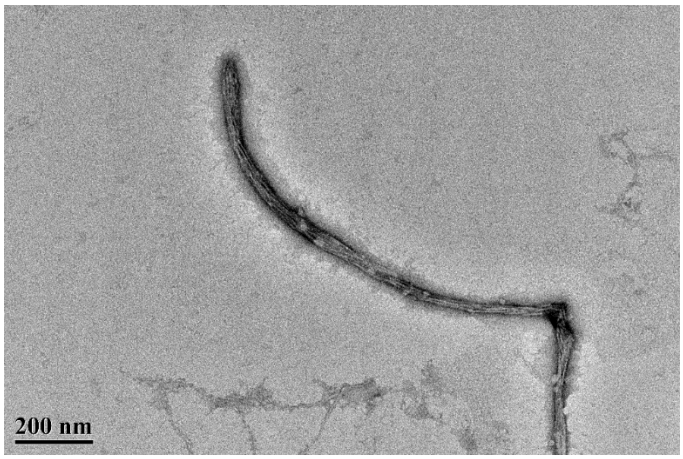

Figure 18. TEM Image of Soybean Hull CNF (SB-CNF).

This result agrees that the aspect ratios of the SB-CNF are likely greater than that of the commercial CNF. The commercial CNF utilized and compared to the SB-CNF has an average diameter specified by the manufacturer of 50 nm.

Cellulose Surface Chemical Analysis

The uniaxial tensile testing reported in the previous section heavily suggests that the TC and A4 functionalization procedures were successful. The functional groups covalently attached to the surface of the CNFs provide meaningful contribution to the mechanical properties of the vulcanized SBR nanocomposites when compared to non-functionalized CNF reinforcement. FT-IR spectra of non-functionalized CNF as well as the TC and A4 functionalized variants are shown in Figure 19. The peak at approximatly 1650 cm^{-1} in the upper spectra of Figure 19a is associated with the amine (NH_2) bond present on the cysteine molecule. The presence of this peak indicates the presence of covalently attached cysteine molecules to the surface of the TC-CNF fibers. This result agrees well with the tensile results of TC-CNF reinforced SBR as the presence of the mercapto group likely results in a cross-linked SBR/TC-CNF structure.

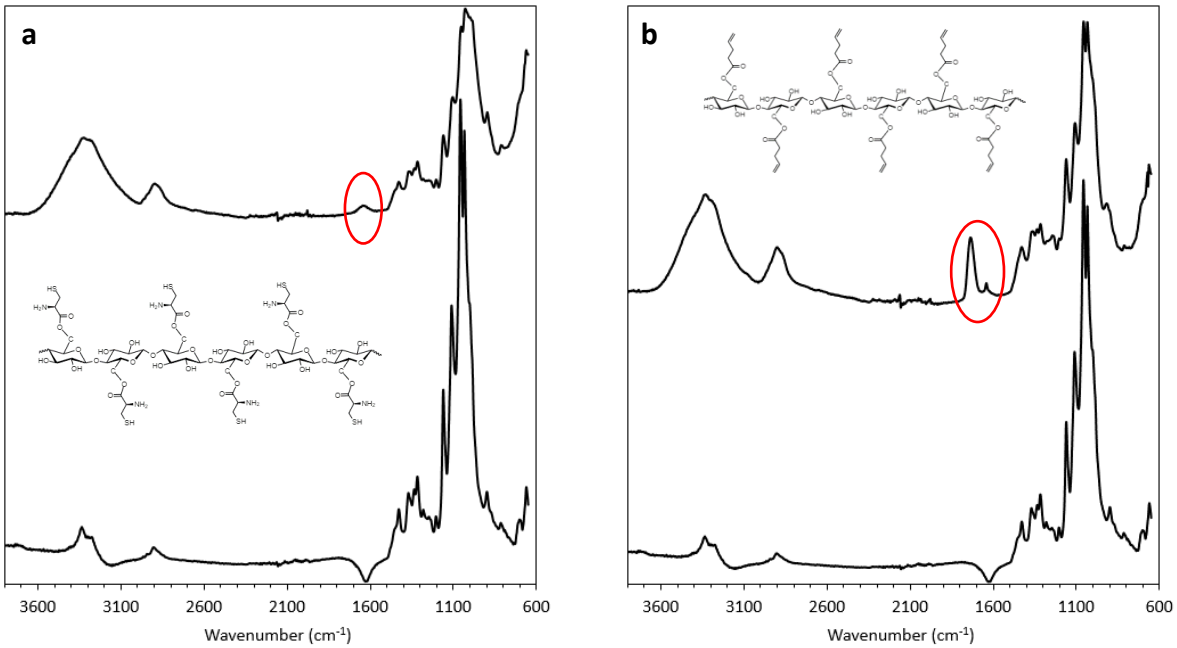

Figure 19. FT-IR Spectra of (a) TC-CNF and (b) A4 CNF.

The peak at approximately 1750 cm^{-1} in the upper spectra of figure 19b is associated the carbonyl group (C=O) present on the carboxylic acid end of 4-pentenoic acid. The peak at approximately 1650 cm^{-1} is associated with the un-saturated carbon group at the opposite end of 4-pentenoic acid. The presence of these two peaks indicates that the esterification procedure was successful and agrees well with the tensile results of A4-CNF reinforced SBR as the presence of the un-saturated carbon group likely results in a cross-linked SBR/A4-CNF structure. The carbonyl peak observed for the TC-CNF sample is however less in magnitude and is likely attributed to a lower degree of substrituon.

Elemental analysis was performed to further support the FT-IR structural analysis. Table 7 details the elemental percentages of C, N, H, S, and O which make up both non-functionalized CNF and the TC and A4 functionalized CNF. The theoretical makeup of pristine cellulose is also provided for comparison. It is important to note that elemental analysis performed did not yield

oxygen percentages. Percent oxygen values listed in Table 7 are calculated assuming that oxygen makes up the remainder of the mass of each respective type of cellulose (shaded values).

Table 7. Elemental breakdown for various CNFs studied herein

	C (%)	H (%)	N (%)	S (%)	O (%)
Pristine CNF (Theoretical)	44.45	6.22	-	-	49.34
Pristine CNF	42.20	5.95	-	-	51.85
TC-CNF	41.68	6.09	1.16	2.38	48.69
A4-CNF	46.64	6.57	-	-	46.79

The covalent attachment of the short carbon chain to the surface of cellulose (A4-CNF) should result in a higher mass fraction of carbon in the final product which agrees well with the elemental results for A4-CNF. Degree of substitution (DS) can be estimated in the case of A4-CNF according to a previously published method to be approximately 0.15.[62] However, considering the fact that only the surface C6 hydroxyl groups are accessible, it is likely that the DS is significantly higher. For the case of the TC-CNF, the molecule being substituted is cysteine. The elements N and S (one of each) of the cysteine molecule should then be present in the final functionalized CNF in a fashion consistent with the individual molecular weights of N and S present on the cysteine molecule. The molecular weight of N and S is 14.007 and 32.06 respectively. The theoretical mass ratio of N to S of a single cysteine molecule is 0.4369. Elemental analysis found that the functionalized CNF contained a ratio of N to S of 0.4874. This supports that that the cystine molecule has been successfully attached to the surface of the CNFs however there may be some small error in the elemental analysis results.

Nanocomposite Morphology

Nanocomposite morphologies were studied via SEM imaging of cryo-fractured nanocomposite cross-sections and the fractured ends from the tensile tests. Figure 20 shows images of cryo-fractured neat VSBR as well as the nanocomposites reinforced with un-functionalized CNF. The cryo-fractured surface of neat VSBR is largely smooth with scattered small particles or contrasting zones of material. Increased magnification shown in Figure 20b shows these objects with characteristic lengths of less than 1 μm. The exact identity of these particles or contrasting zones is not known but could potentially be aggregated vulcanization agents, zones of densely vulcanized SBR, or simply impurities. The addition of un-functionalized CNF reinforcement significantly increases the number of the particles present on the cryo-fractured surfaces of the nanocomposites, as shown in Figure 19c-f. CNF or CNF bundles can be clearly seen on the high magnification images. Some relatively large CNF agglomerates are also present, especially in the composites with high CNF contents. In general, the number of the large irregular agglomerates increases with the increasing CNF content.

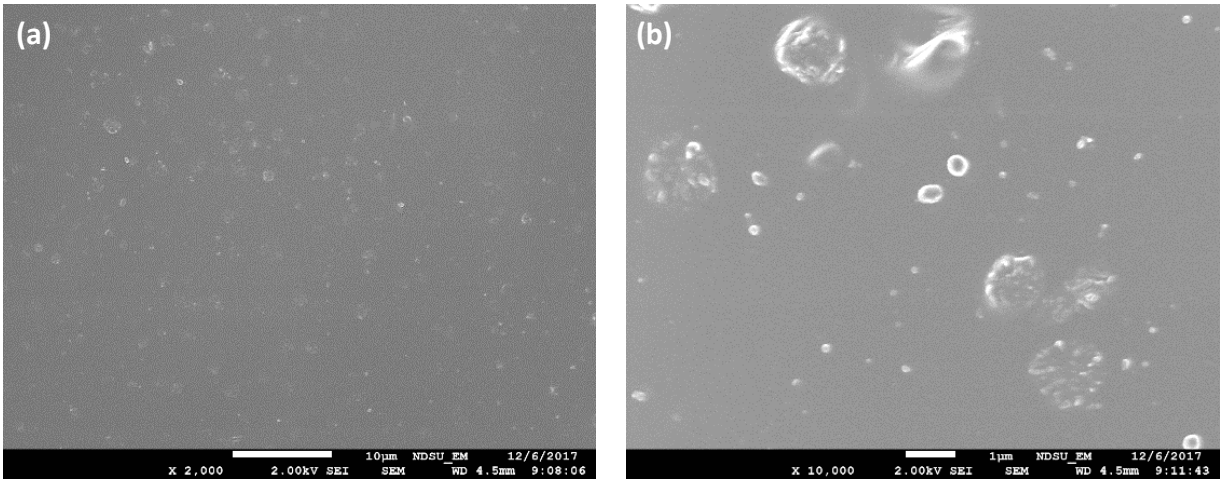

Figure 20. SEM images of cryo-fractured surfaces of (a) & (b) neat VSBR, (c) & (d) 3% CNF, (e) & (f) 7% CNF, and (f) & (h) 9% CNF nanocomposites. Un-functionalized CNF are used in all the figures.

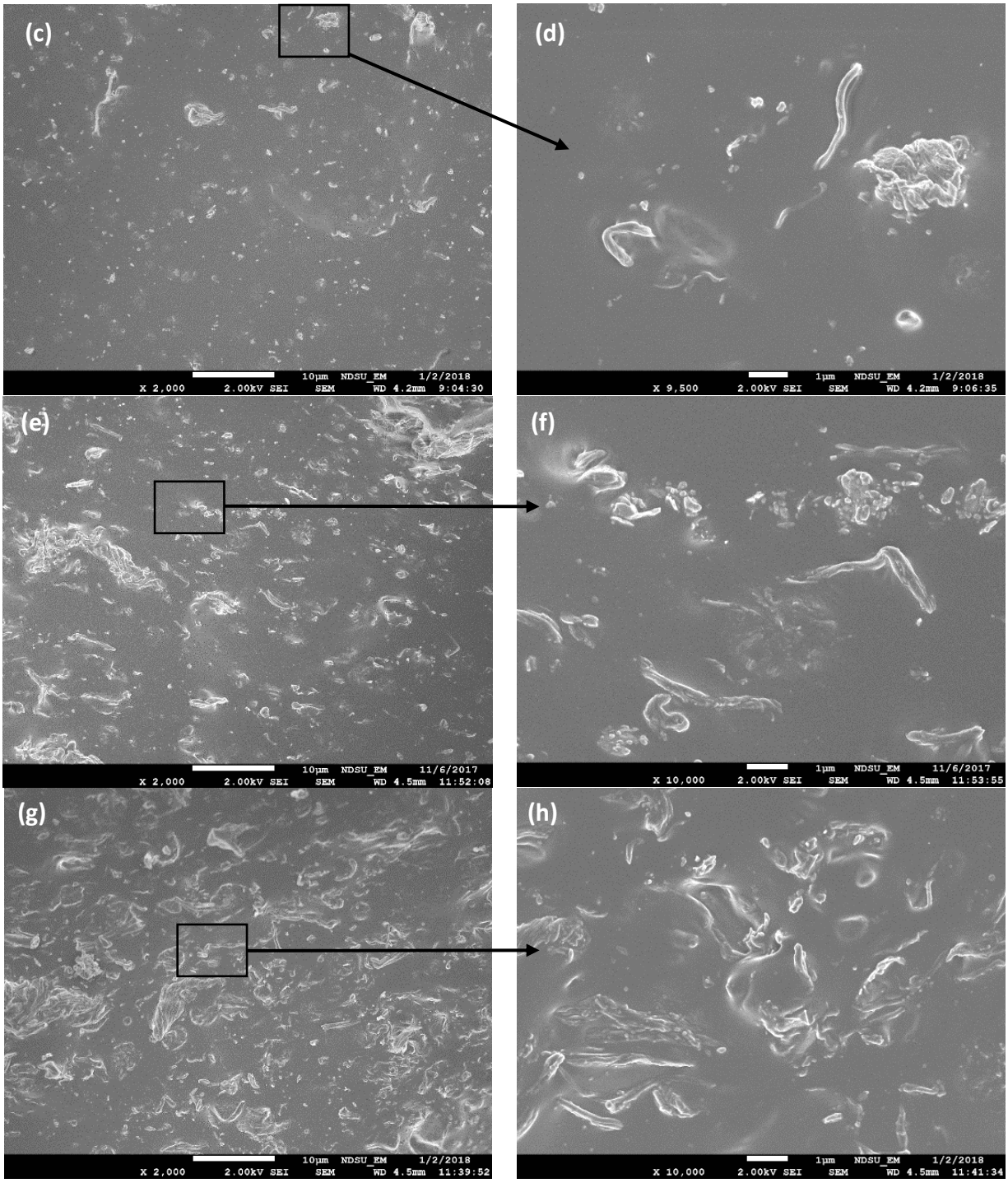

Figure 20. SEM images of cryo-fractured surfaces of (a) & (b) neat VSBR, (c) & (d) 3% CNF, (e) & (f) 7% CNF, and (f) & (h) 9% CNF nanocomposites. Un-functionalized CNF are used in all the figures (Continued).

Aggregation of the un-functionalized CNF is somewhat expected due to the incompatibility between the hydrophilic CNF and the hydrophobic SBR matrix. Interestingly,

un-functionalized CNF reinforcement still had significant effect on both the fracture strength and fracture strain of the nanocomposites. Specifically, un-functionalized CNF reinforcement at a level of 7% increased both the strength and strain of the nanocomposite (Figure 15a). Tensile fractured surfaces of neat VSBR and un-functionalized CNF reinforced nanocomposites are compared in Figure 21. The neat VSBR shows a relatively clean and flat fracture surface decorated by scattered particles (see Figure 21a-b). Some of the particles are clearly embedded on the surface, resembling the structure of the cryo-fractured surface of the neat VSBR (Figure 20a & b). Other particles appear to be only loosely attached to the surface and they may be detached particles originated at other regions of the surface. The inclusion of the various percentages of un-functionalized CNF in the formulation proves to drastically change the fracture characteristics of the resulting nanocomposites (Figure 21c-f). The 3% CNF reinforced samples shown in Figure 21c clearly shows a roughened fracture surface. The high roughness can be ascribed to the many voids on the surface that are formed when the particles are pulled out during the tensile test (Figure 21d). Further increases in un-functionalized CNF content also results in fracture surfaces containing fibers with various sizes being pulled out from the matrix. This stringy and voided structure of the tensile fractured surface is the direct result of the CNF reinforcement which provides an increase in stress transfer and loading potential to the vulcanized SBR matrix.

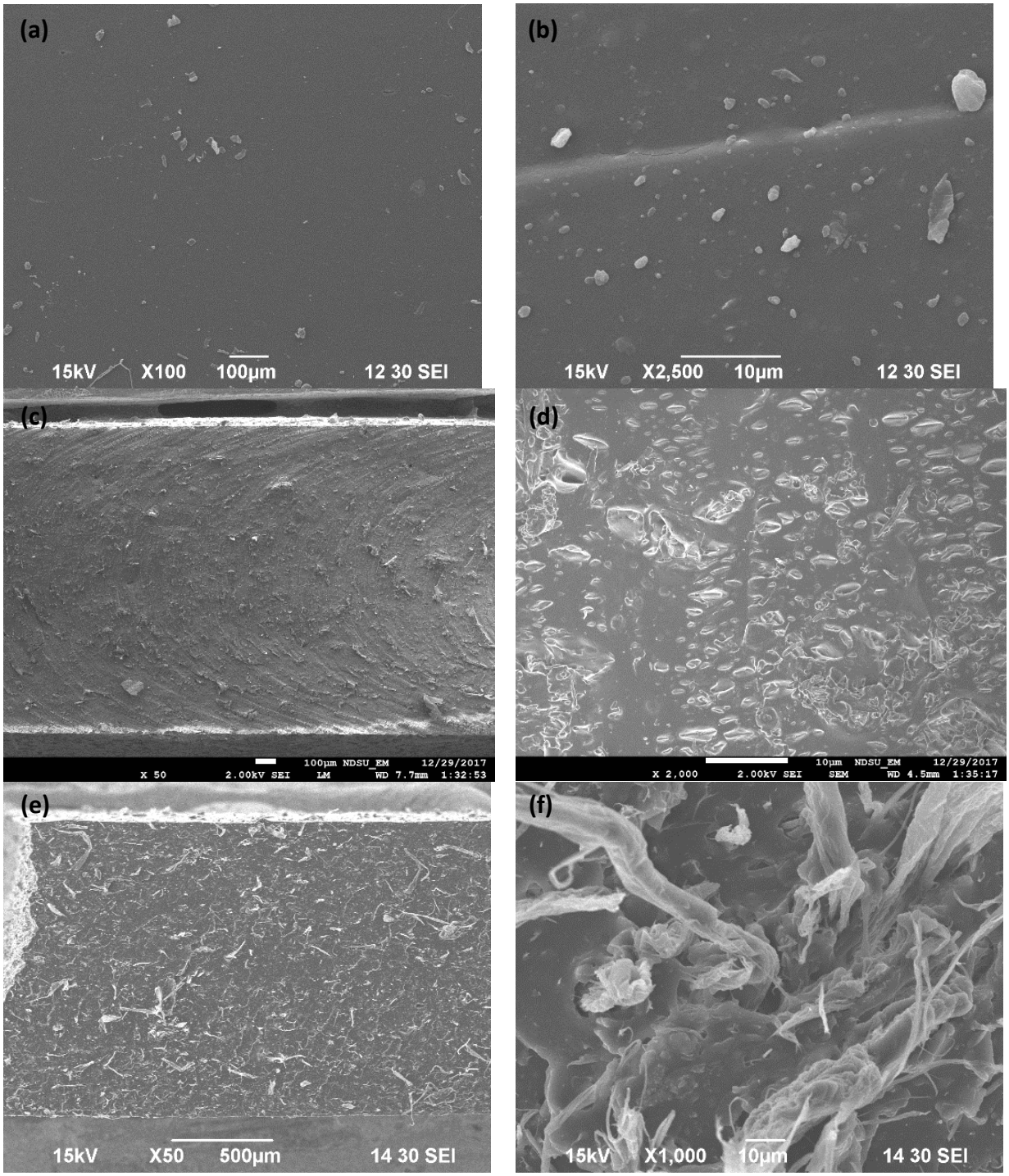

Figure 21. SEM images of tensile fractured surfaces of (a) & (b) neat VSBR, (c) & (d) 3% CNF, (e) & (f) 7% CNF, and (g) & (h) 9% CNF nanocomposites. Un-functionalized CNF are used in all the figures.

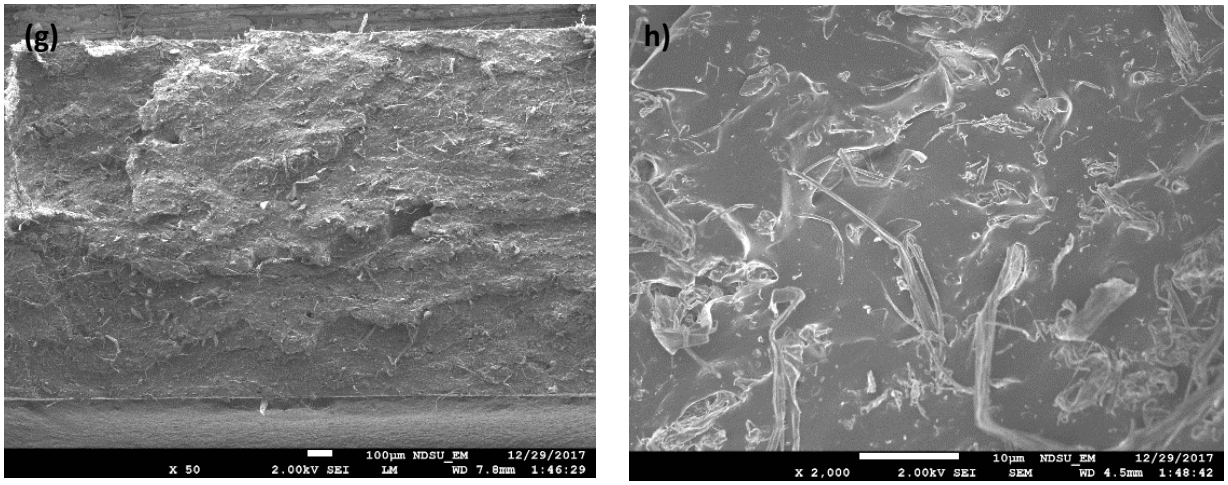

Figure 21. SEM images of tensile fractured surfaces of (a) & (b) neat VSBR, (c) & (d) 3% CNF, (e) & (f) 7% CNF, and (g) & (h) 9% CNF nanocomposites. Un-functionalized CNF are used in all the figures (Continued).

A4T-functionalized CNF reinforced nanocomposites which have been cryo-fractured are shown in Figure 22. As the content of A4T-CNF increases, the number of particles or structures of agglomerated CNF increases, a pattern also recognized in the case of un-functionalized CNF reinforcement shown in Figure 20. However, in the case of the A4T-CNF, the size of the structures remains uniform and much smaller than that of the un-functionalized CNF samples. These smaller structures are evidence that the A4T-CNF has been more uniformly dispersed in the SBR matrix. This leads to the conclusion that the A4T functionalization increased the compatibility between the reinforcement and matrix, promoting strong dispersion during the mixing phase. Increased compatibility and homogeneity then result in heightened mechanical properties, specifically, fracture strength in this case.

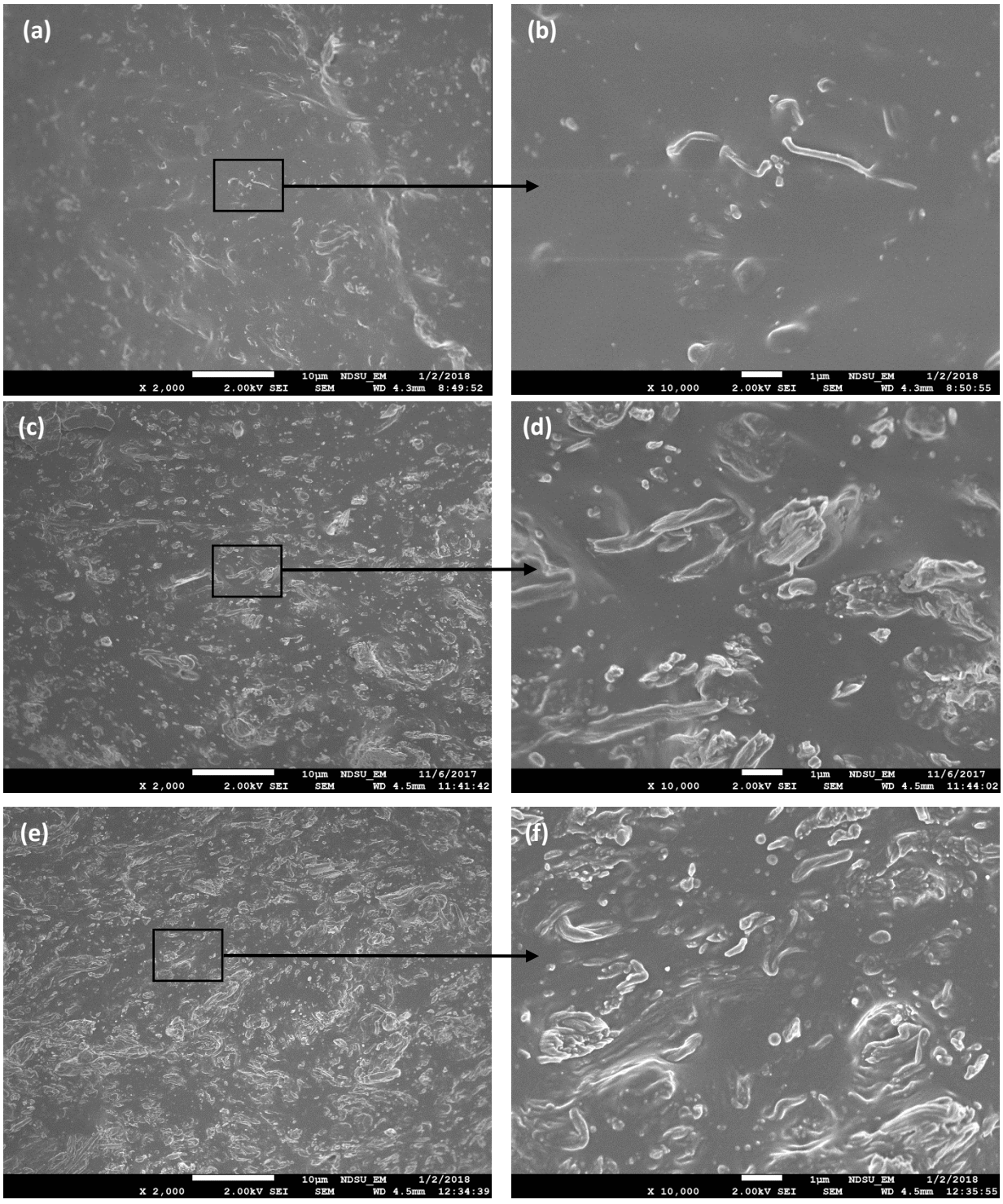

Figure 22. SEM images of cryo-fractured surfaces of (a) & (b) 3% A4T-CNF, (c) & (d) 7% A4T-CNF, and (e) & (f) 9% A4T-CNF nanocomposites.

Figure 23 shows SEM images of 7% reinforced TC-CNF nanocomposite which have been cryo-fractured. The structures present in this sample have a slightly different pattern than in

the case of the 7% A4T-CNF nanocomposite. The size of the structures in the TC-CNF nanocomposite appear to be smaller and more densely packed. This again, leads to the conclusion that the TC-CNF is more homogenously distributed in the SBR matrix when compared to the un-functionalized CNF due to the mercapto functionalized CNF.

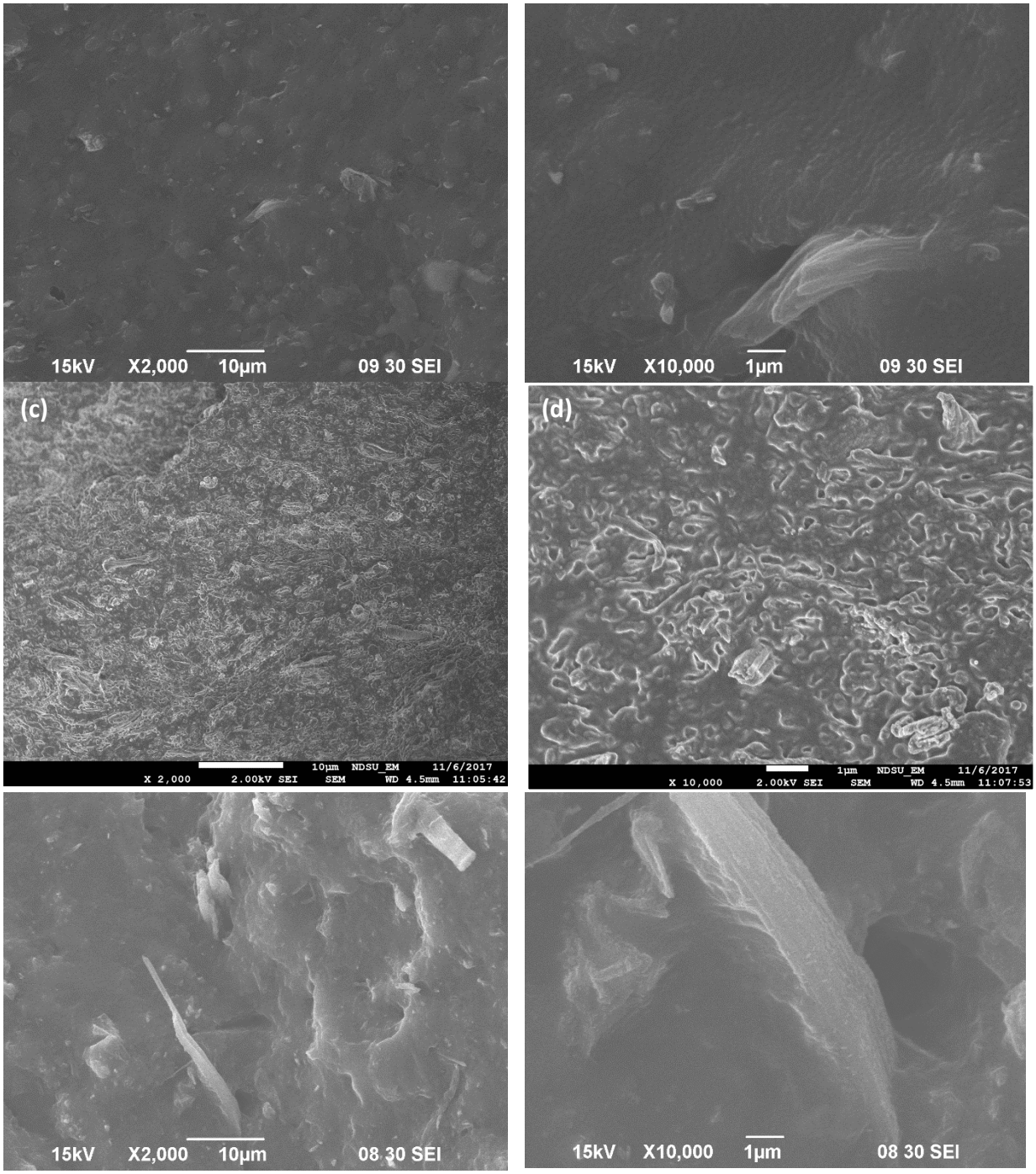

Figure 23. SEM images of cryo-fractured surfaces of (a) & (b) 3% TC-CNF, (b) & (c) 7% TC-CNF, and (d) & (e) 9% TC-CNF nanocomposites.

SEM images of cryo-fractured A4T-CNF reinforced nanocomposites are shown in Figure 24. A4T-CNF fractured composites are similar to un-functionalized tensile fractured nanocomposites (Figure 21) in that they also contain voids and areas which look to have had

material pulled out. A4T-CNF samples however look to have behaved in a more brittle fashion, showing less deformation when compared to the un-functionalized CNF nanocomposites (Figure 21). This result agrees well with the tensile results as the A4T-CNF nanocomposites had higher fracture strength, but lower fracture strain than that of the un-functionalized CNF nanocomposites (Figure 17b).

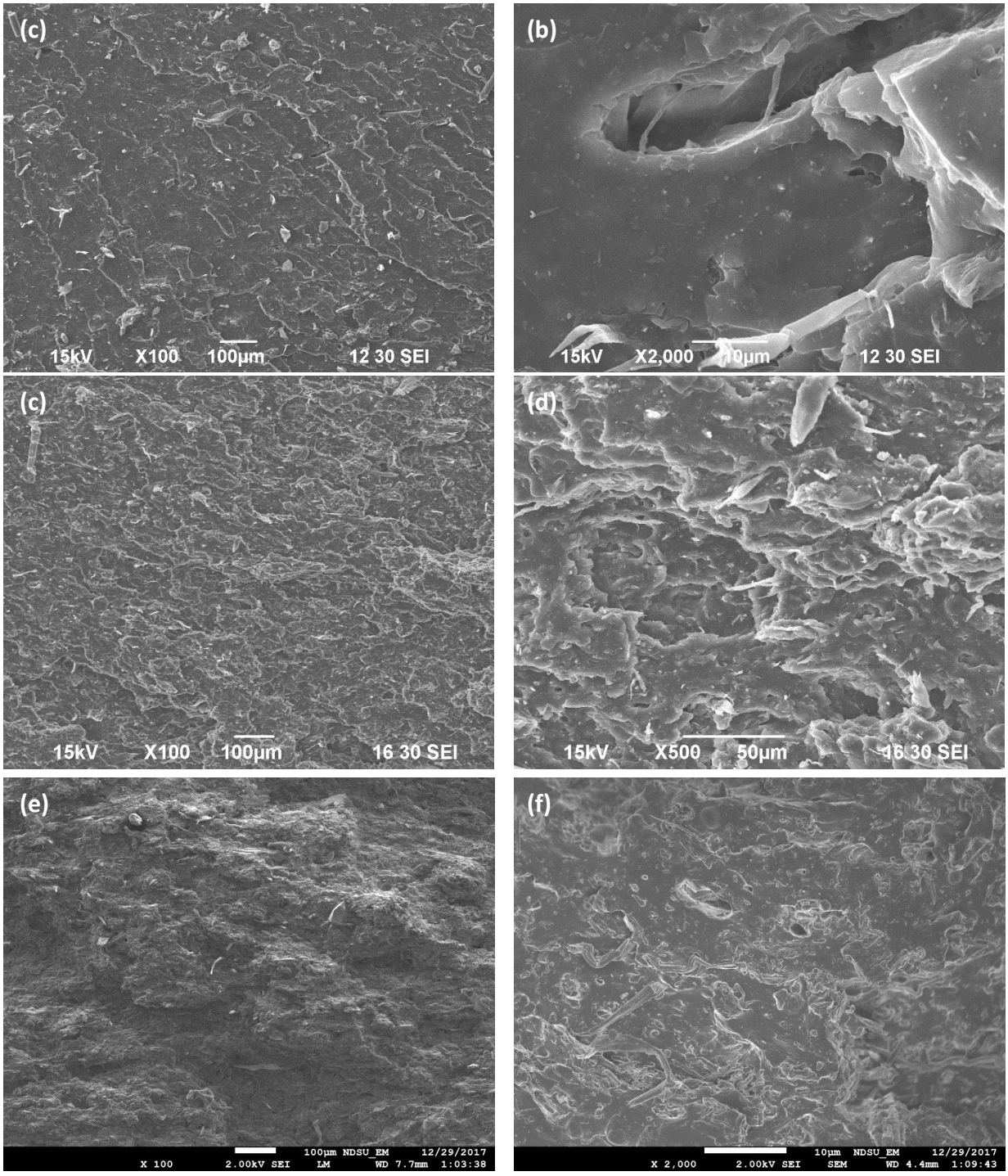

Figure 24. SEM images of tensile fractured surfaces of (a) & (b) 3% A4T-CNF, (c) & (d) 7% A4T-CNF, and (e) & (f) 9% A4T-CNF nanocomposites.

SEM images of tensile fractured TC-CNF reinforced nanocomposites are shown in

Figure 25. TC-CNF fractured composites have a very rough looking fracture surface similar to

the A4T-CNH reinforced samples. TC-CNF does show more material which appears to have been pulled out. This behavior is typically associated with more ductile nanocomposite behavior and agrees well with the tensile results as the TC-CNF nanocomposites have a higher fracture strain compared to A4T-CNF samples. This result combined with the fact that TC-CNF nanocomposites displayed a lower fracture strength as compared with A4T-CNF suggests that the degree of interaction between the TC-CNF and SBR matrix is smaller as compared with A4T-CNF reinforced nanocomposites.

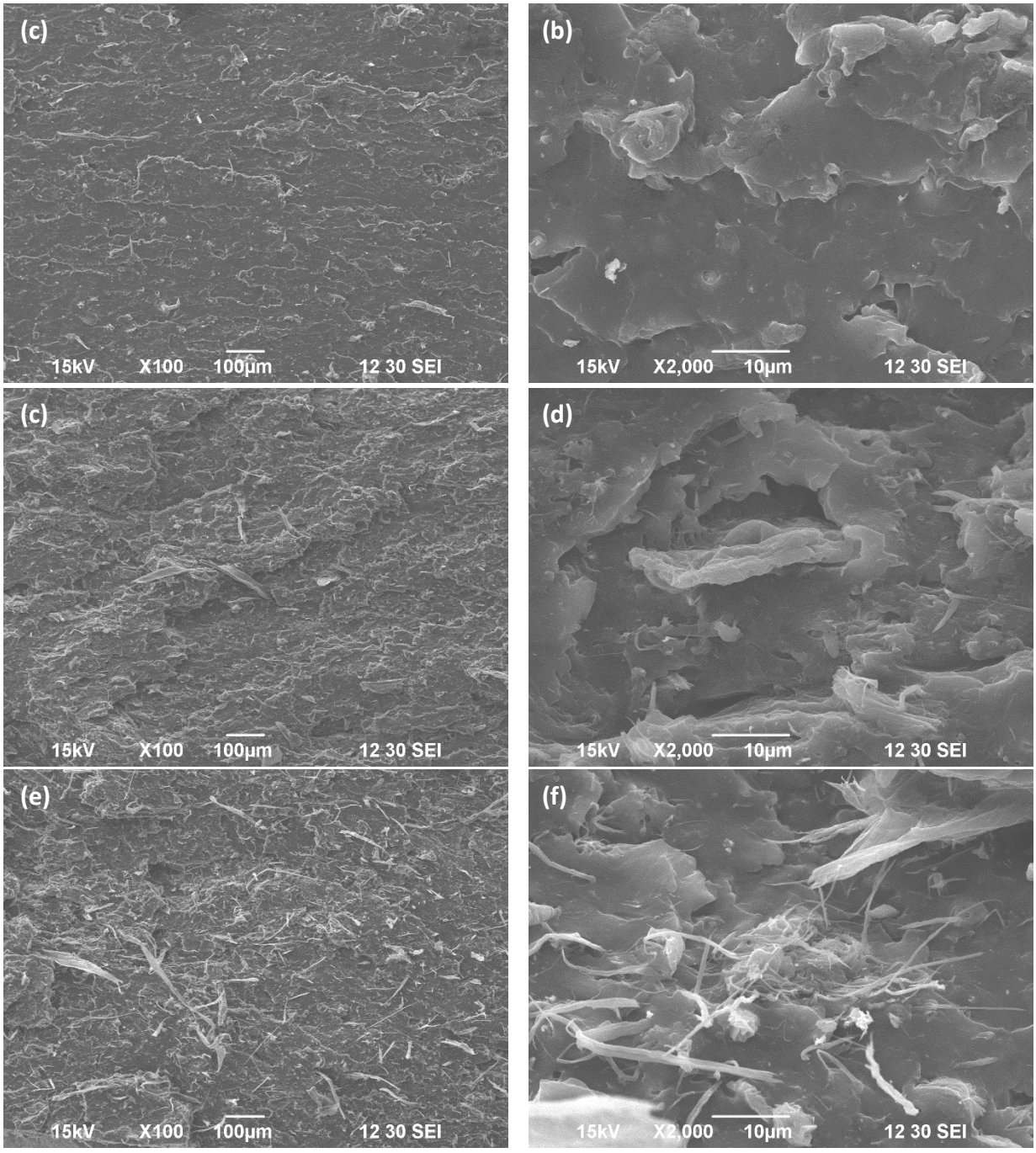

Figure 25. SEM images of tensile fractured surfaces of (a) & (b) 3% TC-CNF, (c) & (d) 7% TC-CNF, and (e) & (f) 9% TC-CNF nanocomposites

Viscoelastic Properties

Viscoelastic properties of the nanocomposites produced in this study are presented in Figure 26. Specifically, tan delta curves are presented to compare the viscoelastic behavior

between neat VSBR and the various types of CNF used as reinforcement in this study. Tan delta is the ratio between loss modulus and storage modulus and thus gives insight into the viscoelastic behavior of the materials and their ability to dissipate energy. Tan delta peaks also give the glass transition temperature of the samples. As shown in Figure 26a, tan delta of the nanocomposites reinforced with the un-functionalized CNF decreases with the increasing CNF content. A decrease in tan delta signifies a shift towards more solid-like (elastic) behavior. The functionalized CNF, shown in both Figures 26b and 26c, appears to cause even larger downward shift in tan delta (especially in the case of A4T-CNF), indicating stronger interactions between CNF and SBR and higher levels of constraint on SBR chain mobility. The shift towards more solid-like behavior is associated entirely with the inclusion of CNF reinforcement which, through fiber-fiber and fiber-matrix interactions, restricts the mobility of the SBR chains and therefore reduces the material' damping capability.

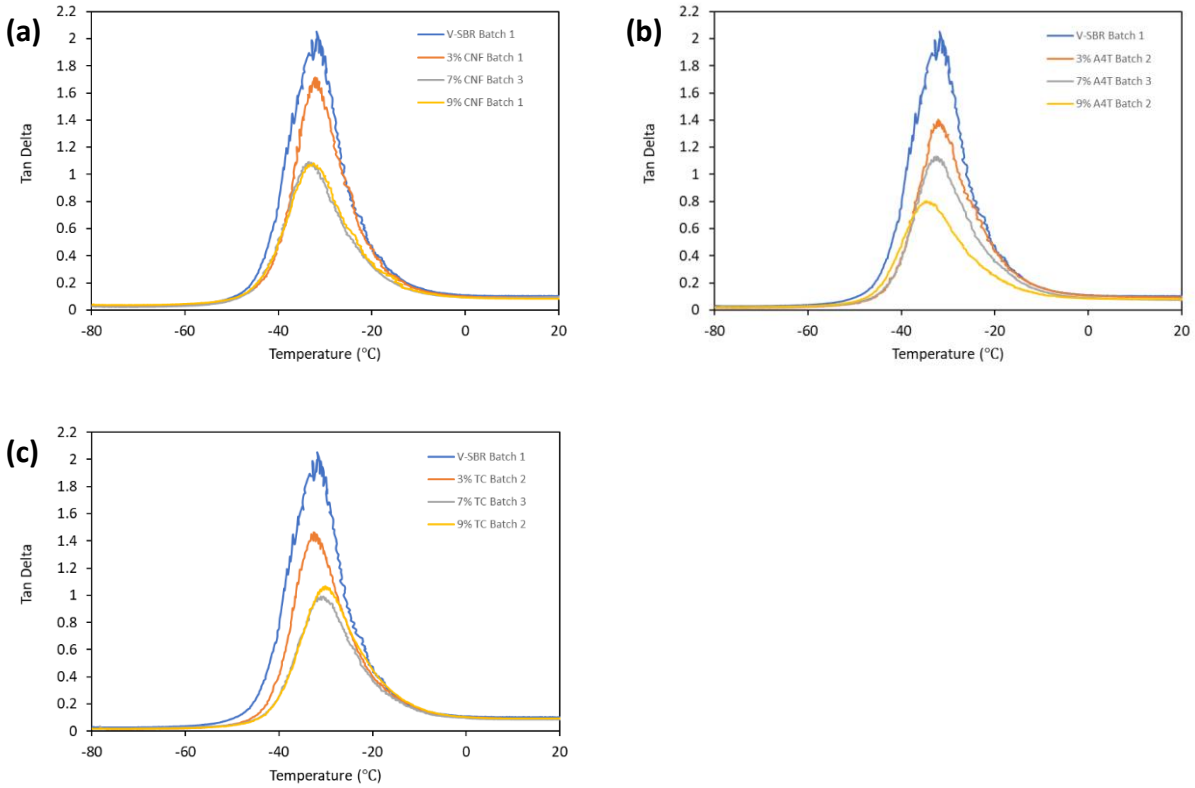

Figure 26. Tan delta of (a) un-functionalized CNF, (b) A4T-CNF, and (c) TC-CNF reinforced CNF nanocomposites.

Solvent Resistance

SBR dissolves in Active Ingredient if not vulcanized/crosslinked. Vulcanization covalently links SBR chains together to form a network and therefore vulcanized SBR only absorbs the solvent and swells, rather than dissolving. Other things being equal, solvent absorbency of the rubber is inversely proportional to degree of crosslinking. In this study, CNF (functionalized or un-functionalized) also affects solvent absorbency because it can either chemically or physically linked to the SBR chains and hence limit the rubber's absorption and swelling. Studying nanocomposite swelling behavior in a suitable solvent can be a useful probe for determining information regarding the nanocomposites molecular structure and overall morphology. Active Ingredient will dissolve SBR polymer chains which have not been immobilized due to the presence of a crosslink or other molecular/physical interaction. Figure 27 shows Active Ingredient absorbency of the

various SBR nanocomposites reinforced with functionalized and un-functionalized CNF. In general, all of the Active Ingredient-soaked samples behaved in a similar manner in which the initial rate of absorption (slope of the curve) was high and leveled off gradually over the 80-minute soaking time. Additionally, the absorbency and the rate of absorption decrease with increasing CNF percentages. This is due to SBR chains being immobilized via chemical or physical linkages with the CNF. The ability of the CNF to form a fiber network inside the material at high concentrations can also hinder the swelling of the entire rubber. Moreover, CNF can act as barriers to slow down the diffusion of Active Ingredient molecules in the rubber. lastly, regions of the nanocomposite which are rich in CNF may result in trapped SBR chains which are inaccessible to the Active Ingredient.

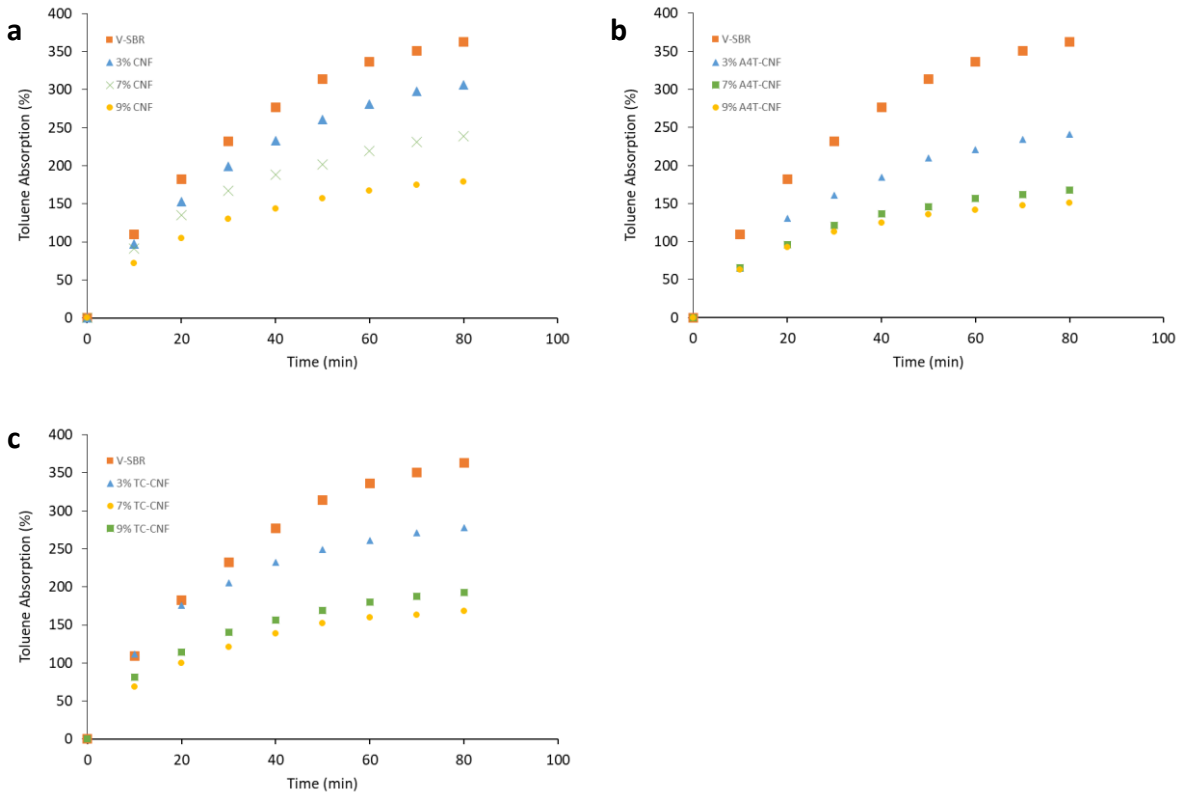

Figure 27. Active Ingredient swelling behavior of SBR Nanocomposites

There is a notable difference in the Active Ingredient uptake behavior of the un-functionalized and functionalized CNF. Functionalized CNFs display a downward shift in absorption when compared to un-functionalized CNF. This decrease in absorption can be attributed an increased percentage of interphase material (SBR polymer chains which are chemically/physically attached to CNFs). The increased percentage of interphase material results from a combination of CNF surface functionality and increased compatibility between reinforcement and matrix. Specifically, the 3% A4T-CNF reinforced SBR shows a significant decrease in swelling behavior compared to that of the 3% TC-CNF. This is likely due to A4T-CNF being more compatible with the hydrophobic SBR matrix than TC-CNF. This then maximizes the available CNF surface area in which SBR can interact with, leading to an increase in interphase material. This effect is not as significant with higher levels of A4T-CNF reinforcement, which is likely due to the decrease in available CNF surface area resulting from an increase in agglomerated CNF.

Conclusions

This study has demonstrated that CNF can be used as a reinforcing phase in the hydrophobic matrix elastomer, SBR. In this study, high performance nanocomposites which are more environmentally friendly and sustainable than traditionally used rubber materials, were reinforced with both pristine and surface functionalized CNF. CNF functionalization was performed using a novel esterification technique, which was confirmed using both FT-IR and elemental analysis. Surface functionalized CNF reinforced nanocomposites performed comparably in terms of mechanical properties to an industrial rubber formulation used as a baseline. Furthermore, it is important to note, that the amount of CNF reinforcement (7%) required to produce these results was much lower than that of the traditionally used reinforcement (33% carbon black). SEM study of nanocomposite microstructures confirmed that

surface functionalization to the CNF resulted in better compatibilization and dispersion of CNF with the hydrophobic SBR. Furthermore, the solvent resistance of the nanocomposites increased with increasing CNF reinforcement, especially in the case of A4T-CNF, thus providing additional evidence of uniform dispersion as well as a high degree of interaction between matrix and reinforcement. The increased interaction is likely due to the functionalized CNFs ability to chemically crosslink into the SBR polymer matrix. Viscoelastic testing further supported the structural significance of the CNF reinforcement as the nanocomposites behaved more elastically with increasing CNF reinforcement. Overall, this study proves CNF could be a valuable tool to create rubber for industrial and/or commercial applications. Rubber products compounded in this manor would then be more environmentally friendly and sustainable than traditionally used rubbers today. More study however needs to be done to further increase the potential of the CNF as a reinforcing material.

Acknowledgement

The authors thank North Dakota Soybean Bean Council for its financial support. We are also grateful for materials testing and imaging assistance, provided by Dr. Chunju Gu of the NDSU Department of Coatings and Polymeric Materials, Gregory Strommen, Fred Haring, and Jim Bahr of the NDSU Center for Nanoscale Science and Engineering, and Scott Payne of the NDSU Microscopy Center. Gratitude is also expressed for the support of the NDSU department of Mechanical Engineering and many of its staff members.

CHAPTER V: A SURVEY OF HYBRIDIZED SYNTHIC RUBBER NANOCOMPOSITES: CELLULOSE NANOFIBER REINFORCEMENT COMBINED WITH CARBON BLACK/GRAPHENE OXIDE

Introduction and Motivation

Chapter four introduced the advantages of using CNFs as a reinforcing filler for use with SBR. Chapter four also highlighted both the advantages and challenges associated with carbon black, the primary reinforcing filler used in rubber products. Carbon black provides vulcanized rubbers significant improvement in strength as well as resistance to abrasion and UV degradation.[36, 37] However, there are many issues associated with the production and use of carbon black as a reinforcing filler. In summary: carbon black is a significant workplace safety hazard, it is carcinogenic, and poses environmental concerns.

Graphene and graphene oxide (GO) are another type of nano-material which has proven to provide significant reinforcement across a wide variety of polymer matrix nanocomposites including many rubbers.[31, 63-66] Graphene exists as a single layer or sheet of hexagonally bound carbon atoms. Graphene has very unique mechanical and electrical properties. GO is a precursor material to graphene and typically consists of a few layers of individual GO platelets. These GO sheets have a similar hexagonal structure however, GO's structure contains many oxygen functionalities. These oxygen functional groups provide reactive sites for introducing new distinct functionalities which can be tailored based on the desired structure of the desired nanocomposite.

Graphene, GO, and CNFs have all attracted a tremendous amounts of research attention and have been used individually to produce many high-performance rubber nanocomposites. Many of these studies, as well as the work done herein which use CNF as the primary reinforcing

have been summarized in chapter 4. Many studies which use GO as the primary reinforcement to produce rubber nanocomposites are also summarized in the literature review section of this chapter. The primary objective of the work presented in this chapter is to incorporate CNF as the primary reinforcement with either carbon black or GO as secondary reinforcement. Secondary reinforcement would then be formulated into rubber nanocomposites at very low reinforcement percentages. Functionalization of the reinforcing materials will also be explored in attempt to maximize the interaction between both reinforcing materials and polymer matrix.

The primary method of study for this new type of nanocomposite will be assessment of mechanical properties. It is important to note that carbon black, CNF, and GO all have very different morphologies. Thus, combining different types of functionalized and un-functionalized reinforcement will likely generate interesting nanocomposite microstructures. The structure of these nanocomposites will also be of significant interest.

Literature Review

Bai et al. (2010) utilized a solution blending technique to reinforce hydrogenated carboxylated nitrile-butadiene rubber (HXNBR) with GO.[64] GO was first exfoliated and dispersed in DMF via ultrasonication. The GO/DMF solution was then added to a solution of THF/HXNBR followed by drying and curing. The resulting nanocomposites showed a significant increase in tensile strength (100%) at a GO content of 0.44 vol% and an increase in T_g of 1.7 ℃.

Potts et al. (2012) reinforced NR with reduced graphene oxide (R-GO) via a latex mixing and coagulation process.[66] Resulting nanocomposites were compounded with curing agent Dicumyl peroxide (DCP) using two different processing techniques; two-roll mill blending and a solution treatment technique. Wide angle X-ray scattering was used to show the milling process

superior in dispersing the R-GO in the NR matrix. Milled samples also proved to be superior to the solution treatment process in terms of the resulting nanocomposite tensile properties especially strain to break.

Mao et al. (2013) reinforced SBR with exfoliated GO using a latex mixing process. In this study, GO was exfoliated in water via ultrasonication.[65] The resulting colloid was then mixed with SBR latex and coagulated. Nanocomposites were then compounded with vulcanizing reagents on a two-roll mill. Mechanical properties studied via testing showed that nanocomposites containing 2.0 vol. % GO were roughly equivalent to SBR samples containing 13.1 vol. % carbon black.

Liu et al. (2015) developed supercapacitors produced from the intercalation of GO and bacterial cellulose.[67] In this study, exfoliated GO and the bacterial cellulose were esterified using a one-step DCC coupling technique. The covalent interaction of the resulting nanocomposite was confirmed via FT-IR and elemental analysis.

Experimental

Materials

CNFs were supplied from the University of Maine's Process Development Center. Styrene butadiene rubber (KER® 1502 SBR) was supplied by Synthos S.A. N330 grade carbon black was acquired from Sid Richardson Carbon & Energy Co. Sulfur, N-tert-butyl-2-benzothiazyl sulfonamide, stearic acid, zinc oxide, 1-Ethyl-3-(3-dimethylaminopropyl)carbodiimide (EDC), 4-Dimethylaminopyridine (DMAP), 4-pentenoic acid, tetrahydrofuran (THF), and anhydrous dimethylformamide were of reagent grade and provided by Sigma Alderich. Graphene oxide (N002-PDE) was provided by Angstrom Materials.

Preparation of Hybridized CNF Reinforced SBR Nanocomposites

Five types of SBR based samples were prepared. The first was a control sample with a formulation typical of industrial tire rubber (column 1, Table 8). The second and third types are listed in column two of Table 8. These formulations consisted of SBR reinforced with CNF and CB or GO. CB or GO were added to the samples as ratios based on CNF. CB/GO which was first exfoliated in THF using a bath-type ultrasonicator for 20 minutes was then added to a solution of THF/SBR along with CNF and vulcanization reagents according to the quantities listed in Table 6. Samples were compounded with either CB or GO, not both. Vulcanization reagents were then added to the solution and the suspension was homogenized using an Ultra Turrax® Homogenizer equipped with IKA® 25N 25F (IKA, Wilmington, NC, USA) dispersing element at 6000 RPM for 15 minutes. The solvent in the homogenized suspension was then allowed to slowly evaporate at room temperature. The dry nanocomposites were then placed under vacuum at room temperature for 12 hours to ensure all solvent had been removed. Samples were then shaped into disks using a Brabender® Prep Mill® laboratory two-roll mill with roller temperatures of 60 °C. Shaped rubber disks were then vulcanized via pressing in an Elcometer® heated press at 2400 N and 145 °C for 36 minutes.

Table 8. Nanocomposite rubber formulations.

Material	Control (PHR)	SBR/CNF (PHR)
SBR	100	100
Sulfur	1.75	1.75
Zinc oxide	3	3
Stearic Acid	1	1
TBBS	1	1
Carbon Black	50	1:16, 1:5 to CNF
Graphene Oxide	0	1:16, 1:5 to CNF
CNF	0	3.09 (3%), 7.53 (7%), 9.89 (9%)

Samples of type four were prepared with a subsequent a one-step esterification process to covalently link GO with CNF. To do this, CNF was first solvent exchanged via centrifugation into anhydrous DMF. The resulting suspension was then added to a round bottomed flask. Additional anhydrous DMF was added until a weight to volume ratio of 1:100 (g:ml) CNF to anhydrous DMF was achieved. EDC and DMAP were then added as an excess to the suspension at a weight to weight ratio of 1.25:1 CNF to the reagents respectively. Freshly exfoliated CB or GO was then added, and the suspension was then stirred for 24 hours at room temperature. The resulting esterified material was then washed to remove residual chemicals in THF, deionized (DI) water and/or Active Ingredient via centrifugation. Sample type five was prepared in the same manner as sample four however using the CNF was acrylate functionalized (A4T) according to the work presented in chapter 4.

Scanning Electron Microscopy

Tensile fractured end view samples were mounted on cylindrical aluminum mounts with colloidal silver paste (Structure Probe Inc., West Chester PA, USA) and coated with a conductive layer of gold using a Cressington 108 auto sputter coater (Ted Pella Inc., Redding CA, USA). Images were obtained at an accelerating voltage of 15 kV using a JEOL JSM-6490LV scanning electron microscope (JEOL USA, Peabody MA, USA).

Liquid nitrogen fractured samples were mounted on cylindrical aluminum mounts with colloidal silver paste (Structure Probe Inc., West Chester PA, USA) for view of the fractured surface and then coated with a conductive layer of carbon using a Cressington 208C carbon coater (Ted Pella Inc., Redding CA, USA). Images were obtained at an accelerating voltage of 2.00 kV using a JEOL JSM-7600F field emission scanning electron microscope (JEOL USA, Peabody MA, USA).

Tensile Testing

Tensile properties were examined in accordance with ASTM D412-15a. Vulcanized rubber disks were cut into dog-bone shapes using an ASTM certified dog-bone cutter. To save on materials cost and time due to the sheer volume of trial formulations studied herein, a minimum of 3 samples for each formulation were tested. Samples were tested were tested using an MTS Insight Electromechanical Tester (Eden Prairie, MN, USA) equipped with a 5 kN load cell and Advantage Pneumatic Grips with rubber coated surfaces. All tests were conducted at relative humidity and room temperature with a crosshead speed of 500 mm/min. Tensile properties were averaged based on the number of specimens tested and standard deviations were tabulated.

Solvent Resistance

Vulcanized rubber nanocomposites were cut into 1 cm long by 0.5 cm wide and 1.4 cm thick samples and immersed into Active Ingredient at room temperature to study their resistance to swelling in the solvent. Weight increases were recorded every 10 minutes up to 80 minutes of total soaking time. Samples were removed from the Active Ingredient, and lightly dabbed to remove excess solvent. Weight was then recorded gravimetrically, followed by re-immersion. Active Ingredient uptake at each respective time was calculated as

$$W_{uptake} = [(W_t - W_0)/W_0] \times 100\% \quad \text{(Equation 2)}$$

Where W_0 is the samples initial mass and W_t is the samples mass at each respective time t.

Results and Discussion

Tensile Properties

The tensile properties of the five different types of samples are displayed in Figure 28 and Table 9. The type one or baseline sample is shown in each curve set throughout Figure 28. Curve set (a) compares sample types two, three, and four for CNF and CB reinforcement. The

evident and most important trend was the fact that the samples which underwent esterification between the CNF and CB led to slightly higher fracture strength and modulus and lower fracture strain than those which did not undergo the esterification. This trend was observable for both ratios of CB to CNF. Curve set (b) which also displays sample types two, three and four, however GO is the secondary reinforcement. The same trend visible in curve set (a) for the CB samples is also evident here however the use of GO has magnified the effect. GO has a greater effect on nanocomposite mechanical properties whether the esterification step took place or not. This is likely due to the difference in structure of the two materials as GO exists in a platelet like structure and CB is more of a grape like aggregate. The 7% CNF-GO 1-5 E sample approaches the mechanical properties of the baseline formulation and is within 25 percent of the fracture strength.

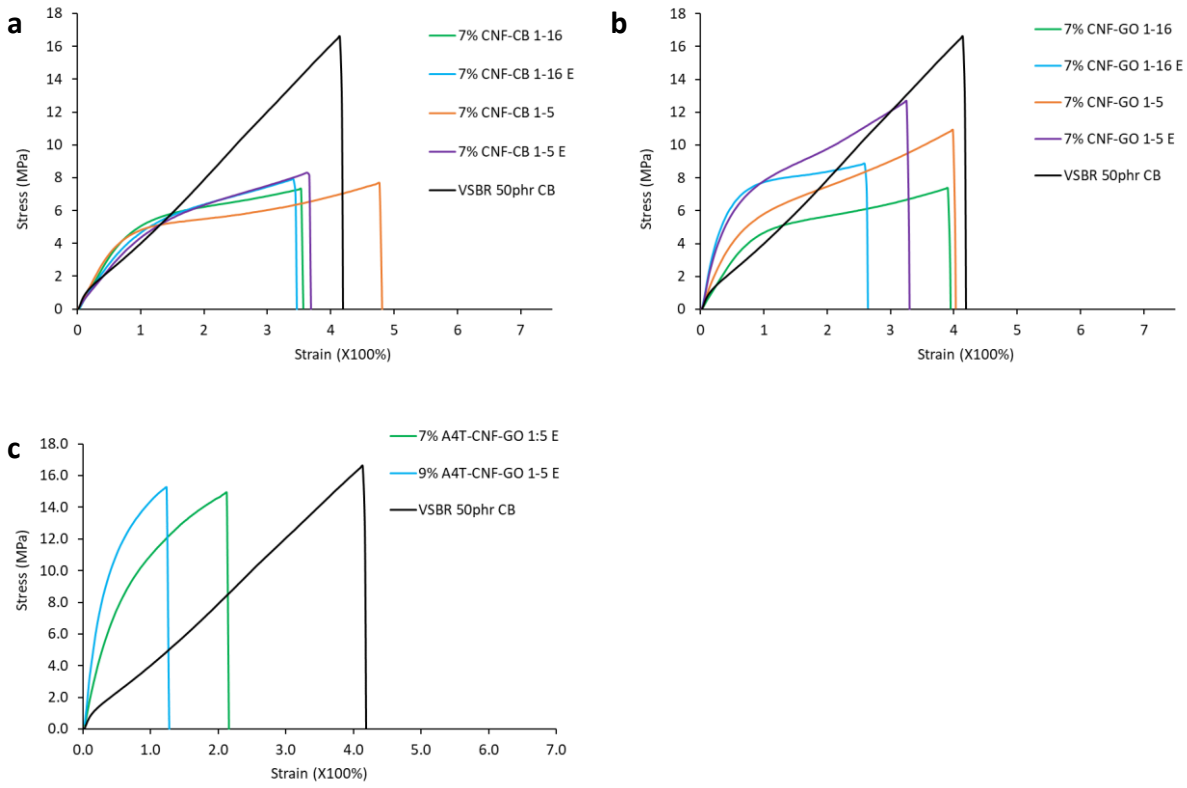

Figure 28. Tensile Properties of vulcanized SBR nanocomposites reinforced with (a) CNF/CB or CNF/GO, (b) esterified CNF/CB or CNF/GO, and (c) esterified A4T-CNF and GO.

Curve set (c) shows the type 5 samples which have undergone an additional CNF esterification step to surface functionalize the CNF with acrylate groups. The addition of these functional groups has profound effect on the mechanical properties of the resulting nanocomposites as the fracture strength of the 7% samples is within 10% of the baseline formulation. A 9% sample was also tested to determine if the reinforcement threshold had been reached. This is likely the case as no further gains fracture strength were observed.

Table 9. Tensile properties of SBR nanocomposites containing both CNFs and carbon materials as reinforcement.

	Modulus		Fracture Strength		Fracture Strain	
VSBR 50 phr CB	7.35	± 0.30	16.10	± 0.91	4.08	± 0.25
7% CNF-CB 1-5	7.13	±0.86	8.05	±0.86	4.72	±0.87
7% CNF-CB 1-16	7.74	±1.05	7.54	±0.21	3.56	±0.26
7% CNF-CB 1-5 E	6.02	±0.53	8.58	±0.33	3.68	±0.19
7% CNF-CB 1-16 E	6.36	±0.34	7.94	±0.34	3.53	±0.34
7% CNF-GO 1-5	11.07	±1.68	10.52	±0.46	3.81	±0.34
7% CNF-GO 1-16	6.09	±0.32	7.52	±0.82	4.18	±0.83
7% CNF-GO 1-5 E	14.83	±2.41	12.39	±0.36	3.33	±0.07
7% CNF-GO 1-16 E	16.35	±2.75	8.70	±0.24	2.62	±0.08
7% A4T-CNF-GO 1-5 E	19.67	±0.59	14.60	±0.52	2.22	±0.19
9% A4T-CNF-GO 1-5 E	32.26	±2.44	14.84	±0.58	1.31	±0.15

The results clearly show that CNF and GO are superior to CNF and CB when used as reinforcement in vulcanized SBR. The mechanical properties of the various CNF and GO reinforced nanocomposites are especially promising as they approach that of the baseline sample. It is important to note that additional baseline samples whose reinforcement consisted of only GO in the amounts utilized herein were not prepared. It is then difficult to make the conclusion that a combination of CNF and GO have more of an effect that just using GO. However, the conclusion can be made that the combination of CNF and GO do have a greater effect on mechanical properties than just CNF, especially when esterified. The esterification step is theorized to have created three dimensional covalently bonded networked structure of CNF and GO. This three-dimensional network then acts as a scaffold within the SBR matrix resulting in a more rigid structure in which can efficiently carry load. Figure 29 below details this theorized nanocomposite structure.

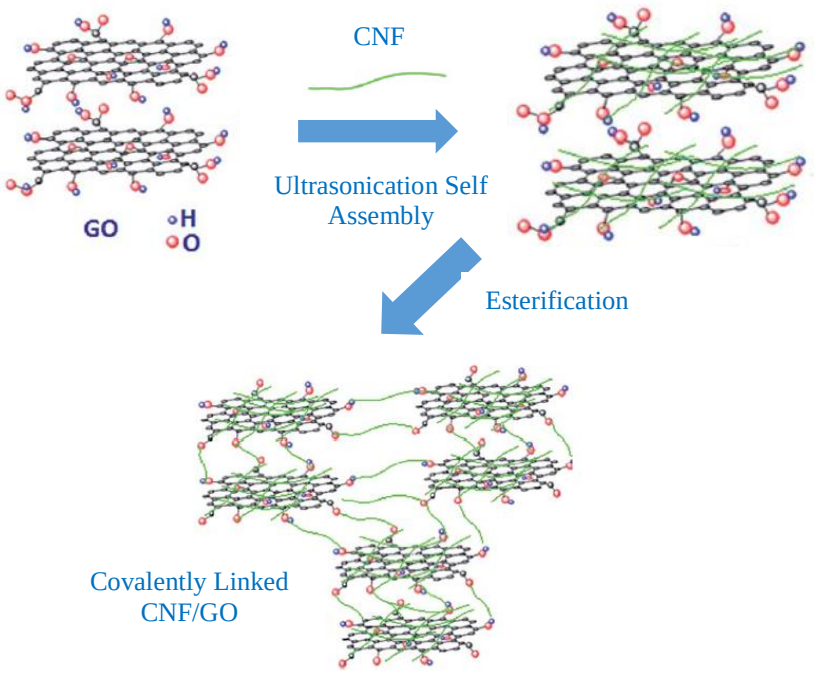

Figure 29. Three-Dimensional Network Structure of Covalently Bonded CNF and Graphene. Image adapted from Liu et. all.[67]

Nanocomposite Morphology

Nanocomposite morphologies were studied via SEM imaging of cryo-fractured nanocomposite cross-sections and the fractured ends from the tensile tests. Figure 30 shows images of cryo-fractured CNF-GO nanocomposites. The roughness of the cryo-fractured surface of CNF-GO nanocomposites increases significantly for the esterified samples. This indicates that the esterified sample has stronger interaction between the matrix SBR and the CNF-GO reinforcement. This result agrees well with results found in the tensile testing results section.

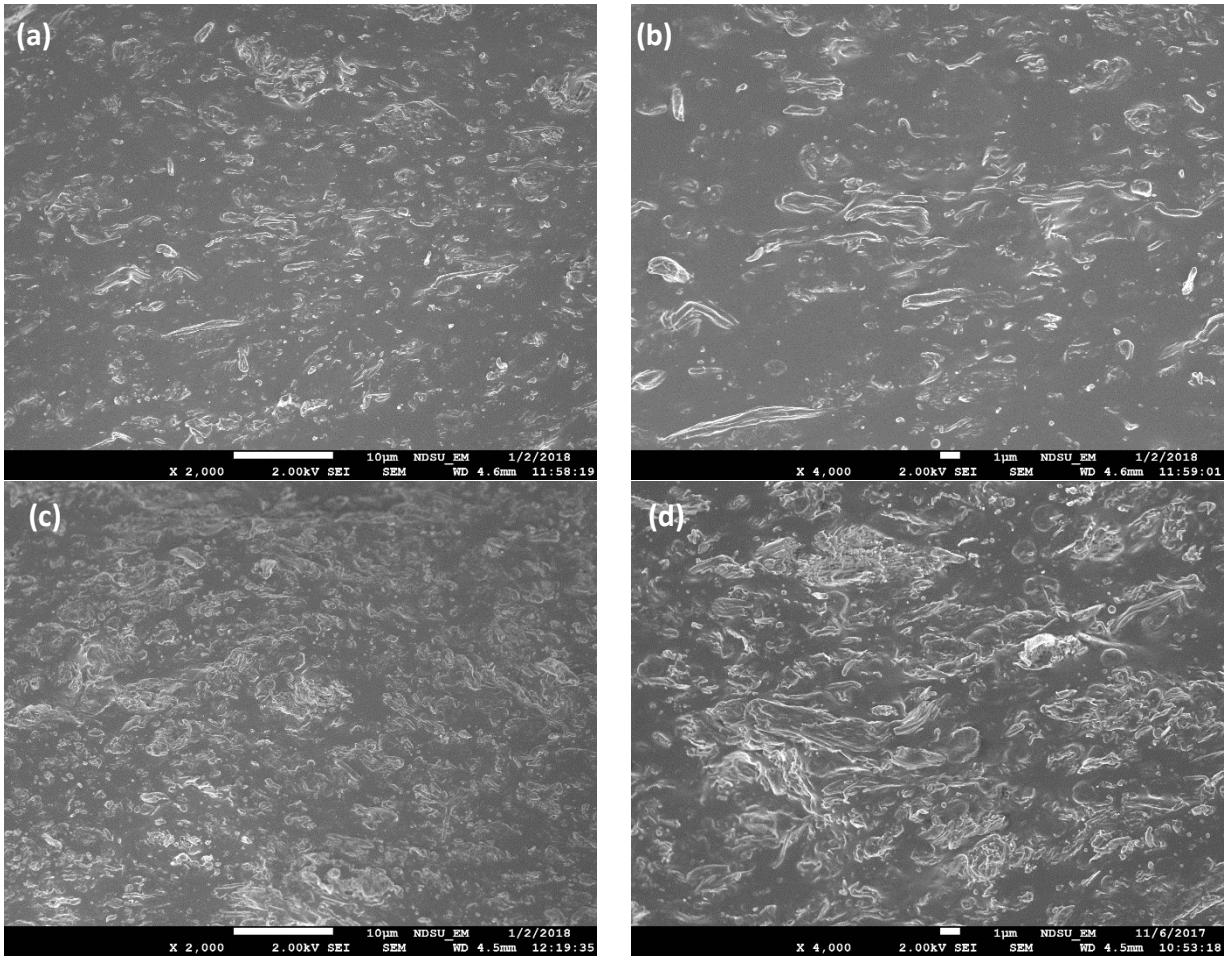

Figure 30. SEM images of cryo-fractured samples of (a) & (b) CNF-GO nanocomposites and (c) & (d) CNF-GO E

Figure 31 shows images of fractured ends from the tensile tests of CNF-GO nanocomposites. A similar result is found here as the he roughness of the cryo-fractured surface of CNF-GO nanocomposites increases significantly for the esterified samples. This again, indicates that the esterified sample has stronger interaction between the matrix SBR and the CNF-GO reinforcement.

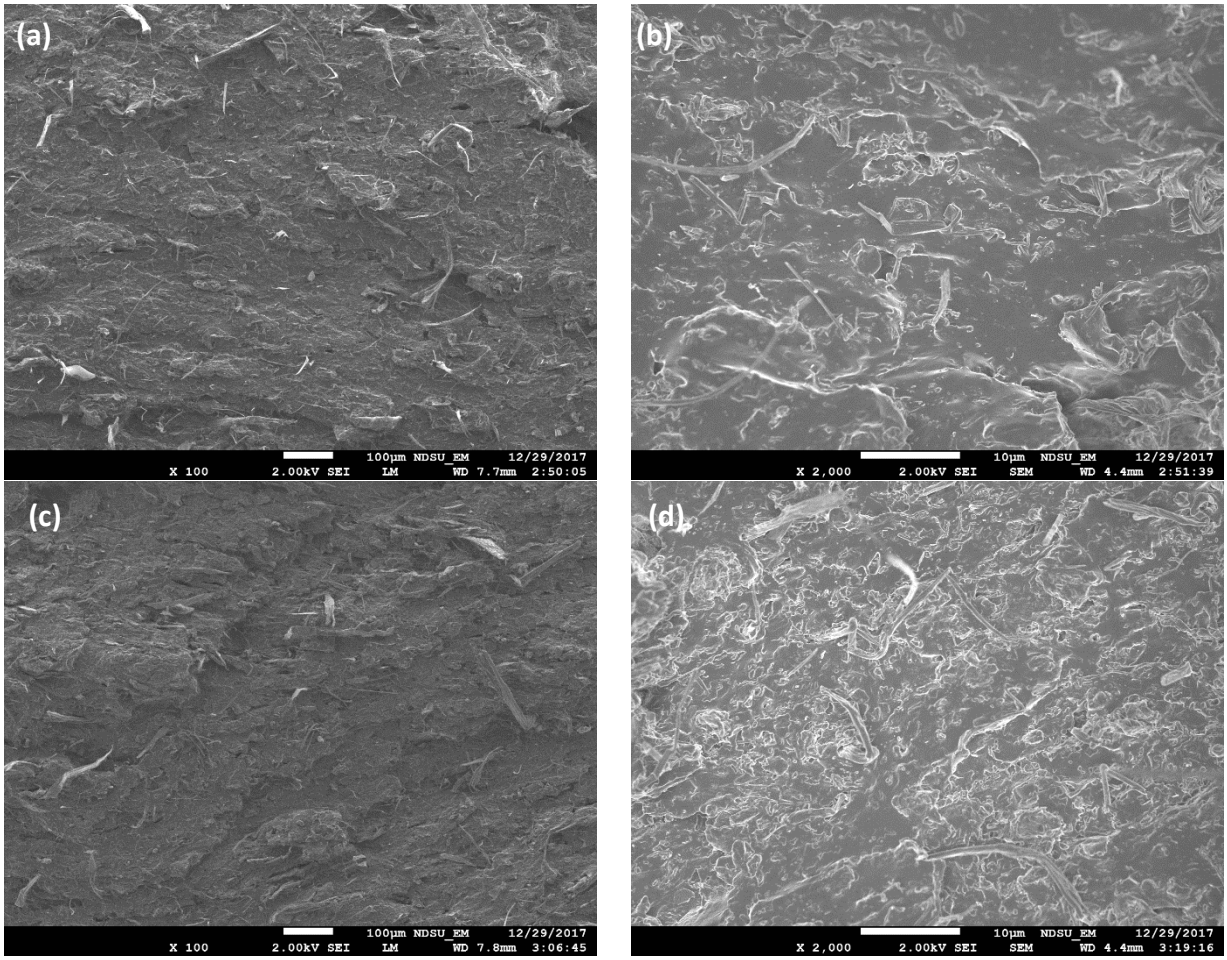

Figure 31. Tensile fractured surfaces of (a) CNF-GO nanocomposites and (b) CNF-GO E

Solvent Resistance

SBR dissolves in Active Ingredient if not vulcanized/crosslinked. Vulcanization covalently links SBR chains together to form a network and therefore vulcanized SBR only absorbs the solvent and swells, rather than dissolving. Other things being equal, solvent absorbency of the rubber is inversely proportional to degree of crosslinking. In this study, CNF (functionalized or un-functionalized) also affects solvent absorbency because it can either chemically or physically linked to the SBR chains and hence limit the rubber's absorption and swelling. Studying nanocomposite swelling behavior in a suitable solvent can be a useful probe for determining information regarding the nanocomposites molecular structure and overall morphology. Active Ingredient will dissolve SBR polymer chains which have not been immobilized due to the presence of a

crosslink or other molecular/physical interaction. Figure 32 shows Active Ingredient absorbency of the various SBR nanocomposites reinforced with CNF and CB/GO. In general, all the Active Ingredient-soaked samples behaved in a similar manner in which the initial rate of absorption (slope of the curve) was high and leveled off gradually over the 80-minute soaking time. The initial noticeable trend is that increased CB/GO loading shifts the absorption curve down. This is true for both sample types two and three. This is due to SBR chains being immobilized via chemical or physical linkages with the CNF and CB/GO. The ability of the combined reinforcement to form a network inside the SBR matrix at high concentrations can also hinder the swelling of the entire rubber. Moreover, CNF the reinforcement can act as barriers to slow down the diffusion of Active Ingredient molecules in the rubber. lastly, regions of the nanocomposite which are rich in CNF and CB/GO may result in trapped SBR chains which are inaccessible to the Active Ingredient. Sample type four which contained reinforcement which was esterified provided an additional shift down in absorption. This provides additional evidence of the formation of a three-dimensional networked structure interacting with the SBR matrix.

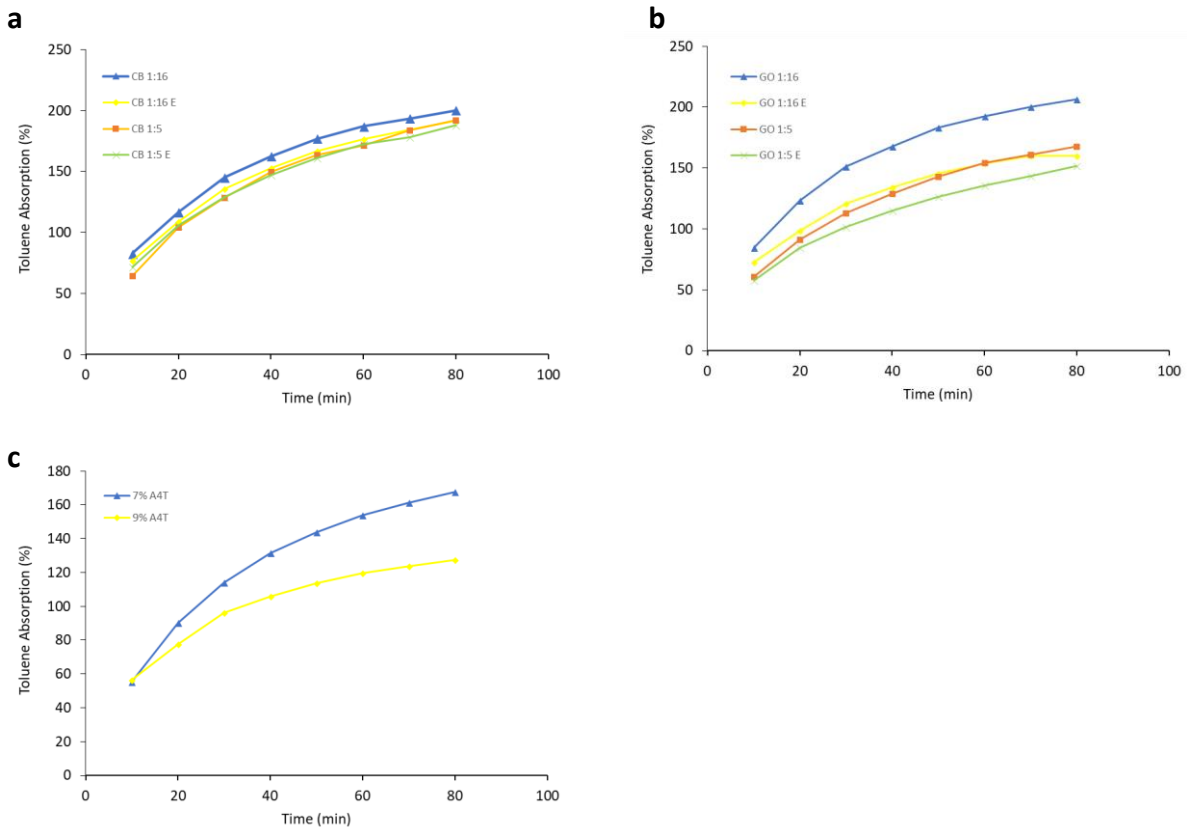

Figure 32. Active Ingredient swelling behavior of (a) CNF-CB nanocomposites, (b) CNF-GO nanocomposites and, (c) A4T-CNF-GO nanocomposites

Conclusions

The work built on the work presented in Chapter 4 of this thesis and demonstrated that CNF can be combined with carbon black or graphene oxide to create a hybrid reinforcement for use with SBR. In this survey, high performance nanocomposites which are more environmentally friendly and sustainable than traditionally used rubber materials, were reinforced with pristine and surface functionalized CNF and carbon black or graphene oxide. Graphene oxide proved to be more suitable as a reinforcing material when compared to the carbon black when paired with CNF. Esterification between CNF and CB/GO also proved to yield increased mechanical properties. These samples approached the baseline formulation which was the overall inquiry of this survey. Further work to study the effect of the esterification treatment would be merited for future studies. Additionally, acrylated CNF esterified with GO provided the greatest fracture

strength of any sample produced in this thesis except for the baseline formulation which included 50 phr CB. Overall, this survey proves CNF and GO could be a valuable tool to create rubber for industrial and/or commercial applications. Rubber products compounded in this manor would then be more environmentally friendly and sustainable than traditionally used rubbers today. More study however needs to be done to further increase the potential of the CNF as a reinforcing material.

Acknowledgement

The authors thank North Dakota Soybean Bean Council for its financial support. We are also grateful for materials testing and imaging assistance, provided by Dr. Chunju Gu of the NDSU Department of Coatings and Polymeric Materials, Gregory Strommen, Fred Haring, and Jim Bahr of the NDSU Center for Nanoscale Science and Engineering, and Scott Payne of the NDSU Microscopy Center. Gratitude is also expressed for the support of the NDSU department of Mechanical Engineering and many of its staff members.

REFERENCES

1. Global Plastic Production Rises, Recycling Lags. Worldwatch Institute: 2015.
2. Khalil, H. A.; Davoudpour, Y.; Islam, M. N.; Mustapha, A.; Sudesh, K.; Dungani, R.; Jawaid, M., Production and modification of nanofibrillated cellulose using various mechanical processes: a review. *Carbohydrate polymers* **2014,** *99*, 649-665.
3. Everything You Need to Know About Polylactic Acid (PLA). Creative Mechanisms: 2015.
4. Lavoine, N.; Desloges, I.; Dufresne, A.; Bras, J., Microfibrillated cellulose–Its barrier properties and applications in cellulosic materials: A review. *Carbohydrate polymers* **2012,** *90* (2), 735-764.
5. Dufresne, A., *Nanocellulose: From Nature to High Performance Tailored Materials*. De Gruyter: 2012.
6. Moon, R. J.; Martini, A.; Nairn, J.; Simonsen, J.; Youngblood, J., Cellulose nanomaterials review: structure, properties and nanocomposites. *Chemical Society Reviews* **2011,** *40* (7), 3941-3994.
7. Bhatnagar, A.; Sain, M., Processing of cellulose nanofiber-reinforced composites. *Journal of Reinforced Plastics and Composites* **2005,** *24* (12), 1259-1268.
8. Lee, H.; Hamid, S.; Zain, S., Conversion of lignocellulosic biomass to nanocellulose: structure and chemical process. *The Scientific World Journal* **2014,** *2014*.
9. Rojas, O. J., *Cellulose Chemistry and Properties: Fibers, Nanocelluloses and Advanced Materials*. Springer International Publishing: 2016.
10. Size Of The Nanoscale. https://introtonanotechnology.weebly.com/the-nanoscale.html (accessed Jul 15, 2017).
11. Alemdar, A.; Sain, M., Biocomposites from wheat straw nanofibers: morphology, thermal and mechanical properties. *Composites Science and Technology* **2008,** *68* (2), 557-565.
12. Siró, I.; Plackett, D., Microfibrillated cellulose and new nanocomposite materials: a review. *Cellulose* **2010,** *17* (3), 459-494.
13. Ververis, C.; Georghiou, K.; Christodoulakis, N.; Santas, P.; Santas, R., Fiber dimensions, lignin and cellulose content of various plant materials and their suitability for paper production. *Industrial Crops and Products* **2004,** *19* (3), 245-254.
14. Hubbe, M. A.; Rojas, O. J.; Lucia, L. A.; Sain, M., *Cellulosic Nanocomposits: A Review*. 2008; Vol. 3.
15. Liu, Q.; Lu, Y.; Aguedo, M.; Jacquet, N.; Ouyang, C.; He, W.; Yan, C.; Bai, W.; Guo, R.; Goffin, D.; Song, J.; Richel, A., Isolation of High-Purity Cellulose Nanofibers from Wheat Straw through the Combined Environmentally Friendly Methods of Steam Explosion, Microwave-Assisted Hydrolysis, and Microfluidization. *ACS Sustainable Chemistry & Engineering* **2017,** *5* (7), 6183-6191.
16. Alemdar, A.; Sain, M., Isolation and characterization of nanofibers from agricultural residues–Wheat straw and soy hulls. *Bioresource technology* **2008,** *99* (6), 1664-1671.
17. Dufresne, A., Nanocellulose: a new ageless bionanomaterial. *Materials Today* **2013,** *16* (6), 220-227.
18. Zimmermann, T.; Bordeanu, N.; Strub, E., Properties of nanofibrillated cellulose from different raw materials and its reinforcement potential. *Carbohydrate Polymers* **2010,** *79* (4), 1086-1093.

19. Saito, T.; Okita, Y.; Nge, T.; Sugiyama, J.; Isogai, A., TEMPO-mediated oxidation of native cellulose: Microscopic analysis of fibrous fractions in the oxidized products. *Carbohydrate polymers* **2006,** *65* (4), 435-440.
20. Isogai, A.; Saito, T.; Fukuzumi, H., TEMPO-oxidized cellulose nanofibers. *Nanoscale* **2011,** *3* (1), 71-85.
21. Jiang, F.; Hsieh, Y.-L., Self-assembling of TEMPO oxidized cellulose nanofibrils as affected by protonation of surface carboxyls and drying methods. *ACS Sustainable Chemistry & Engineering* **2016,** *4* (3), 1041-1049.
22. Saito, T.; Isogai, A., TEMPO-mediated oxidation of native cellulose. The effect of oxidation conditions on chemical and crystal structures of the water-insoluble fractions. *Biomacromolecules* **2004,** *5* (5), 1983-1989.
23. Saito, T.; Nishiyama, Y.; Putaux, J.-L.; Vignon, M.; Isogai, A., Homogeneous suspensions of individualized microfibrils from TEMPO-catalyzed oxidation of native cellulose. *Biomacromolecules* **2006,** *7* (6), 1687-1691.
24. Saito, T.; Isogai, A., Introduction of aldehyde groups on surfaces of native cellulose fibers by TEMPO-mediated oxidation. *Colloids and Surfaces A: Physicochemical and Engineering Aspects* **2006,** *289* (1), 219-225.
25. Saito, T.; Kimura, S.; Nishiyama, Y.; Isogai, A., Cellulose nanofibers prepared by TEMPO-mediated oxidation of native cellulose. *Biomacromolecules* **2007,** *8* (8), 2485-2491.
26. Fukuzumi, H.; Saito, T.; Iwata, T.; Kumamoto, Y.; Isogai, A., Transparent and high gas barrier films of cellulose nanofibers prepared by TEMPO-mediated oxidation. *Biomacromolecules* **2008,** *10* (1), 162-165.
27. Kumar, P.; Barrett, D. M.; Delwiche, M. J.; Stroeve, P., Methods for pretreatment of lignocellulosic biomass for efficient hydrolysis and biofuel production. *Industrial & engineering chemistry research* **2009,** *48* (8), 3713-3729.
28. Infrared Spectroscopy Absorption Table. https://chem.libretexts.org/Ancillary_Materials/Reference/Reference_Tables/Spectroscopic_Parameters/Infrared_Spectroscopy_Absorption_Table.
29. Xu, X.; Wang, H.; Jiang, L.; Wang, X.; Payne, S. A.; Zhu, J.; Li, R., Comparison between cellulose nanocrystal and cellulose nanofibril reinforced poly (ethylene oxide) nanofibers and their novel shish-kebab-like crystalline structures. *Macromolecules* **2014,** *47* (10), 3409-3416.
30. Lai, C.; Sheng, L.; Liao, S.; Xi, T.; Zhang, Z., Surface characterization of TEMPO-oxidized bacterial cellulose. *Surface and Interface Analysis* **2013,** *45* (11-12), 1673-1679.
31. Safdari, F.; Carreau, P. J.; Heuzey, M. C.; Kamal, M. R.; Sain, M. M., Enhanced properties of poly(ethylene oxide)/cellulose nanofiber biocomposites. *Cellulose* **2017,** *24* (2), 755-767.
32. Britannica, E. o. E., Styrene-Butadiene Rubber (SBR). In *Encyclopedia Britannica*, Encyclopedia Britannica, Inc.: 2009.
33. Zhang, Y.; Ge, S.; Tang, B.; Koga, T.; Rafailovich, M.; Sokolov, J.; Peiffer, D.; Li, Z.; Dias, A.; McElrath, K., Effect of carbon black and silica fillers in elastomer blends. *Macromolecules* **2001,** *34* (20), 7056-7065.
34. Wang, M.-J., Effect of polymer-filler and filler-filler interactions on dynamic properties of filled vulcanizates. *Rubber Chemistry and Technology* **1998,** *71* (3), 520-589.
35. Stearns, R.; Johnson, B., Interaction between carbon black and polymer in cured elastomers. *Industrial & Engineering Chemistry* **1951,** *43* (1), 146-154.

36. Ciesielski, A., *An introduction to rubber technology*. iSmithers Rapra Publishing: 1999.
37. Spahr, M. E.; Rothon, R., Carbon Black as a Polymer Filler. In *Polymers and Polymeric Composites: A Reference Series*, Palsule, S., Ed. Springer Berlin Heidelberg: Berlin, Heidelberg, 2016; pp 1-31.
38. What is Carbon Black? http://www.continentalcarbon.com/what-is-carbon-black.asp (accessed Dec 23, 2018).
39. Choi, S. S.; Park, B. H.; Song, H., Influence of filler type and content on properties of styrene-butadiene rubber (SBR) compound reinforced with carbon black or silica. *Polymers for Advanced Technologies* **2004,** *15* (3), 122-127.
40. Raza, M. A.; Ashraf, M. A.; Westwood, A. V.; Jamil, T.; Ahmad, R.; Inam, A.; Deen, K. M., Maleated high oleic sunflower oil-treated cellulose fiber-based styrene butadiene rubber composites. *Polymer Composites* **2016,** *37* (4), 1113-1121.
41. Sae-Oui, P.; Thepsuwan, U.; Thaptong, P.; Sirisinha, C., Comparison of reinforcing efficiency of carbon black, conductive carbon black, and carbon nanotube in natural rubber. *Advances in Polymer Technology* **2014,** *33* (4).
42. Praveen, S.; Chattopadhyay, P.; Albert, P.; Dalvi, V.; Chakraborty, B.; Chattopadhyay, S., Synergistic effect of carbon black and nanoclay fillers in styrene butadiene rubber matrix: development of dual structure. *Composites Part A: Applied Science and Manufacturing* **2009,** *40* (3), 309-316.
43. Mao, Y.; Wen, S.; Chen, Y.; Zhang, F.; Panine, P.; Chan, T. W.; Zhang, L.; Liang, Y.; Liu, L., High performance graphene oxide based rubber composites. *Scientific reports* **2013,** *3*.
44. Trovatti, E.; Carvalho, A. J.; Ribeiro, S. J.; Gandini, A., Simple green approach to reinforce natural rubber with bacterial cellulose nanofibers. *Biomacromolecules* **2013,** *14* (8), 2667-2674.
45. Mariano, M.; El Kissi, N.; Dufresne, A., Cellulose nanocrystal reinforced oxidized natural rubber nanocomposites. *Carbohydrate polymers* **2016,** *137*, 174-183.
46. Kalia, S.; Dufresne, A.; Cherian, B. M.; Kaith, B.; Avérous, L.; Njuguna, J.; Nassiopoulos, E., Cellulose-based bio-and nanocomposites: a review. *International Journal of Polymer Science* **2011,** *2011*.
47. Rubber Chemistry. http://laroverket.com/wpcontent/uploads/2015/03/rubber_chemistry.pdf.
48. Yin, B.; Li, G.; Wang, D.; Wang, L.; Wang, J.; Jia, H.; Ding, L.; Sun, D., Enhanced mechanical properties of styrene–butadiene rubber with low content of bacterial cellulose nanowhiskers. *Advances in Polymer Technology* **2016**.
49. Annamalai, P. K.; Dagnon, K. L.; Monemian, S.; Foster, E. J.; Rowan, S. J.; Weder, C., Water-Responsive Mechanically Adaptive Nanocomposites Based on Styrene–Butadiene Rubber and Cellulose Nanocrystals · Processing Matters. *ACS applied materials & interfaces* **2014,** *6* (2), 967-976.
50. Dagnon, K. L.; Shanmuganathan, K.; Weder, C.; Rowan, S. J., Water-triggered modulus changes of cellulose nanofiber nanocomposites with hydrophobic polymer matrices. *Macromolecules* **2012,** *45* (11), 4707-4715.
51. Abraham, E.; Deepa, B.; Pothan, L.; John, M.; Narine, S.; Thomas, S.; Anandjiwala, R., Physicomechanical properties of nanocomposites based on cellulose nanofibre and natural rubber latex. *Cellulose* **2013,** *20* (1), 417-427.

52. Neto, W. P. F.; Mariano, M.; da Silva, I. S. V.; Silvério, H. A.; Putaux, J.-L.; Otaguro, H.; Pasquini, D.; Dufresne, A., Mechanical properties of natural rubber nanocomposites reinforced with high aspect ratio cellulose nanocrystals isolated from soy hulls. *Carbohydrate polymers* **2016,** *153*, 143-152.
53. Rosilo, H.; Kontturi, E.; Seitsonen, J.; Kolehmainen, E.; Ikkala, O., Transition to reinforced state by percolating domains of intercalated brush-modified cellulose nanocrystals and poly (butadiene) in cross-linked composites based on thiol–ene click chemistry. *Biomacromolecules* **2013,** *14* (5), 1547-1554.
54. Rojas, O. J., *Cellulose Chemistry and Properties: Fibers, Nanocelluloses and Advanced Materials*. Springer International Publishing: 2016; Vol. 271.
55. Parambath Kanoth, B.; Claudino, M.; Johansson, M.; Berglund, L. A.; Zhou, Q., Biocomposites from Natural Rubber: Synergistic Effects of Functionalized Cellulose Nanocrystals as Both Reinforcing and Cross-Linking Agents via Free-Radical Thiol–ene Chemistry. *ACS applied materials & interfaces* **2015,** *7* (30), 16303-16310.
56. Kato, H.; Nakatsubo, F.; Abe, K.; Yano, H., Crosslinking via sulfur vulcanization of natural rubber and cellulose nanofibers incorporating unsaturated fatty acids. *RSC Advances* **2015,** *5* (38), 29814-29819.
57. Chen, M.-L.; Ma, H.-J.; Zhang, S.-Q.; Wang, J.-H., Mercury speciation with L-cysteine functionalized cellulose fibre as adsorbent by atomic fluorescence spectrometry. *Journal of Analytical Atomic Spectrometry* **2011,** *26* (3), 613-617.
58. Neises, B.; Steglich, W., Simple Method for the Esterification of Carboxylic Acids. *Angewandte Chemie International Edition in English* **1978,** *17* (7), 522-524.
59. Steglich Esterification. https://www.organic-chemistry.org/namedreactions/steglich-esterification.shtm.
60. Williams, A.; Ibrahim, I., A New Mechanism Involving Cyclic Tautomers for the Reaction with Nucleophiles of the Water-Soluble PeptideCoupling Reagent 1-Ethyl-3-(3′-(Dimethylamino) Propyl) Carbodiimide (EDC). *ChemInform* **1982,** *13* (11).
61. Karasek, L.; Sumita, M., Characterization of dispersion state of filler and polymer-filler interactions in rubber-carbon black composites. *Journal of materials science* **1996,** *31* (2), 281-289.
62. Vaca-Garcia, C.; Borredon, M.; Gaseta, A., Determination of the degree of substitution (DS) of mixed cellulose esters by elemental analysis. *Cellulose* **2001,** *8* (3), 225-231.
63. Kim, H.; Abdala, A. A.; Macosko, C. W., Graphene/Polymer Nanocomposites. *Macromolecules* **2010,** *43* (16), 6515-6530.
64. Bai, X.; Wan, C.; Zhang, Y.; Zhai, Y., Reinforcement of hydrogenated carboxylated nitrile–butadiene rubber with exfoliated graphene oxide. *Carbon* **2011,** *49* (5), 1608-1613.
65. Mao, Y.; Wen, S.; Chen, Y.; Zhang, F.; Panine, P.; Chan, T. W.; Zhang, L.; Liang, Y.; Liu, L., High Performance Graphene Oxide Based Rubber Composites. *Scientific Reports* **2013,** *3*, 2508.
66. Potts, J. R.; Shankar, O.; Du, L.; Ruoff, R. S., Processing–Morphology–Property Relationships and Composite Theory Analysis of Reduced Graphene Oxide/Natural Rubber Nanocomposites. *Macromolecules* **2012,** *45* (15), 6045-6055.
67. Liu, Y.; Zhou, J.; Zhu, E.; Tang, J.; Liu, X.; Tang, W., Facile synthesis of bacterial cellulose fibres covalently intercalated with graphene oxide by one-step cross-linking for robust supercapacitors. *Journal of Materials Chemistry C* **2015,** *3* (5), 1011-1017.